5-2014

Kinesthetic Haptics Sensing and Discovery with Bilateral Teleoperation Systems

Tian Qiu
University of Tennessee - Knoxville, tqiu@utk.edu

To the Graduate Council:

I am submitting herewith a dissertation written by Tian Qiu entitled "Kinesthetic Haptics Sensing and Discovery with Bilateral Teleoperation Systems." I have examined the final electronic copy of this dissertation for form and content and recommend that it be accepted in partial fulfillment of the requirements for the degree of Doctor of Philosophy, with a major in Mechanical Engineering.

William R. Hamel, Major Professor

We have read this dissertation and recommend its acceptance:

Dongjun Lee, Seddik Djouadi, Xiaopeng Zhao, Joseph Boulet

Accepted for the Council:

Carolyn R. Hodges

Vice Provost and Dean of the Graduate School

(Original signatures are on file with official student records.)

Kinesthetic Haptics Sensing and Discovery with Bilateral Teleoperation Systems

A Dissertation Presented for the

Doctor of Philosophy

Degree

The University of Tennessee, Knoxville

Tian Qiu

May 2014

To my parents:

Ning Qiu,

Chang Liu

Acknowledgements

First and foremost I would like to thank my advisers, Dr. Hamel and Dr. Lee, for supporting me during the past five years. Dr. Lee hired me after I graduated from Tsinghua. He always actively took part in every part of my research and gave me helpful advice. His guidance covered every aspect of graduate student work: designing experiment protocols, writing papers, reading and analyzing other people's results and so on. His enthusiasm for his research deeply affected me. Dr. Hamel became my adviser and continued my assistantship after Dr. Lee left the University of Tennessee. He always gave me maximum flexibility in research and trusted my judgment. Discussion with him was always very constructive. He has very good instincts about mechanical and electronic system design because of his long and extensive experience in various robotics engineering projects. These instincts helped to improve my results substantially. He also provided ample funding to support my research, which was essential to the completion of this project.

I would also like to express gratitude for the support I received from all the other graduate and undergraduate students that I have been working with. Dr. Huang, Mr. Xu, Mr. Zuo and Mr. Davis worked with me under the supervision of Dr. Lee. Dr. Nycz, Mr. Young and Mr. Anderson worked with me under the supervision of Dr. Hamel. Dr. Huang and I were supported by the same grant from the National Science Foundation, so our work has a lot in common. Dr. Huang always went out of his way to help me. He picked me up at the airport when I first arrived in Knoxville

and provided me with temporary housing. He then taught me a lot about the software and hardware we were going to use in our research and helped me initialize my first computer program. Mr. Xu and Mr. Zuo worked in the same laboratory with me but on a different project. Our projects shared many of the same research problems. They offered a lot of valuable suggestions about my projects.

When I joined Dr. Hamel's lab three years ago, Dr. Nycz and Mr. Young had already worked for Dr. Hamel for some time. They gave me many suggestions and offered a lot of support to help make transitional period very smooth. We all spent a large amount of time setting up and upgrading the Robotics Systems Laboratory. Mr. Young also helped me learn Solidworks, which saved me a lot of precious time. He also offered helpful suggestions about my research project. Dr. Nycz is a senior member of our laboratory who had experience in many aspects of our research. His sharp opinions often helped clarify many issues. Dr. Nycz and I also shared an interest in world history and we often discussed historical events when we had time. Mr. Anderson joined our lab in Fall 2013. He was also a great person to work with. I often asked him to proofread my papers and to build parts using 3D printers. He always responded in a very timely manner.

The undergraduate research assistants also helped me in many ways: Mr. McNeil helped me proofread my papers; he and Mr. Penney helped a lot when we setup my lab; Ms. Hurst also helped me with numerous things.

I also appreciate the help of Dr. Noakes from Oak Ridge National Lab. He collaborated extensively with us during the course of my dissertation.

My thesis could never have happened without the help of Mr. Higdon from the departmentâĂŹs instrumentation technology support and Mr. Graham from the departmentâĂŹs machine shop. We have various electronics experimental systems, and when any one of them had a problem, Mr. Higdon was always the first person I went to for help. Mr. Graham diligently manufactured many parts for our research project.

My great thanks to my committee members: Dr. Boulet, Dr. Djouadi and Dr. Zhao. I appreciate their time spent on my dissertation.

Last but not least, many thanks to my parents for their support and guidance during all those years of my study. They started teaching me about engineering when I was very young. This gave me a significant head start in most science subjects, which I felt to be invaluable. Also, their commitment to hard work set a very good example for me.

"The world of the future will be an even more demanding struggle against the limitations of our intelligence, not a comfortable hammock in which we can lie down to be waited upon by our robot slaves."

—- Norbert Wiener, The Human Use Of Human Beings: Cybernetics And Society

Abstract

In the mechanical engineering field of robotics, bilateral teleoperation is a classic but still increasing research topic. In bilateral teleoperation, a human operator moves the master manipulator, and a slave manipulator is controlled to follow the motion of the master in a remote, potentially hostile environment. This dissertation focuses on kinesthetic perception analysis in teleoperation systems. Design of the controllers of the systems is studied as the influential factor of this issue. The controllers that can provide different force tracking capability are compared using the same experimental protocol. A 6 DOF teleoperation system is configured as the system testbed. An innovative master manipulator is developed and a 7 DOF redundant manipulator is used as the slave robot. A singularity avoidance inverse kinematics algorithm is developed to resolve the redundancy of the slave manipulator. An experimental protocol is addressed and three dynamics attributes related to kineshtetic feedback are investigated: weight, center of gravity and inertia. The results support our hypothesis: the controller that can bring a better force feedback can improve the performance in the experiments.

Table of Contents

List of Tables

List of Figures

Chapter 1

Introduction

1.1 Motivation

There are many hostile work environments where it is impossible for humans to be present, for example, outer space, deep ocean or high nuclear radiation areas. Researchers from all over the world have been working for years to develop and improve telerobotic systems to replace humans, as shown in Fig. 1.1, or at least isolate them from hostile environments. For example, Oak Ridge National Laboratory developed several teleoperators to clean up contaminated waste tanks and other facilities to keep the operator away from radioactive materials. Another important telerobotics application is the deep sea exploration, for example, the opening scene in the movie Titanic, where a dual arm robotic submersible explored the wreckage of Titanic. This makes remote environment exploration a very important robotics research area.

Haptics research has a long history and has gained increasing attention recently. There are three types of haptics: human haptics, machine haptics and computer haptics. Human haptics is the study of human sensing and is generally considered a psychological study. In those studies, subjects are usually asked to directly perceive objects, for example, touch or lift them. The subjects then answer questions about

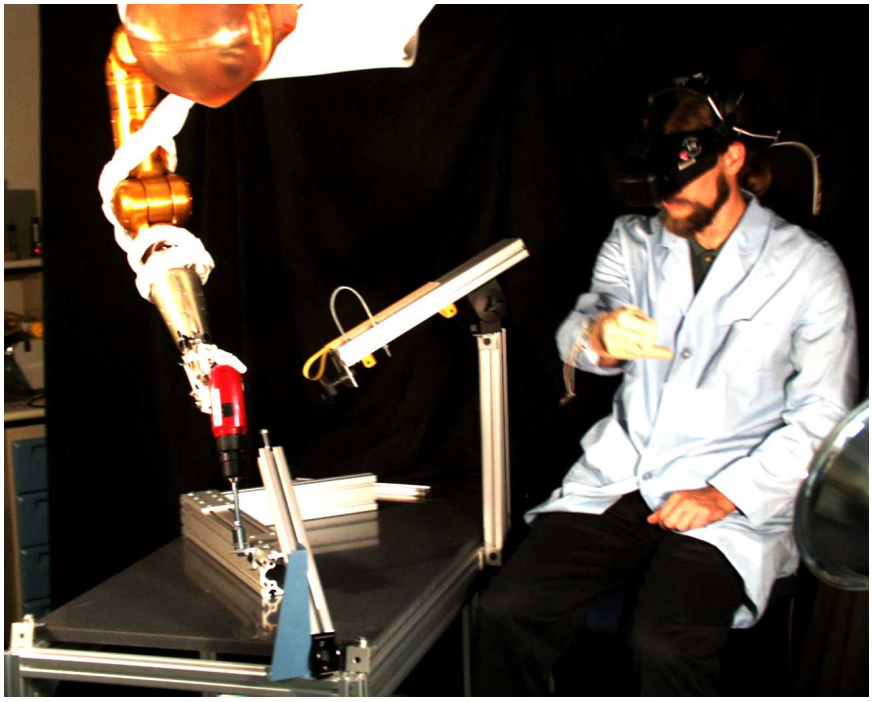

Figure 1.1: Teleoperation*
*Images courtesy of NASA Johnson Space Center

certain properties of the objects, such as their weight, inertia, texture and so on. These studies provide an understanding of the process of haptics exploration. Machine haptics is about design and optimization of the machines that replace or augment human touch. Force/position tracking errors are often used as the performance index for the controller design. Computer haptics is a newly emerging area which deals with software and algorithms to render virtual objects that mimic certain real things. High performance computers provide the possibility of running simulation models made up of millions of nodes.

Haptics sensation can also be categorized either as "kinesthetic" or "tactile." Kinesthetic sensation is about the motion and forces the body experiences during a haptics interaction. Kinesthesia has been considered in teleoperation research with force reflection. Tactile sensation usually refers to the interaction between objects and the fingers or skin; it covers temperature, pressure, texture and many other areas.

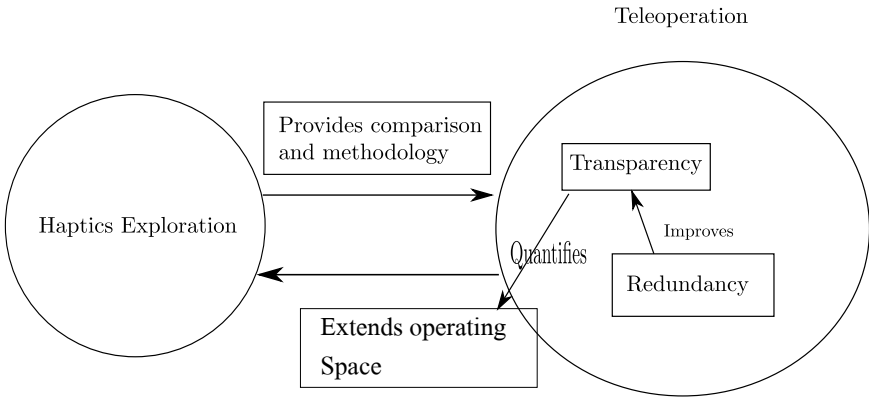

Figure 1.2: Haptics Teleoperation Research Area Structure

A variety of experimental equipment has been built to investigate the tactile sensing capabilities of humans.

1.2 Summary

This dissertation focuses on a generalized theory of kinesthetic haptics exploration of an unknown remote environment using a full-size teleoperation system. Human haptics research methodology is used to guide and evaluate the design of the teleoperator.

The philosophy adopted is that the human should remain in direct control of the whole system. When interaction between the teleoperator and environment occurs, the teleoperator should provide feedback that is as close to the actual interaction as possible. Since a kinesthetic teleoperator provides force feedback, force tracking is very important in providing appropriate feedback. The ideal case of exploration through a teleoperator is that the performance is as good as direct interaction between the operator and the slave work environment. This falls into the area of transparency analysis in telerobotics research. In this way, the influence of human factors in a teleoperator can be fully investigated.

1.3 Outline

This dissertation is organized as follows: chapter two discusses previous related literature, chapter three proposes the research methodology used in our research, chapter four summarizes the fundamental contributions of this project, chapter five describes the system testbed configured for the experiments, chapter six reviews all the experiment assessments carried out during the course of this research project, chapter seven gives the conclusions of the dissertation and chapter eight provides a perspective of future work.

Chapter 2

Literature Review

2.1 Introduction

A bilateral teleoperation system is a robotic system with two robots: a slave and a master, as shown in Fig. 2.1. The human operator operates the master robot and the master robot sends commands to the slave robot through a communication network; the slave robot then mimics the motion of the master robot. The slave also sends feedback to the master robot. Force interaction between the slave robot and the remote environment can be reflected to the human operator through the master robot. The workspace and the capability of a human operator can be extended and the operator can be isolated from the hostile environment. As pointed out in [43], there are two primary means to improve the performance of a teleoperation system: (1) increasing the transparency of the system and (2) adding task automation to make the system more time efficient. We will focus on the first method.

The first bilateral kinesthetic teleoperation system was built by Dr. Goertz in the 1950s [23].The slave and the master robots were connected using rigid mechanical linkages and the operator had to look directly at the slave workspace to get visual feedback. In the 1970s and 80s, electrical servos replaced mechanical linkages and camera-monitor based vision systems replaced direct visual feedback. Numerous

bilateral teleoperation systems were developed by various laboratories [39] and utilized for handling radioactive materials in Oak Ridge National Laboratory.

2.2 Generalized Teleoperation Systems

The very first teleoperation system built by Dr. Goertz [23] consisted of two manipulators with similar kinematics. Later electrical servo teleoperation systems also adopted this design method. The advantage of this method is that the controller design is simple, as joint angles of the master manipulator can be sent to the slave without having to go through any computation or transformation. However this method poses serious limitations on the design of the manipulators.

Later, another type of teleoperation systems, the generalized teleoperation systems, were developed [10, 9, 16], in which the master and slave manipulators do not have to have a similar mechanism. Their controllers have to have kinematics and inverse kinematics algorithms. The joint angles of the master manipulators need to be converted to the master manipulator position in Cartesian space and then transformed into the desired slave manipulator position and orientation. The communication network passes this information on to the slave robot. Then the slave manipulator controller needs to convert the desired position and orientation into the desired joint angles. If the teleoperation system has feedback, then the original information from the slave environment needs to be transmitted and transformed to the master space.

Recently, a new research area called trilateral teleoperation emerged [34, 37, 36]. In [37, 36], a redundant slave manipulator is considered and the two master manipulators control different spaces of the slave motion: one for the null space and another one for the solution space. In [34], the trilateral haptics collaboration system is modeled as a six port control system, and its passivity condition is considered.

2.3 Transparency and Stability in Controller Design of Teleoperation Systems

The controller design of a teleoperation system plays a vital role in its performance. Reducing position tracking error is one of the first goals considered by teleoperation researchers; feedforward controllers are used to cancel the dynamics of the manipulators, but they usually suffer from the noise brought on by the differentiation of the position signals and the inaccuracy of the dynamics modeling.

Improving transparency and maintaining stability are the two primary tasks for teleoperator system design. Previously, kinesthetic force feedback was computed using the PID controllers. This brought about a problem: a small position tracking error could result in a very low force feedback. For this reason, force direct measurement and feedback are now used. In [29], Dr. Lawrence systematically analyzed the efficacy of this type of controller and proposed the well-known four channel transparent control architecture. Psychophysics experiments are largely used in teleoperation control design [54]. Dynamics feedforward has been used, but it is notorious for amplifying the noise [33] and an accurate modeling of the robot is required. Hannaford summarized all possible control architectures and analyzed their transparency based on their transmitted impedance [41]. Even though these analyses provided significant theoretical results, they have not been connected with the direct hand kinesthetic exploration tasks. Also, these transparency studies all focus on single degree of freedom systems and the theories lack actual application potential. This dissertation considers a 6 DOF teleoperation system, which is commonly used in various remote handling tasks.

Stability is also very important in that it affects the safety of the system. Time delay in the communication network could harm the systemâĂŹs stability [2, 52]. Control algorithms considering time delay have been proposed in various papers [29, 48, 25]. In [25], Dr. Hannaford presented a novel passivity based haptics interface

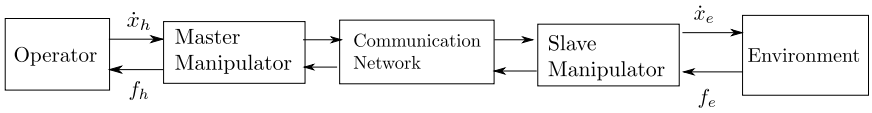

Figure 2.1: General Framework of a Teleoperation System

control algorithm. All of these publications focus on improving stability or reducing tracking errors. None of them considered human factors in teleoperation tasks. In this thesis we investigate the effect of control algorithms on the performance of the system.

2.4 Haptics and Teleoperation

As mentioned above, haptics exploration consists of two major fields: tactile and kinesthetic. Most of the existing haptics exploration research is about tactile sensing [30, 8, 28, 44]. In [30], the natural procedure of a human exploring an unknown object is discussed, and potential guidelines to improve teleoperation system are given. An H_2 based control architectural analysis is provided in [8], where the ability of reflecting the change of compliance of the object is considered the primary fidelity of the system. [44] used a robotic finger to explore the features of an object. All of these papers focus on tactile sensing and exploration; research about kinesthetic exploration is needed.

Kinesthetic feedback was considered in [26], where the teleoperation system is modeled as a two port system. The limitation of this work is obvious: the system is modeled as a one degree of freedom, linear system. In an actual teleoperation system application, most of the equipments are 6 DOF.

Teleoperators with kinesthetic feedback have seen applications in many areas, for example, outer space, deep ocean or high nuclear radioactive environments [38, 12, 24, 43]. Teleoperation systems can extend the reach of human operators but they also compromise the sense of immersion. In other words, the teleoperation systems are not transparent enough for humans to perceive as perfectly as they could in direct contact exploration. Issues about internet-based teleoperations are discussed in [24]. In [43],

the weight perception limitation is determined to be 3 lb (1.36 kg). An example of a force feedback teleoperation system is presented in [12]. A solution to improve the kinesthetic feedback in nuclear clean-up is proposed in [38].

2.5 Performance Evaluation

Evaluation of the performance of a haptic device divides into two major streams. The first one focuses on the mechanical or control engineering properties of the system [62, 19]. The second one addresses this issue based on psychology evaluations [64, 51, 58]. In [64, 51], the effect of time delay on haptics performance is discussed. The experiment is based on haptics devices interacting with a virtual environment and response time is used as the major haptics performance index. In [58], haptic feedback provides a great advantage in surgical training for physicians. But none of the papers mentioned uses non-linear, multi-dimension, full size bilateral teleoperation systems. A variety of haptics performance indexes will be used.

2.6 Redundant Manipulators

A manipulator requires 6 joints to place the end-effector in an arbitrary position with an arbitrary orientation. Most industrial robots are 6 DOF, such as PUMA560, ABB IRB series. Any manipulator that has more than six joints is redundant. There are many methods that use this redundancy to provide better performance of the robot [6, 17, 15, 18, 53]. [6] provides a comprehensive analysis on the design of kinematic redundant robot. [18] focuses on the design and analysis of an innovative parallel manipulator. [53] provides a tutorial report of the literature on kinematics control of redundant robot manipulators. [17] proposes a computational efficient gradient projection optimization scheme for a 7 DOF redundant robot. A controller based on task performance measures is discussed in [15].

2.7 Direct Contact Kinesthetic Exploration

Previous research in experimental psychology has been conducted regarding the weight perception [1]. Some methods and testing protocols are used in this dissertation and extended to the teleoperation scenario in an effort to bridge the gap between these two areas [66]. There has been some research about the psychophysical evaluation of teleoperation systems [40] and [54], where researchers consider environment as a virtual wall with stiffness and damping. Haptics refers to the sense of touch, including weight, temperature, inertia, stiffness perceptions and so on. It is one of the most classic research areas in experimental psychology. Haptics has two major sub-areas: kinesthetic [1] and tactile [31]. Kinesthetics sensing is about the motion and force of muscles and joints while tactile sensing is about the touch between the fingers and objects. Therefore, kinesthetic sensing in experimental psychology is very important to the teleoperation research. One of the first kinesthetic sensing tasks used in experiments was the weight and inertia perception. We adopted these experimental protocols as our major testing method. In teleoperation, many performance indices were proposed in the previous literature [57]. Most of them are task dependent which is difficult to generalize into other applications. Draper categorizes all the indices into two major categories in his human factor analysis paper [14].

Weight perception is a very important research area in experimental psychology [1, 61, 30]. The earliest studies dated back to 1834 when Ernest Weber proposed his famous Weber's law. The roles of the size and inertia of objects in weight perception are investigated. [61] provided a comprehensive review of the recent haptics psychology research. In [1], the patterns of objectsâĂŹ inertia tensor and their eigenvalue and eigenvectors were analyzed.

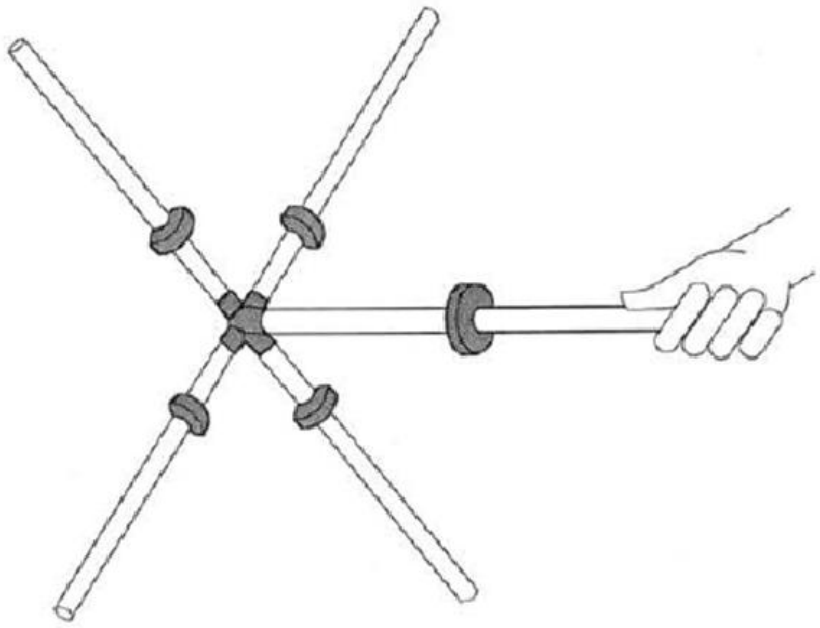

Figure 2.2: Weight Perception Object [1]

2.8 Master Controller Design

A haptic device with 6 DOF force feedback is essential in providing exact and complete kinesthetic feedback. There are several off-the-shelf haptics devices with 6 DOF of force feedback [13, 47, 21]. Force Dimension offers several haptic devices with 6 active joints. A product called "Sigma 7" even has a seventh active grasping joint to mimic the motion of a pair of scissors [13]. Geomagic provides a haptic device called "Phantom Premium" which can provide a fairly large workspace and force capacity [21]. Another notable product called "Haptic Wand" is also available from Quanser, a research equipment company [47]. It offers five active degrees of freedom and a sixth joint which is passive. All of them are quite expensive for many research groups. So a lot of researchers have designed their own 6 DOF haptic devices for their projects. There are two ways of building a 6 DOF haptic device: 1) designing and building

the whole system from scratch [60, 65, 59, 63] or 2) integrating existing, off-the-shelf haptics products with fewer degrees of freedom and coordinating them to provide a higher degrees of freedom force feedback.

Examples of the first method were presented in [60, 65]. This method makes the developing process lengthy and costly. Researchers have to deal with the issue of machining all the parts and interfacing with the motors. It could also take a long time to calibrate and adjust the design. On the other hand, building an advanced haptic device based on the off-the-shelf haptic devices can be very cost effective. Novint Falcon is developed and used widely as a haptics research device and computer gaming equipment. Many researchers have integrated multiple Falcons together to develop new haptic devices with higher degrees of freedom. Instructions about how to build a novel haptic device using two Falcons were provided in [50]. A similar device has seen application in device calibration for fingernail imaging [35].

2.9 Summary

Force reflection of the teleoperation system is very important in kinesthetic exploration tasks. Previous research on teleoperation systems has provided valuable results. The general structures of the controller of the teleoperation systems are constantly being modified and upgraded to enhance their performance. In haptics and human factors analysis, many experiments have been conducted to explore the human perception capability. However, most of the analysis focused on a one degree of freedom system, which lacked application potential. Also, there have not been sufficient attempts to connect the engineering side of the problem to the perception side of the research.

Chapter 3

Research Methodology

3.1 Overview

There are many factors that contribute to the efficacy of the teleoperation systems, such as the hardware, the level of training of the operators and the controller design. In this dissertation, we focus on the influence of the controller design.

The earliest teleoperation systems used two channel position to position controllers. In this type of control system, the master controller sends its position to the slave, and the slave sends its position back to the master. The slave and master both compute control effort to compensate for position errors; the most simple and widely used example is the PID controller. This type of controller provides good position convergence, but its kinesthetic perception is poor.

In a direct contact kinesthetic perception case, the operator interacts with the unknown object directly; he/she perceives the exact position and force information of the object. When an operator operates a teleoperation system through a master controller, such as a joystick, a haptic device, etc., he/she senses the position of his/her arm through the muscles and nerves in his/her arm as before, so the operators know the exact position of the desired master controller. Since the position tracking functions very well in most of the teleoperation systems, the position

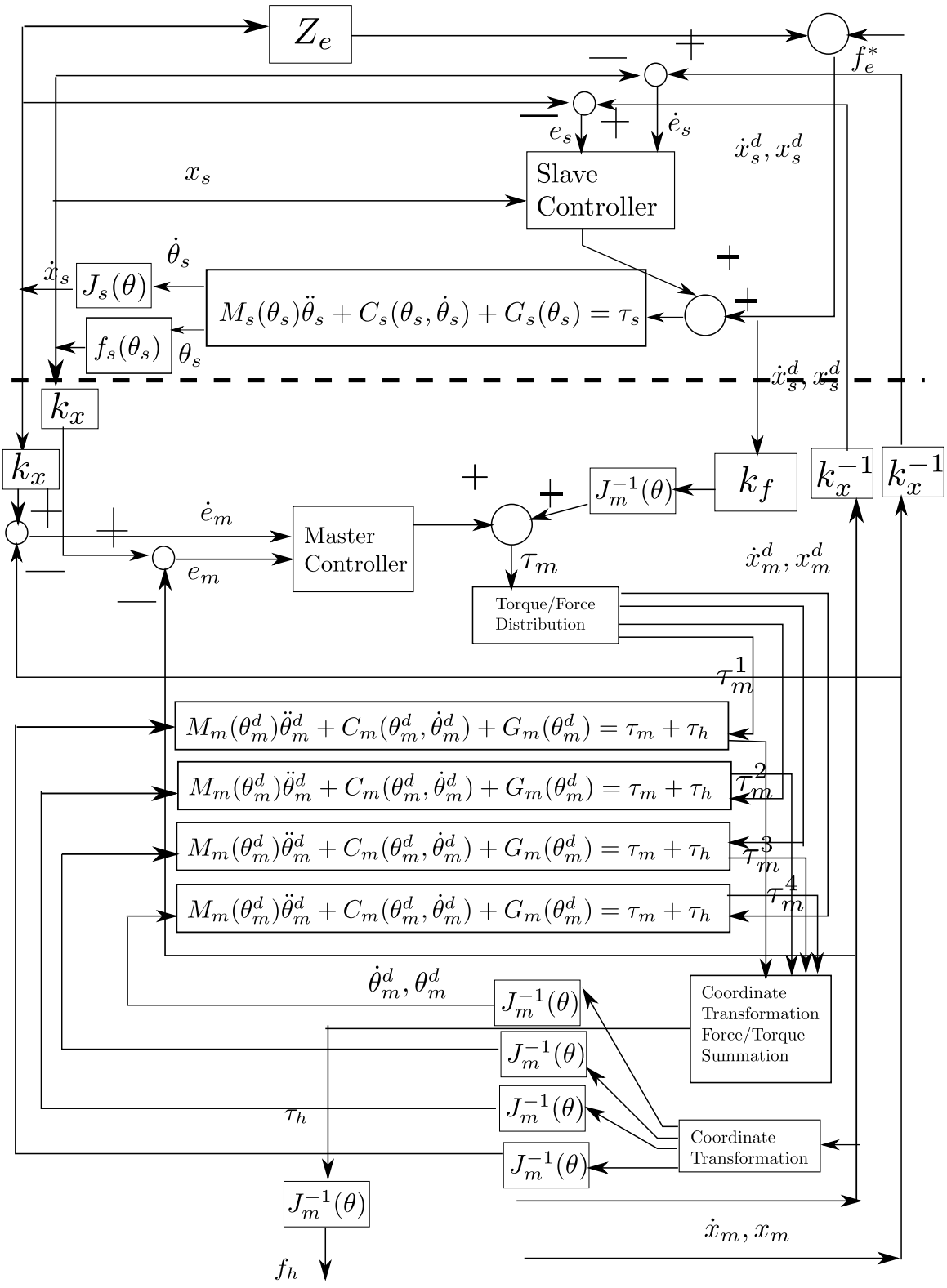

Figure 3.1: Three-channel Control Architecture of Bilateral Teleoperation Systems

error information is not significant in kinesthetic perception, while force is. During operation, the operator should be expecting an interaction force between the object and the slave robot, but he/she perceives the force feedback, f_h, from the devices. In other words, we model the human perception as a "flow source". Flow is a generalized term in engineering. In dynamics, flow refers to velocity, while in electrical engineering it refers to current. Flow source means that humans can inject velocity commands into the system and the system responds with effort. Effort is also a generalized engineering term, referring to force or torque in dynamics and voltage in electrical engineering. Flow times effort equals power. Force tracking is essential to transparency because of the nature of kinesthetic perception. Hampered force feedback makes it difficult for the operator to determine the dynamic attributes of the object that the system is handling, which diminishes the haptics sensation. Previously, impedance, the ratio between force and velocity was commonly used to analyze the transparency of a teleoperation system. However, it is an engineering term that may be confusing to non-engineers taking part in human factor experiments. Therefore analyzing and improving the force instead of perceived impedance is a better choice.

The force feedback f_h that the operator perceives is different from the actual interacting force f_e^* between the slave robot and the object, as shown in Fig. 2.1.

The slave manipulator in our system is a redundant robot. That is to say, instead of having one solution for the inverse kinematics of the robot, the system can provide an infinite number of solutions that all lead to the same end-effector position and orientation. In order to improve the kinesthetic perception in the experiments, one of the configurations has to be chosen as the desired configuration of the slave manipulator.

3.2 Preliminary

3.2.1 Environment Modeling

Previous research considers the environment as a stiffness/damping virtual wall. The environment considered in this project is modeled as a pure inertia component. This is to assume that the robot is holding a rigid object firmly in the end-effector and the object has exactly the same orientation, position and velocity as the end-effector. So the ideal kinesthetic feedback should provide a force/torque feedback that matches exactly the effort needed to accelerate a rigid body. A pure inertia component is a linear component, so if the robot works in the configurations that are relatively close to a certain configuration, frequency domain analysis can be applied around that linear operation point.

The inertial parameters of any rigid body in a three dimensional space is fully defined by the following constant symmetric positive-definite 3 by 3 matrix:

$$I = \begin{pmatrix} I_{xx} & I_{xy} & I_{xz} \\ I_{xy} & I_{yy} & I_{yz} \\ I_{xz} & I_{yz} & I_{zz} \end{pmatrix}$$

Because of the symmetry, there are only six independent constants in the matrix; these six constants are the parameters that the operator tries to determine and evaluate during the haptics exploration task. The equation of motion of a general rigid body is given by:

$$f_d = ma + mg \tag{3.1}$$

$$\tau_d = I\alpha + \omega^T I \times \omega + \tau_g(\theta) \tag{3.2}$$

Where f_d, a, g, ω and α are all 3×1 vectors. Human kinesthetic perception is the process of combining and analyzing information of f, ω, α and τ and tries to estimate

I, m, $\tau_g(\theta)$. The ideal teleoperation system should be able to provide exactly the same feedback f_d, τ_d that the environment provides.

3.2.2 Robot Dynamics, Gravitational compensation and PD controllers

The dynamic model of a robotic arm is given by:

$$M(\theta_*)\ddot{\theta}_* + C(\theta_*, \dot{\theta}_*)\dot{\theta}_* + G(\theta_*) = \tau_* \quad * = s, m \tag{3.3}$$

where θ is the configuration of the robot, $M(\theta)$ is the inertia matrix, $C(\theta, \dot{\theta})$ is the Coriolis matrix, $G(\theta)$ is gravity and τ is the torque applied at the joints. Eq. 3.3 is based on two commonly accepted assumptions: 1) the torque τ's is applied at the joint and 2) the links of the robot under investigation are all rigid bodies.

The most commonly used controller for a bilateral teleoperation system is the PD controller. This control architecture will be used as a comparison group in our project to show the superiority of our novel methods.

$$\tau_* = K_*^p(\tilde{\theta}_* - \theta_*) + K_*^d(\dot{\tilde{\theta}}_* - \dot{\theta}_*) \quad * = s, m \tag{3.4}$$

Therefore, the combined dynamics of the manipulator is given by

$$M(\theta_*)\ddot{\theta}_* + C(\theta_*, \dot{\theta}_*)\dot{\theta}_* + G(\theta_*) = K_s^p(\tilde{\theta}_* - \theta_*) + K_*^d(\dot{\tilde{\theta}}_* - \dot{\theta}_*) + J^{-1}(\theta_*)F_* \quad * = s, m \tag{3.5}$$

Gravitational compensation is commonly used to reduce the tracking error of a teleoperation system and to improve the haptics sensation. The basic idea is to predict the control effort to compensate for gravity based on the desired position and known system parameters. If there is no such effort, then the operator has to provide the force to lift both the manipulator and the object in the gripper of the

robot. This would hamper kinesthetic perception . The challenge in using this kind of controller is that it heavily depends on system modeling. Therefore, the manufacturer of our robot, the WAM (Whole Arm Manipulator), provided a special program called "bt-wam-gravitycal" to control the robot through nine configurations, measure the torque applied at the joints and compute the inertia parameters of the arm. These parameters were saved in a file and used whenever gravity compensation was enabled.

Force and position scaling is commonly used in teleoperation systems to reduce fatigue or increase dexterity where:

$$f_m^d = k_f f_s \qquad x_m^d = k_x x_s \tag{3.6}$$

$$f_s^d = \frac{f_m}{k_f} \qquad x_s^d = \frac{x_m}{k_x} \tag{3.7}$$

Where k_f is the force scaling factor and k_x is the position scaling factor. There are three special cases for scaling factors. If $k_x = 1$, then the human operator experiences the same motion as the slave robot. If $k_f = 1$, then the human operator experiences the same force feedback as the slave robot. If $k_x = k_f$, then the human operator experiences the same impedance/admittance as the slave robot.

3.3 Singularity Avoidance of a Redundant Robotic Arm

To improve the transparency of a robot, we have to overcome the singularity issue of the robotic arm. Given our specific application, wrist singularities are studied and wrist singularity avoidance is considered in the inverse kinematics of our robotic arm.

3.3.1 Singularity of Non-redundant robot

A robot arm requires at least six joints to place the end-effector at a given configuration in its workspace; however, a 6 DOF manipulator may have singularity

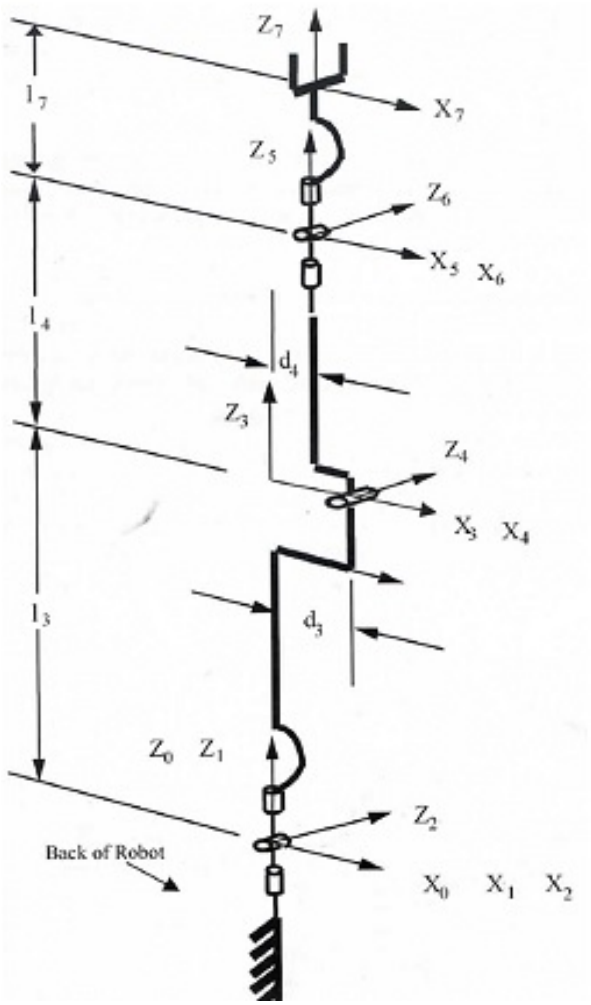

Figure 3.2: Coordinate Frames of WAM

issues when the arm is at some particular configuration and lose the capability to move in certain directions. When a robotic arm is in a singular configuration, it may have a sudden motion that completely hampers the kinesthetic feedback or even causes a safety threat.

To demonstrate this argument, the geometric inverse kinematics method explained in Appendix C.1 is used; joint three is locked to turn WAM into an anthropomorphic robotic arm. Since WAM has a spherical wrist, its Jocabian matrix is can be written as:

$$J(\theta) = \begin{pmatrix} J_{11} & 0 \\ J_{12} & J_{22} \end{pmatrix} \tag{3.8}$$

Where J_{11} is the linear velocity matrix, J_{22} is the wrist angular velocity matrix and J_{12} is the arm angular velocity matrix. The upper right corner of the matrix is zero because the spherical wrist joints do not have any effect on the linear velocity of the robot.

$$J_{22} = R(\theta_1, \theta_2, \theta_3, \theta_4) \begin{pmatrix} 0 & -s_5 & c_5 s_6 \\ -1 & 0 & -c_6 \\ 0 & c_5 & s_5 s_6 \end{pmatrix} \tag{3.9}$$

Where $R(\theta_1, \theta_2, \theta_3, \theta_4)$ is the transformation can be found in Appendix. C.1. Take the determinant of Eq. 3.9

$$|J_{22}| = |R(\theta_1, \theta_2, \theta_3, \theta_4)| \times |-\sin(\theta_6)| \tag{3.10}$$

$$= -\sin(\theta_6) \tag{3.11}$$

This simplification is possible because $R(\theta_1, \theta_2, \theta_3, \theta_4)$ is a rotational matrix and its determinant is 1. From Eq. 3.11, we can see that the wrist singularity happens when joint six is zero and axis five and seven are parallel to each other; therefore it is important to keep joint six away from zero. The results from simulation, as shown in Fig. 3.3 demonstrate the effect of singularity; those sharp turns show that there is dramatic change in the slave robot at joints five and seven.

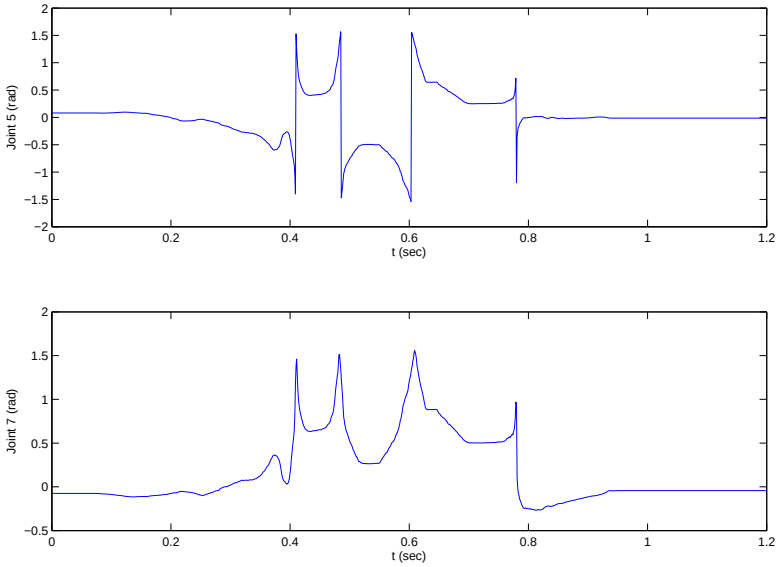

Figure 3.3: Wrist Singularity of An Anthropomorphic Arm
The sharp turns at 0.4, 0.5, 0.6 and 0.8 are all caused by the wrist singularity.

3.3.2 Redundant Robot

When computing the inverse kinematics of a robotic arm, if the manipulator has more degrees of freedom than the constraints, then there is redundancy in the system. For example, a three dimensional space only requires six independent coordinates to fully define the configuration (position, orientation) of the end-effector, and if the manipulator has seven joints, then it has (7-6)=1 degree of redundancy. This mapping is defined by.

$$U : x \in Re^6 \rightarrow \theta \in Re^7 \tag{3.12}$$

This means that an infinite set of robot joint angles can bring exactly the same end-effector configuration. This can provide the controller with extra flexibility to achieve extra performance indicators, for example, response speed, stability region, load capacity and so on. In our project, the redundancy is used to avoid singularities.

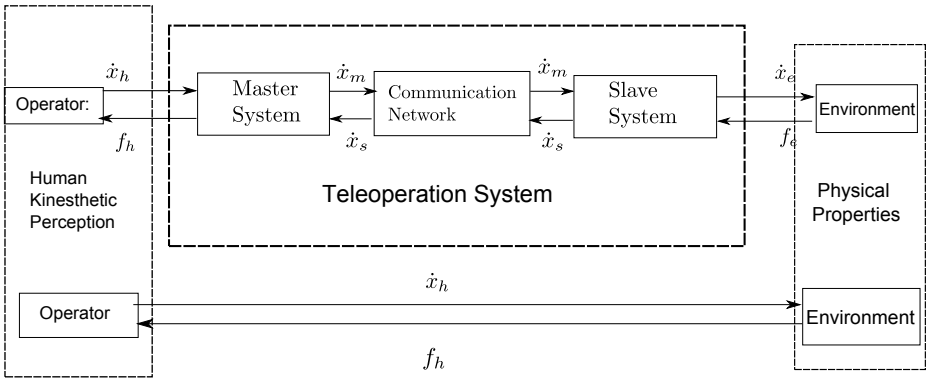

Figure 3.4: Haptics Exploration (Top-Bilateral Teleoperaton; Bottom-Direct)

There are several types of singularity for robots. In our experiment, due to the specific workspace of the arm, the elbow and base pitch joint stay significantly away from their singular positions. Therefore, the only singularity issue we have to consider is the wrist joint singularity. This type of singularity occurs when a pitching joint goes to a zero angle, making the two neighboring rolling joints align with each other and hence losing one degree of freedom. Since our robot has only one more degree of freedom than required, the redundancy can be resolved by imposing one extra constraint. The detailed equations can be found in Appendix C.2.

3.4 Kinesthetic Perception with Teleoperation Systems

3.4.1 Performance

Simple PD controllers result in poor haptics feedback. The manipulator inertia gets reflected to the operator, which completely hampers the kinesthetic perception. This is because the manipulators are usually at least three to four times heavier than the objects in their end-effectors. The operator experiences a lot of force feedback caused by the manipulatorâĂŹs weight rather than the interaction force between the environment and the manipulator. The force feedback of a teleoperation system can

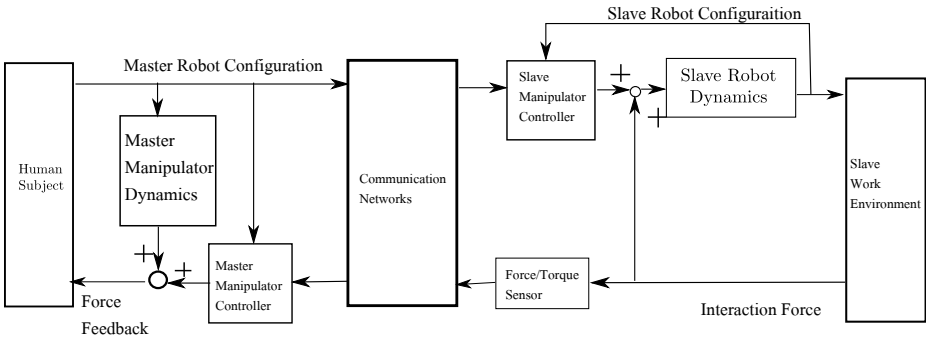

Figure 3.5: Model for Human Kinesthetic Perception with Bilateral Teleoperation Systems

be modeled as in Fig. 3.5. Therefore the force feedback can be computed using Eq. 3.13. The first term represents the dynamics of the master robot. Operators need to provide the force to manipulate it to generate the desired position for the slave robot; therefore that force is added on top of the system force feedback. The second term is the force feedback from the direct force measurement from the slave robot. Since the signal is usually noisy, as defined in Eq. 3.14, the signal is filtered using a first order low pass filter. The third and fourth terms show the PID controllers to enforce the position tracking, where x_s and v_s stand for the master robot configuration, and x_d, v_d stands for the slave robot configuration. This equation shows only one degree of freedom force feedback. All 6 DOF share the same type of force/torque feedback.

$$\begin{aligned} F_{\text{error}} =& (Ms^2 + bs)x_s + G + \frac{1}{1+\tau s}\tilde{F}_{ext} \\ &+ k_p(x_s - x_d) + k_d(v_s - v_d) - F_{ext} \end{aligned} \tag{3.13}$$

$$\tilde{F}_{ext} = F_{ext} + e_f \tag{3.14}$$

The goal of our control is to minimize this force error. There are three parameters that we can change: τ as the cutoff frequency of the first order low pass filter, k_p,the proportional gain and k_d, the derivative gain. Previous research shows that human motion usually has a frequency lower than 5Hz, so τ is picked so that all components greater than 5Hz are eliminated. Given the force capability given by the haptic device,

we keep the k_p and k_d to make room for the F_{ext}, because that is what the operator needs to feel.

3.5 Design of An Innovative 6 DOF Master Controller

The kinesthetic teleoeperation exploration tasks we proposed require 6 DOF force and torque feedback. Our current Omni only has 3 DOF force feedback. Also, its pen shaped handle is not very commonly used in teleoperation tasks. Therefore, we designed and built an innovative master controller.

Our master controller is integrated from four off-the-shelf haptic devices. The Phantom haptics device is the most widely used commercially available haptic device. It provides 3 DOF force feedback to the operator. It has 6 joints, of which the first three joints are actuated and the last three joints are passive. We integrated them into a 6 DOF force feedback haptic device and manufactured a handle with 3D printing technology.

The challenge of our work is that the system we build has actuation and kinematic redundancy. All Phantom Omnis devices return position information of their end-effectors; the system needs to compute the handles' position and orientation based on this information. This includes coordinate transformation and vector computation. The force feedback from the devices also needs to be coordinated to ensure precision while minimizing the total load of the system.

The advantages of our system include: low cost, greater force/torque feedback, more degrees of freedom in feedback and better position resolution. One Phantom Omni costs $1500. So the total cost of our systemâĂŹs hardware is less than $6100, which is very affordable. The force feedback provided by the new system is the summation of four individual Omnis together, so the maximum force feedback is four times the original device's. Also, the devices are configured in such a way that torque

feedback can be provided to the operator, which is critical in many applications. For example, in a case in which an operator is teleoperating a robot with an impact wrench as its end-effector, the resistive torque provided to the operator can provide him/her with ample information. Details are discussed in Sec. 5.2.1.

However there are also some limitations to the proposed master controller. First, since this manipulator is based on haptic devices, its workspace is limited to that of the original devices. Second, the maximum force feedback is limited by the force capacity of the original devices. Last but not least, the new device only provides kinesthetic feedback and lacks a tactile sensation component.

3.6 Stability Analysis

Stability is one of the most important factors in the design of a control system. Here we prove that our system is stable using the Lyapunov theory and Hilbert network; this method is very similar to [3].

3.6.1 Hilbert Network

The Hilbert network is a model that can transform a mechanical system into an electrical system that is easier to analyze. It is made up of four types of passive circuit elements: inertia, damping, stiffness and transfer. These elements correspond to similar components on the mechanical engineering side. An inertia component can be modeled as an inductor, where

$$f_i = \frac{d}{dt}(M_i v_i) \tag{3.15}$$

The damping components can be viewed as a resistor, where

$$f_i = B_i v_i \tag{3.16}$$

The stiffness component is where potential energy is stored, and therefore is equivalent to the capacitive element, where

$$f_i = K_i x_i \tag{3.17}$$

3.6.2 Teleoperation System Stability

The stability is proved by applying the Hilbert network properties to the Lyapunove function of the teleoperation system. Define x_m and x_s as the composite stiffness position vector for the master and slave manipulator. In the actual PD controller, they are the position errors between the master and the slave systems. Define the v_m and v_s as the master and slave system velocity. Define k_p and k_f as the position and force scaling factor. Define the following function as the Lyapunove function of the teleoperation system:

$$L(x,v) = \frac{1}{2}k_p k_f(||x_m||^2_{km} + ||v_m||^2_{mm}) + \frac{1}{2}(||x_s||_{ks} + ||v_s||_{ms}) \tag{3.18}$$

Take its derivative:

$$\dot{L}(x,v) = k_p k_f(< x_m, v_m >_{km} + < v_m, \dot{v}_m >_{mm}) + (< x_s, v_s >_{ks} + < v_s, \dot{v}_s >_{ms}) \tag{3.19}$$

$$= k_p k_f(< f_m, v_m >_{km} + < v_m, f_m >_{mm}) + (< f_s, v_s >_{ks} + < v_s, f_s >_{ms}) \tag{3.20}$$

Applying Property 1

$$\dot{L}(x,v) = k_p k_f(< f_{bm}, v_{bm} >_{bm} + < v_m, f_m >_{mm}) + (< f_{bs}, v_{bs} >_{bs} + < v_s, f_s >_{ms}) \tag{3.21}$$

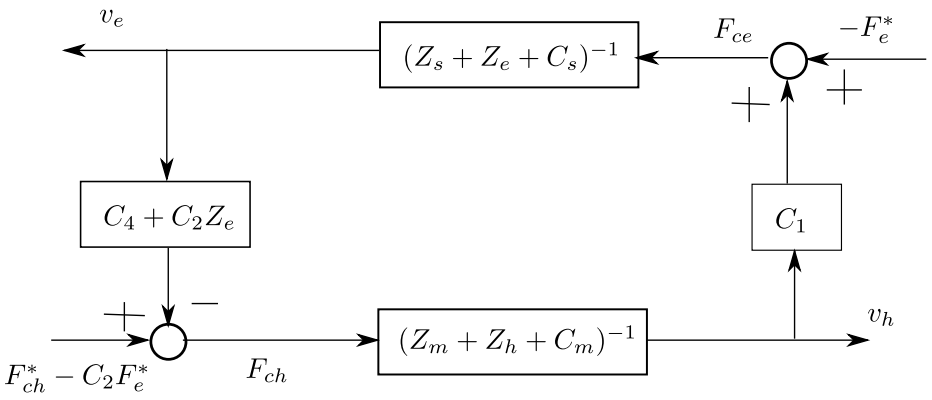

Figure 3.6: Single loop representation of the general teleoperator system[29]

Apply the definition of position and velocity,

$$\dot{L}(x, v) = -k_p k_f < f_{bm}, v_{bm} >_{bm} - < f_{bs}, v_{bs} >_{bs} \leq 0 \tag{3.22}$$

Therefore, the system is passive.

3.6.3 Stability of the System for Three-Channel Controller

In order to analyze the stability of a teleoperation system with three communication channels (Two velocity and one force/torque), the four-channel architecture proposed by Dr. Lawrence needs to be transformed into Fig. 3.6. This figure is adopted from [29], the only difference is that we didn't use the force/torque feedforward channel from master to slave, so C_3 in the original diagram is eliminated.

$$F_{ce} = (Z_s + Z_e + C_s)V_e \tag{3.23}$$

$$= -F_e^* + C_1 V_h \tag{3.24}$$

$$F_{ch} = (Z_m + Z_h + C_m)V_h \tag{3.25}$$

$$= -C_2 F_e^* + F_h^* - (C_4 + C_2 Z_e)V_e \tag{3.26}$$

Denote:

$$S_1 = (C_4 + C_2 Z_e)(Z_s + Z_e + C_s)^{-1}(C_1 - C_3 Z_h) \tag{3.27}$$

$$S_2 = (Z_m + Z_h + C_m)^{-1} \tag{3.28}$$

According to theorem 1 of [29], the sufficient condition to ensure the system stability is:

a) S_1 is a strictly positive real transfer function (exponentially stable, and $S_1(j\omega) + S_1^T(-j\omega)$ uniformly positive definite over all frequencies ω).

b)S_2 is a strictly positive real transfer function ($S_1(j\omega) + S_1^T(-j\omega)$ positive semi-definite over all frequencies ω).

c) The transfer functions $(C_4 + C_2 Z_e)(Z_s + Z_e + C_2)^{-1}$,$Z_s + Z_e + C_s)^{-1}$, and $(C_1 - C_3 Z_h)(Z_m + Z_e + C_m)^{-1}$ are stable.

In our system, we don't use the force/torque measurement and feedback from master to slave, so C_3 is zero for both PD and the three-channel controllers. For the PD case, there is no force/torque signal send from the slave to master, so

$$C_2 = 0 \tag{3.29}$$

So the S_1 becomes

$$S_1 = C_4(Z_s + Z_e + C_s)^{-1} C_1 Z_h \tag{3.30}$$

and S_2 is the same as in Eq. 3.28. The S_1 is obviously strictly proper, because

$$C_1 = K_d^1 + \frac{K_p^1}{s} \tag{3.31}$$

$$C_4 = K_d^4 + \frac{K_p^4}{s} \tag{3.32}$$

The C_1 and C_4 are the controllers for velocity signals, so Eq. 3.31 and Eq. 3.32 are PD controllers for position signals. Therefore, S_1 is

$$(K_d^4 + \frac{K_p^4}{s})\frac{1}{Z_s + Z_e + C_s}(K_d^1 + \frac{K_p^1}{s})Z_h \tag{3.33}$$

Z_s, Z_e are both second order component, and C_s is a first order component. Therefore S_1 is positive real.

For the three-channel controller case, the C_2 channel is added, which is the force/torque feedback from slave to master and it is equal to the force scaling coefficient.

$$C_2 = K_f \tag{3.34}$$

So,

$$S_1 = (K_f Z_e + C_4)(K_d^4 + \frac{K_p^4}{s})\frac{1}{Z_s + Z_e + C_s}(K_d^1 + \frac{K_p^1}{s})Z_h \tag{3.35}$$

Therefore, as we can see S_1 is still strictly proper because the Z_e is the impedance of the objects, which is a second order system. The denominator still have higher order than the numerator, but their order difference reduced. In other words, the stability of Eq. 3.33 is better than Eq. 3.35.

Chapter 4

Fundamental Contributions

Bilateral coupling between the master and the slave manipulators provides kinesthetic feedback to the human operator. The operator then takes proper action based on the feedback he/she receives. Providing accurate kinesthetic feedback is therefore important. The ideal kinesthetic feedback occurs when the system provides a force feedback that is exactly the same as in the interaction between the environment and the slave robot. This means the fundamental goal of designing a robot controller is to provide feedback that is as close to the ideal case as possible. Therefore, the fundamental contributions of this dissertation can be summarized into the following three points:

4.1 Improved Force Tracking to Improve Kinesthetic Feedback

Position to position control architecture has been used by many 6 DOF teleoperation systems. It can enforce position tracking but compromises the kinesthetic feedback. A three channel controller is developed and implemented on a 6 DOF teleoperation system to improve force tracking. An additional wrist force/torque sensor is used to

generate feedback to the master robot. The performance of our system supports our hypothesis.

4.2 Developed Wrist Singularities Avoidance Algorithm to Improve Kinesthetic Feedback

A redundant manipulator provides the control engineers with extra flexibility. This advantage has been used in singularity avoidance, collision avoidance and control effort optimization. In this project, we developed a singularity avoidance algorithm for the wrist. This algorithm is completely geometrical; every intermediate step has specific physical meanings. It is also minimizes computation as compared to the psudo-inverse of the Jacobian matrix.

4.3 Developed An Innovative Master Manipulator for the Teleoperation Systems

The kinesthetic perception we studied requires 6 DOF force and torque feedback to the operator. We developed an innovative manipulator that functions as the master of the system and provides the necessary feedback to the operators.

4.4 Developed An Experimental Framework for Studying the Efficacy of Kinesthetics Feedback in Haptics Exploration

Any experiments using human subjects require a standard experimental protocol to ensure that the results are general and objective. We developed an experimental framework that enabled us to investigate the relative weight, center of gravity

and inertia between the objects. The system setup, examiner's behavior during the experiments and the testing objects were all regularized. The experimental protocol also enabled us to compare the direct contact and the teleoperation haptics exploration performances.

Chapter 5

System TestBed

5.1 System Overview

The previously described research methodology was tested on a bilateral teleoperation system. This chapter begins with the hardware set up of the experimental teleoperation system. Computers are used as controllers to the manipulators. An Ethernet is setup as the communication network. The systemâĂŹs software is also covered in this chapter.

5.2 Hardware

The teleoperation system used in this project is a bilateral teleoperation system with one master and one slave manipulator. Its structure is shown in Fig. 5.1. The master manipulator consists of four haptic devices and can provide 6 DOF force feedback to the operator. High performance computers ensure the computation power for both the control loop and the graphic interface. The phantoms are connected in a cascade style on a Firewire network. The two Firewire ports on the master control computer are used. The master control computer is connected to an Ethernet switch through an Ethernet cable. The slave manipulator computer, with a real time Linux operating system, is connected to the same switch. The CAN bus port on the slave

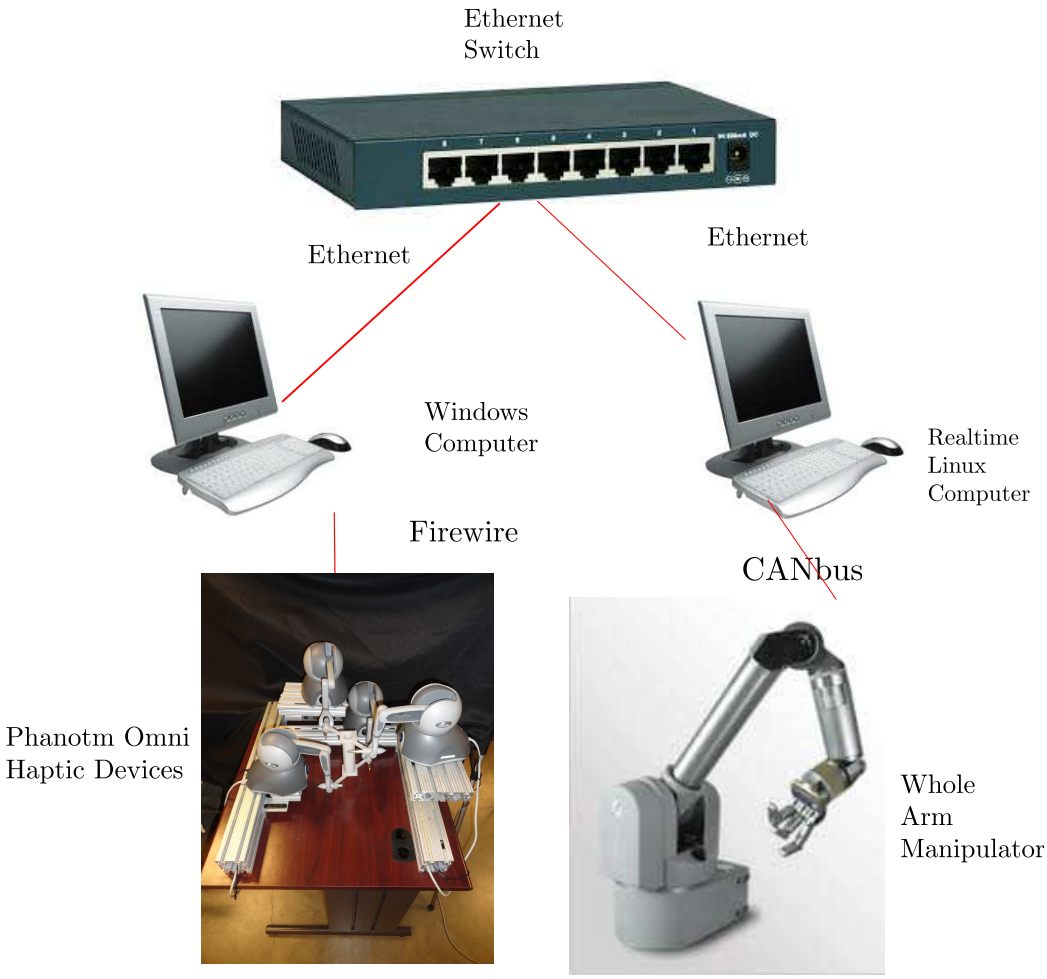

Figure 5.1: Hardware Schematics

manipulator computer is used to connect the WAM manipulator, the remote or "slave" manipulator.

5.2.1 Master Manipulator

Phantom Omnis, designed by Sensable Inc., have been used as the master robots in many research projects [45]. They have low inertia [7], low friction, high position and force reflection resolution [46], all of which are important merits for a master robot. They are very transparent, since the low inertia makes them easy to manipulate and there is very low gravitational force even without gravity compensation. Also, they

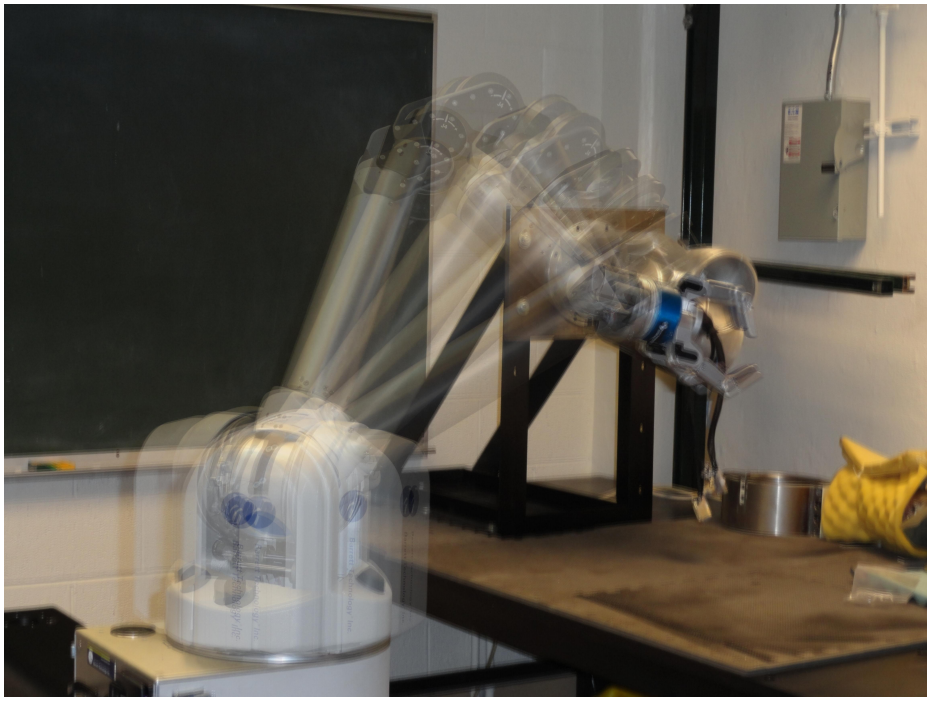

Figure 5.2: Illustration of Redundancy of WAM

have a universal connection, which enables a fast update rate. They can measure 6 DOF (three rotational and three translational) motion and provide 3 DOF force feedback. In the system testbed, four of them are combined together to form a master controller that can provide 6 DOF force feedback.

System Design and Kinematics In this section, the general design of the proposed controller is presented. Its mechanism and capacity are discussed.

Mechanism Four Phantom Omni devices were used in our system as shown in Fig. 5.3. All of them were fixed onto the 80/20 aluminum frame with fasteners that are not shown in the figure. The original handles on the Omnis were removed. A new "integrating" handle we built was attached to the end links. The Omnis are electronically connected in cascade style using Firewire. Two Omnis are used in each cascade, so there are two cascades in total. According to the manual, each cascade

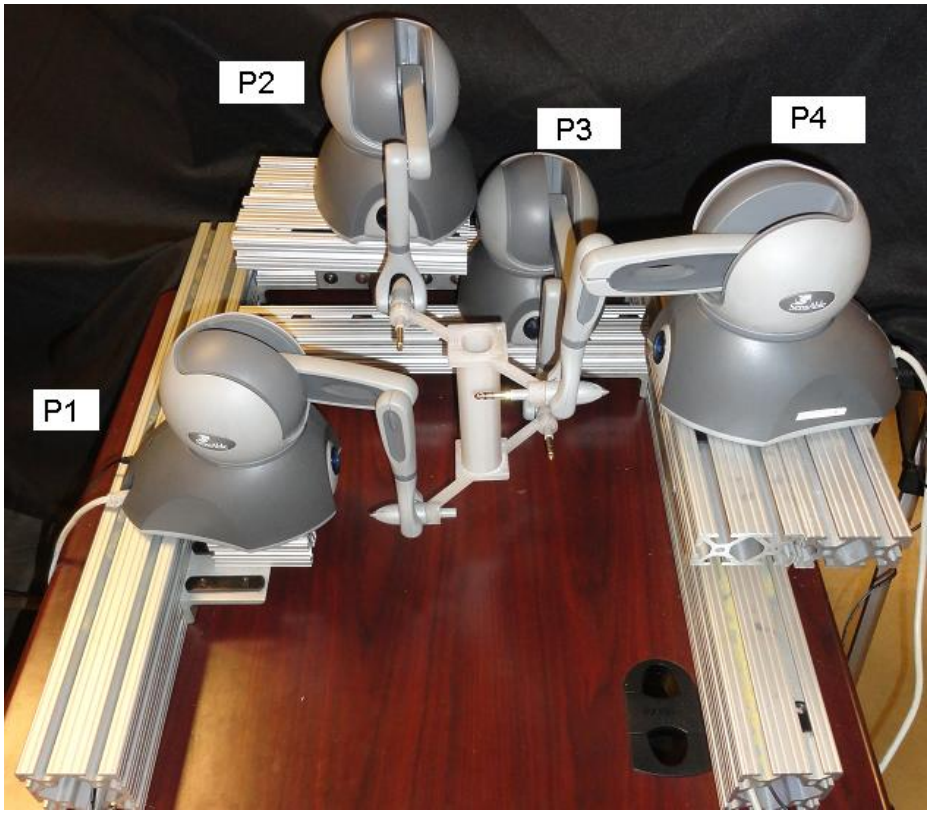

Figure 5.3: Innovative Master Manipulator

can have a maximum of 20 haptic devices, so the amount of devices we used was far below the capacity and therefore the update rate would not be affected.

Range of Motion and Force Capacity The haptic devices are placed to maximize the range of motion of the new master controller. The range of motion of the Phantom Omni is 6.4"× 4.8" × 2.8" (160 × 120 × 70mm) [49]. The definition of the coordinate system for an Omni is shown in Fig. 5.4. If the new device travels along the vertical axis, all the Omnis reach their maximum and minimum Y-axis values simultaneously, so the range of motion on the Y-axis is the same as on the original Omni specifications. As shown in Fig. 5.3, two Omni devices, P1 and P4, were placed sideways to the other two. The range of motion on the horizontal plane is limited by the Z-axis motion of P1 and P4. Therefore, the range of motion of the new system is smaller than the Phantom Omni: 2.8'× 4.8' × 2.8' (70 × 120

Figure 5.4: World Coordinate of An Phantom Omni

× 70mm). When in the center of the workspace, the rotational range of motion of the new system is the same as the original Phantom Omni. However, it should be noted that when close to the boundary of the workspace, significant rotational range of motion was lost.

The maximum exertable force of a Phantom Omni is 0.75 lbf (3.3 N)[49]. The maximum force feedback that can be offered by the proposed system is the sum of the force feedback from the four Omnis, and therefore 3 lbf (13.2 N).

Handle The handle of the new system was designed to connect the four Omnis together. It has four holes which fit tightly with each haptic device. In order to reduce its weight, the handle is hollow. The light weight is essential because the gravity of haptic devices is added on top of the force feedback provided by the active joints. Any extra weight hampers kinesthetic perception. 3-D printing has shown great potential in new equipment prototyping. The flexibility of 3-D printing has brought about significant gains in engineering. Parts created in this way are lightweight and comparatively sturdy. The handle was printed using a Stratsys Fortus 250mc 3D printer.

Kinematics The general control architecture of the proposed device is shown in Fig. 5.5. The purpose of this section is to present the solution for the "Kinematic coordinate transformation" and "Kinematic" block of that figure.

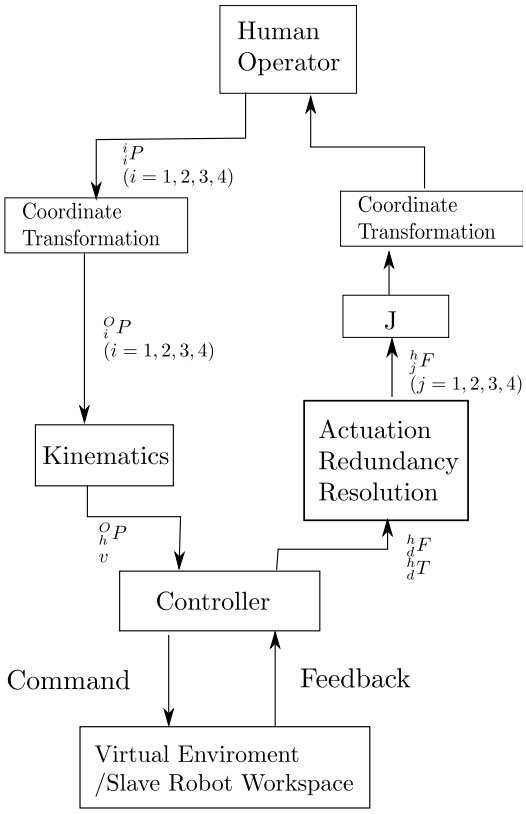

Figure 5.5: Control System of the Novel 6 DOF Haptic Device

Kinematics of Phantom Omni Each Omni can measure the position of its end link with respect to its own world frame. We use that as the position of the corner of the handle, O_1, O_2, O_3 and O_4. Each of the coordinates corresponds to one Omni in Fig. 5.3; all four Omni's needed to be transformed into the common world frame first according to Eq. 5.1 and Eq. 5.2.

$$ {}^{O}_{1}P = {}^{o}_{1}R^{1}_{1}P \qquad {}^{O}_{2}P = {}^{o}_{2}R^{2}_{2}P \tag{5.1} $$

$$ {}^{O}_{3}P = {}^{o}_{3}R^{3}_{3}P \qquad {}^{O}_{4}P = {}^{o}_{4}R^{4}_{4}P \tag{5.2} $$

Since the Omnis are rigidly attached to the aluminum frame, all the coordinate transformation terms in Eq. 5.5 are constant homogeneous transformations.

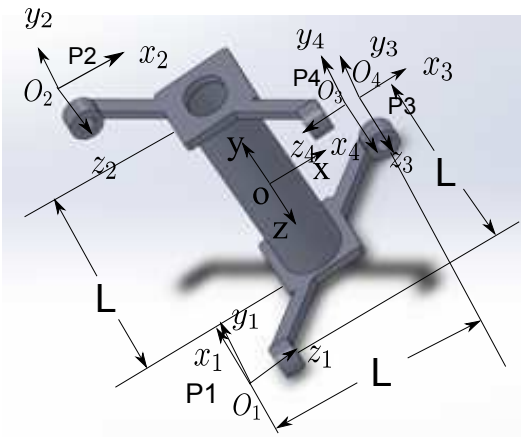

Figure 5.6: Coordinate of the Handle, All of Them Are Fixed with the Handle

$$
{}^{o}_{1}R = \begin{bmatrix} 0 & 0 & 1 & -\frac{L}{2} \\ 0 & 1 & 0 & -\frac{L}{2} \\ -1 & 0 & 0 & \frac{L}{2} \\ 0 & 0 & 0 & 1 \end{bmatrix} \quad {}^{o}_{2}R = \begin{bmatrix} 1 & 0 & 0 & -\frac{L}{2} \\ 0 & 1 & 0 & \frac{L}{2} \\ 0 & 0 & 1 & -\frac{L}{2} \\ 0 & 0 & 0 & 1 \end{bmatrix} \tag{5.3}
$$

$$
{}^{o}_{3}R = \begin{bmatrix} 1 & 0 & 0 & \frac{L}{2} \\ 0 & 1 & 0 & -\frac{L}{2} \\ 0 & 0 & 1 & -\frac{L}{2} \\ 0 & 0 & 0 & 1 \end{bmatrix} \quad {}^{o}_{4}R = \begin{bmatrix} 0 & 0 & -1 & \frac{L}{2} \\ 0 & 1 & 0 & \frac{L}{2} \\ 1 & 0 & 0 & \frac{L}{2} \\ 0 & 0 & 0 & 1 \end{bmatrix} \tag{5.4}
$$

The position and orientation of the handle with respect to the center of the home position can be determined using Eq. 5.5. This summation and average process also reduces the position error [55].

$$
{}^{o}_{h}P = \frac{1}{4}({}^{1}_{1}P + {}^{2}_{2}P + {}^{3}_{3}P + {}^{4}_{4}P) \tag{5.5}
$$

Where ${}^{i}_{i}P$'s are the positions of each Omni given in their own frame, and ${}^{o}_{i}R$'s are the coordinate transformation between their world frames and the common world frame. Their values are shown in Eqs. 5.3 and 5.4.

Kinematics The orientation of the controller is derived using Eqs. 5.7, 5.8 and 5.9. All the position data (p_{1-4}) are in the common world coordinate. Therefore, only the position data from each Omni is used to derive the orientation of the handle. Those position data are derived from the waist, shoulder and elbow joint angles. Thus the singularity problem that usually happens at the last three passive joints is avoided. Denote:

$$v = [v_x, v_y, v_z] \tag{5.6}$$

Then,

$$v_x = v_y \times v_z \tag{5.7}$$

$$v_y = \frac{({}^{O}_{4}P - {}^{O}_{2}P) \times ({}^{O}_{3}P - {}^{O}_{1}P)}{||({}^{O}_{4}P - {}^{O}_{2}P) \times ({}^{O}_{3}P - {}^{O}_{1}P)||_2} \tag{5.8}$$

$$v_z = \frac{({}^{O}_{3}P - {}^{O}_{2}P) \times ({}^{O}_{4}P - {}^{O}_{1}P)}{||({}^{O}_{3}P - {}^{O}_{2}P) \times ({}^{O}_{4}P - {}^{O}_{1}P)||_2} \tag{5.9}$$

The results of Eq. 5.7, 5.8 and 5.9 are the three unit vectors along the handle coordinate system with respect to the common world frame.

Force Feedback This section addresses the "Actuation Redundancy Resolution" in Fig. 5.5. The actuation redundancy issue is formulated into a convex optimization problem and a solution is provided.

Force Coordinate Transformation When computing the command force for each device, the desired force and torque is first represented in the frame located at the center of the handle, as shown in Fig. 5.6; the rest of the coordinates represent the force each Omni exerted on the handle. The reason why we selected this coordinate frame is that the leverage for each force exerted on the handle would be constant based on the chosen coordinate frame. This simplifies the optimization

of the distribution of the load. After the optimization process, the computed force vector will be transformed into world frames of each haptic device respectively.

Actuation Redundancy The four haptic devices have three actuated joints each. Therefore, there are twelve DOF of actuation in the system, but the force/torque feedback requires only 6 degrees of freedom.

This actuation redundancy allocation problem is formulated as an optimization problem. The objective function is the squared sum of the torque applied on each joint. The justification for this objective function is that the torques are proportional to the current for each motor, and therefore to the power consumption of the haptic device. Minimizing the sum of the torques is the same as minimizing the force feedback of the whole control system. The constraints, as shown from Eq. 5.10 to Eq. 5.15, for this optimization problem are the desired torque and force feedback to the operator.

Desired Force Feedback The desired force and torque at the new handle are given by the following equations. The subscripts stand for the index of haptic devices, the superscripts stand for the axis of the corresponding device. The terms from Eq. 5.10 to Eq. 5.15 are defined in the free body diagram of the handle, Fig. 5.6.

$$ {}^{h}_{d}F^{x} = {}^{h}_{1}F^{z} + {}^{h}_{2}F^{x} + {}^{h}_{3}F^{x} - {}^{h}_{4}F^{z} \tag{5.10} $$

$$ {}^{h}_{d}F^{y} = {}^{h}_{1}F^{y} + {}^{h}_{2}F^{y} + {}^{h}_{3}F^{y} + {}^{h}_{4}F^{y} \tag{5.11} $$

$$ {}^{h}_{d}F^{z} = -{}^{h}_{1}F^{x} + {}^{h}_{2}F^{z} + {}^{h}_{3}F^{z} + {}^{h}_{4}F^{x} \tag{5.12} $$

$$ \begin{aligned} {}^{h}_{d}T^{x} = & \frac{L}{2}({}^{h}_{1}F^{x} - {}^{h}_{1}F^{y}) + \frac{L}{2}({}^{h}_{2}F^{y} + {}^{h}_{2}F^{z}) \\ & + \frac{L}{2}({}^{h}_{3}F^{y} - {}^{h}_{3}F^{z}) + \frac{L}{2}({}^{h}_{4}F^{x} - {}^{h}_{4}F^{y}) \end{aligned} \tag{5.13} $$

$$
\begin{aligned}
{}^{h}_{d}T^{y} =& \frac{L}{2}(-{}^{h}_{1}F^{x} + {}^{h}_{1}F^{z}) + \frac{L}{2}(-{}^{h}_{2}F^{x} + {}^{h}_{2}F^{z}) \\
&+ \frac{L}{2}(-{}^{h}_{3}F^{x} - {}^{h}_{3}F^{z}) + \frac{L}{2}(-{}^{h}_{4}F^{x} - {}^{h}_{4}F^{z})
\end{aligned} \tag{5.14}
$$

$$
\begin{aligned}
{}^{h}_{d}T^{z} =& \frac{L}{2}(-{}^{h}_{2}F^{y} + {}^{h}_{3}F^{z}) + \frac{L}{2}(-{}^{h}_{2}F^{x} - {}^{h}_{2}F^{y}) \\
&+ \frac{L}{2}(+{}^{h}_{3}F^{x} + {}^{h}_{3}F^{y}) + \frac{L}{2}({}^{h}_{4}F^{y} + {}^{h}_{4}F^{z})
\end{aligned} \tag{5.15}
$$

Each of the four Phantoms provides 3 DOF force feedback, so the number of unknowns here is twelve. There are a total of six constraints on them, from Eq. 5.10 to Eq. 5.15. Motors in the haptic devices provide the force feedback, and forces are proportional to the currents passing through the motors. In order to minimize the power consumption of the system, we proposed the following objective function:

$$
\min \Sigma_{i=1}^{4}(({}^{h}_{i}F^{x})^{2} + ({}^{h}_{i}F^{y})^{2} + ({}^{h}_{i}F^{z})^{2}) = \frac{1}{2}F^{T}PF \tag{5.16}
$$

where

$$
\begin{aligned}
F =& [{}^{h}_{1}F^{x}, {}^{h}_{1}F^{y}, {}^{h}_{1}F^{z}, {}^{h}_{2}F^{x}, {}^{h}_{2}F^{y}, {}^{h}_{2}F^{z}, \\
& {}^{h}_{3}F^{x}, {}^{h}_{3}F^{y}, {}^{h}_{3}F^{z}, {}^{h}_{4}F^{x}, {}^{h}_{4}F^{y}, {}^{h}_{4}F^{z}]^{T}
\end{aligned} \tag{5.17}
$$

This function is the sum of the squares of the norm of the force feedback vectors provided by the four Omnis.

$$
P = \begin{bmatrix}
2 & 0 & 0 & 0 & 0 & 0 \\
0 & 2 & 0 & 0 & 0 & 0 \\
0 & 0 & 2 & 0 & 0 & 0 \\
0 & 0 & 0 & 2 & 0 & 0 \\
0 & 0 & 0 & 0 & 2 & 0 \\
0 & 0 & 0 & 0 & 0 & 2
\end{bmatrix}
$$

$$J = \begin{bmatrix} 0 & 0 & 1 & 1 & 0 & 0 & 1 & 0 & 0 & 0 & 0 & -1 \\ 0 & 1 & 0 & 0 & 1 & 0 & 0 & 1 & 0 & 0 & 1 & 0 \\ -1 & 0 & 0 & 0 & 0 & 1 & 0 & 0 & 1 & 1 & 0 & 0 \\ -\frac{L}{2} & -\frac{L}{2} & 0 & 0 & \frac{L}{2} & -\frac{L}{2} & 0 & \frac{L}{2} & -\frac{L}{2} & \frac{L}{2} & -\frac{L}{2} & 0 \\ -\frac{L}{2} & 0 & \frac{L}{2} & -\frac{L}{2} & 0 & \frac{L}{2} & -\frac{L}{2} & 0 & -\frac{L}{2} & -\frac{L}{2} & 0 & \frac{L}{2} \\ 0 & -\frac{L}{2} & -\frac{L}{2} & \frac{L}{2} & -\frac{L}{2} & 0 & -\frac{L}{2} & \frac{L}{2} & 0 & 0 & \frac{L}{2} & -\frac{L}{2} \end{bmatrix} \tag{5.20}$$

Putting Eq. 5.10 through Eq. 5.15 into matrix form and denoting:

$$b = [{}^h_d F^x, {}^h_d F^y, {}^h_d F^z, {}^h_d T^x, {}^h_d T^y, {}^h_d T^z]^T \tag{5.18}$$

we can get Eq. 5.19, where J is shown in Eq. 5.20. This matrix is the Jacobian matrix of the system. Since the output of each Omni is force, and the output of our new system is force and torque, the first three lines of the matrix are unitless, and the remaining three lines have the dimension of length.

$$JF = b \tag{5.19}$$

After deriving F, all the force components have to be transformed into the form with respect to the ground frame of the Omnis.

$${}^i_i F = {}^i_h R^h_i F \quad i = 1, 2, 3, 4 \tag{5.21}$$

where ${}^i_h R$ represents the transformation matrix between the handle frame and the ground frames.

Convex Optimization Methods

We applied the "Karush-Kuhn-Tucker"(KKT) condition to solve the optimization problem. The generalized KKT condition for

$$\text{minimize } f_0(x) \tag{5.22}$$

$$\text{subject to } f_i(x) \leq 0, i = 1, \ldots, m \tag{5.23}$$

$$h_i(x) \leq 0, i = 1, \ldots, p \tag{5.24}$$

is

$$\begin{aligned} f_i(x*) &\leq 0,\ i = 1, \ldots, m \\ h_i(x*) &= 0,\ i = 1, \ldots, p \\ \lambda_i^* &\geq 0,\ i = 1, \ldots, m \\ \lambda_i^* f_i(x*) &= 0,\ i = 1, \ldots, m \\ \bigtriangledown f_0(x*) + \Sigma_{i=1}^m \lambda *_i \bigtriangledown f_i(x*) + \Sigma_{i=1}^p v_i * \bigtriangledown h_i(x*) &= 0 \end{aligned} \tag{5.25}$$

Where on the condition that the objective function $f_0(x)$, inequality constraint functions $f_i(x*)$ and equality constraint functions $h_i(x*)$ are all differentiable. If the objective function is quadratic, all the equality constraints are linear and there are no inequality constraints, the problem can be simplified into:

$$\text{minimize } \frac{1}{2} x^T P x + q^T x + r \tag{5.26}$$

$$\text{subject to } Ax = b \tag{5.27}$$

The KKT condition is simplified into

$$Ax* = b \tag{5.28}$$

$$Px* + q + A^T v* = 0 \tag{5.29}$$

Eq. 5.26 and Eq. 5.27 are exact matches to our problem; therefore, Eq. 5.28 and Eq. 5.29 are the answers to our optimization algorithm. Given the objective function in Eq. 5.16, and linear equality constraints in Eq. 5.19, then applying the KKT condition [5], we have Eq. 5.30.

$$\begin{bmatrix} P & J^T \\ J & 0 \end{bmatrix} \begin{bmatrix} F^* \\ v^* \end{bmatrix} = \begin{bmatrix} -q \\ b \end{bmatrix} \tag{5.30}$$

The matrix on the left side of Eq. 5.30 is invertible by inspection, so the optimal value can be found by directly taking the matrix inverse. Since this is a constant matrix, matrix inversion doesn't have to be processed for every iteration. It can be computed offline and stored in the computerâĂŹs memory.

$$v^* = -2(JJ^T)^{-1}b \tag{5.31}$$

$$F^* = J^T(JJ^T)^{-1}b \tag{5.32}$$

Where F^* is the optimal solution for the haptic devicesâĂŹ desired force defined in Eq. 5.17 and v^* is the optimal value of the dual problem [5].

5.2.2 Slave Manipulator

The slave robot used is the WAM. It is widely known that a manipulator requires six joints to go to an arbitrary position and orientation in its workspace. WAM has seven joints, which means it is a redundant robot; its kinematics are given in Appendix B. The redundancy is shown in Fig 5.7, where several WAM pictures are superimposed together. All of the different configurations take the end-effector to the same position and orientation. This redundancy can be used to avoid singularities, collisions or joint limits. Every joint of WAM is powered by an electric motor. They are controlled by a compact controller called the "puck." Each puck has temperature, torque and position sensors. All of the "puck" are connected in parallel on a CANbus$^{\text{TM}}$(Controller

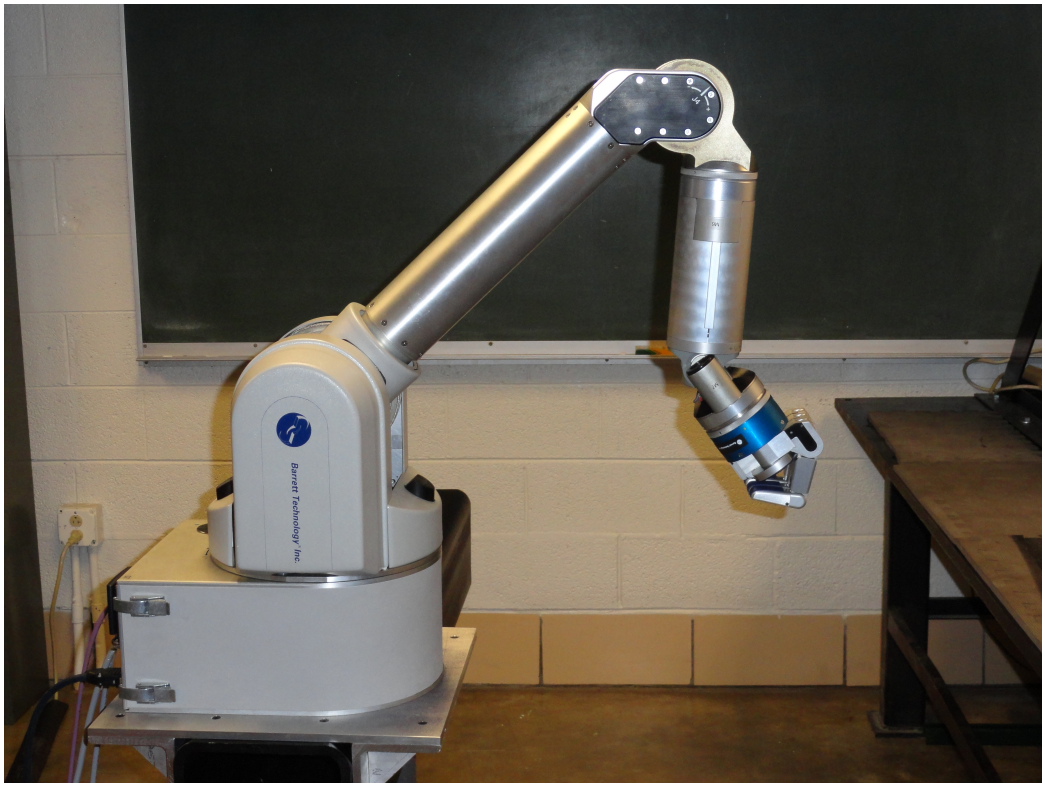

Figure 5.7: Whole Arm Manipulator (WAM)

Area Network). The robot can be controlled in two ways: internal and external modes. During internal mode, the computer inside the base of the robot is used. A wireless router on the robot base gives off wireless signals. Any computer with wifi connection capability can connect to it and control it. In external mode, the internal computer relinquishes its control to an external computer that is connected to the CANbus^{TM}connector on the back of the robot. It can be controlled in position mode or torque mode. Position mode is mostly used in supervisory control when it is easy to implement safety measures that can constraints the maximum velocity and position. In torque control mode, the controller can send direct torque commands to each joint through CANbus^{TM}. This offers greater flexibility to the controller.

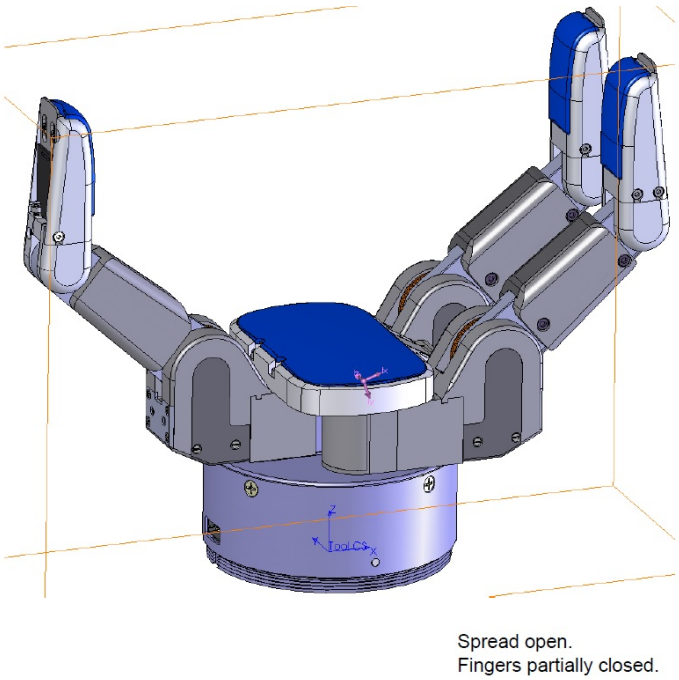

Figure 5.8: Barrett Hand

5.2.3 End-Effector

The end effector used in this project is a three finger robotic hand made by Barrett Technology. The robotic hand is controlled by four pucks. Each finger is controlled by one puck; the fourth one controls the spread motion of the fingers. Every finger has two joints, and in free space, the bottom joint is activated and the top joint is locked. When the bottom link applies pressure on the object that it is grasping, a locking mechanism activates the top joint and locks the bottom joint. There are tactile sensors on every finger and on the palm of the hand. A 1 DOF finger torque sensor is also installed on every finger. In this project, those sensors are not used.

5.2.4 Force Torque Sensor

A force torque sensor is installed between the end-effector and the WAM. This sensor can provide 3 DOF force and 3 DOF torque measurement. The data provided by this sensor is the force/torque applied on the hand by the arm. There are two

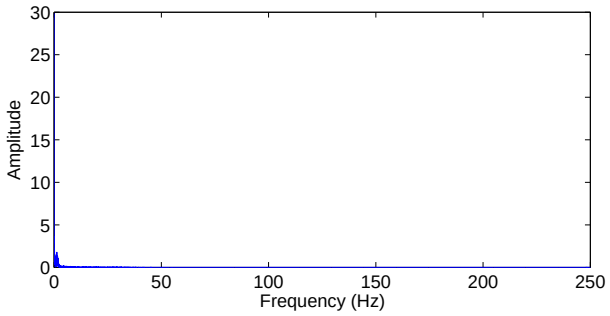

Figure 5.9: The Frequency Spectrum of the Force Torque Sensor Data

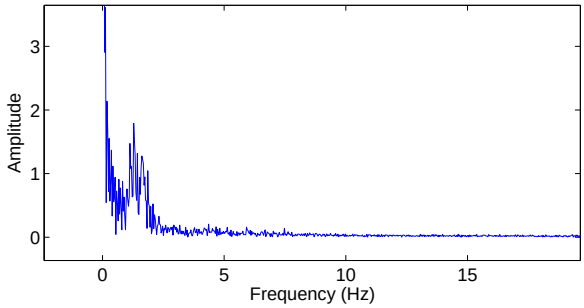

Figure 5.10: Zoom-In View of the Frequency Spectrum of the Force Torque Sensor Data

portions of this force: the force that moves the hand around and the force that moves the object around. Therefore, when sending this force as a signal back to the operator, the hand portion data should be subtracted. So before every experiment, there will be a calibration process where there would be no object in the hand and the controller remembers the sensor reading as the "hand force"; then this "hand force" will be subtracted from later sensor readings to derive the force associated with the object. This sensor is strain gauge based and therefore sensitive to temperature, so it is necessary to perform calibration before every experiment. Also, the sensor data includes high frequency noise that is eliminated using a low pass filter, as is shown in Fig. 5.9 and Fig. 5.10.

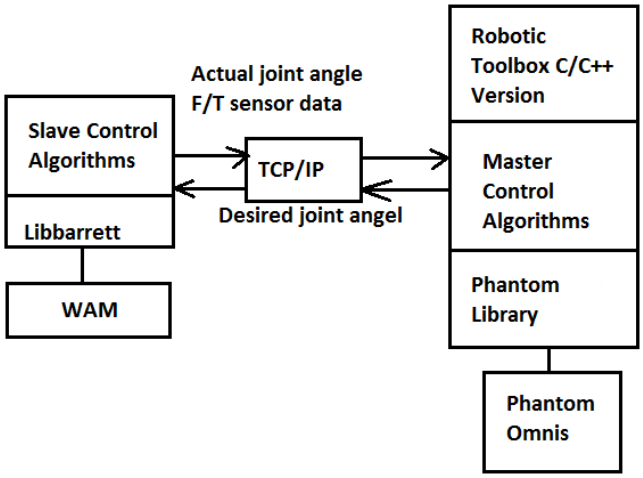

Figure 5.11: Experiment Software Schematics

5.2.5 Ethernet Switch

An intranet is set up between the master and slave control computer. Communication protocol is a commonly used internet protocol. A sixteen port Ethernet switch is used as the central hub. Static IP addresses are assigned to the computers. The number of ports available at the Ethernet switch makes the system very flexible for future expansions. The size of the Ethernet packet from the master to the slave is 28 bytes and the size of the package from slave to master is 56 bytes. The system has an update rate of 500 Hz; therefore, the total data transmission rate is:

$$(28 + 56) \times 500 = 336kbps \tag{5.33}$$

a lot lower than the 100mpbs maximum transfer rate of the switch. Therefore, the information currently transferred on this network is relatively small compared to the hardware capability.

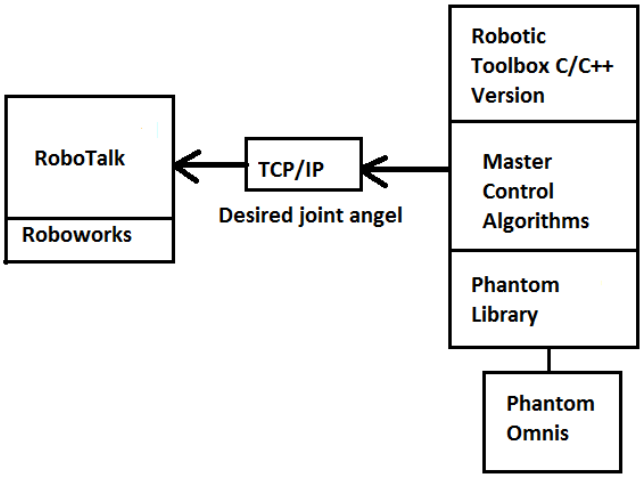

Figure 5.12: Simulation Software Schematics

5.3 Software

Various types of software are used in this project. Simulation software such as MATALB^{TM}and Roboworks^{TM}are used to test the algorithms before application to the robot in order to ensure safety and to visualize the algorithm's performance. Visual Studio 2005 is the main programming software. RoboTalk^{TM}is an interface library that communicates between the visual studio and Roboworks^{TM}. Phantom software and Libbarrett^{TM}, provided by the hardware manufacturers, function as the interface between WAM and a Linux computer. The general software architectures are shown in Fig. 5.12 and Fig. 5.11.

5.3.1 MATLAB^{TM}and Robot Toolbox

MATLAB^{TM}is a commonly used computation software with various toolboxes developed by users to expand its capabilities. Dr. Corke developed a robotics simulation tool box decades ago [11]. After being upgraded for more than two decades, the current version is applicable to our application. It provides most of the forward kinematic and conventional D-H modeling functions required for robotics research.

A plot function is also included to visualize the configuration of the robot. Both kinematics and dynamics of the robotics can be simulated. Also, there is a C/C++ version of this toolbox that can be imported into Visual Studio.

5.3.2 RoboWorks™and RoboTalk™

RoboWorks™and RoboTalk™are two robotic simulation software packages developed by Newtonium [42]. The lower arm with four joints was built by a former member of our lab and is available for download from Newtonium's company website. The three wrist joints were built from the Solidworks™model provided by Barrett. RoboWork™allows visualization of the robot in an animated graphic dialog; engineers can input the configuration in a window and see the pose of the robot. RoboTalk™provides an interface between the RoboWorks™and other software packages. It can interact with other programs through TCP/IP protocol. Another program can send configuration data to RoboWorks™to simulate the robot under control. The purpose of using this type of simulation is to ensure the safety of our equipment. Any algorithm has to be tested on the simulation before use with the actual robot system. One limitation for RoboWorks™and RoboTalk™is that the graphical interface requires significant computation power, which may slow down the overall update rate.

5.3.3 Microsoft™Visual Studio

Visual Studio (VS) is the main programming software for the master controller. The master controller is based on an example program provided by Sensable™. That program controls two Phantom Omni devices simultaneously. We used the 2005 version of VS. Although, there are newer versions which provide many new features, the 2005 version is the most compatible with the Phantom examples. The library files of all other software packages are imported into VS. After importing the library files, the functions predefined for the RoboTalk™and the Phantom devices can be used.

C/C++ is used as the programming language. TCP/IP is used as the interfacing protocol between the master and the slave robot.

5.3.4 Phantom Configuration and Phantom Test

Sensable™, the manufacture of the Phantom, provided these two software packages. The Phantom Configuration reads the serial numbers from the devices connected to the computer and assigns names to them. Those names are used in the computer codes written in VS. Phantom Test provides several simple testing programs that help diagnose the hardware status. It also helps the programmer get familiar with the devices and identifies the coordinates of the devices. Sensable™also provides library files for C/C++ programs and several example codes for their product.

5.3.5 Libbarrett™

The Libbarrett™file contains the control software for WAM. There are twelve example programs in the Libbarrett™folder. All of them are provided as source code and must be compiled into executable before testing. The first example is the process of turning on and off the WAM and is always a good starting point for any type of programming. Functions for various operations can be seen in the source files.

Our program is based on example one. Codes about TCP/IP protocol and robot motion control are added to the original code. Several configuration files are also modified.

A very good trouble shooting command is "btutil." It can list all the available pucks on the current CAN bus. If the computer reports a problem with any of the pucks, Barrett should be contacted for repair.

Chapter 6

Experimental Assessments

To verify the efficacy of the control architecture and the system setup, several experiments are developed here. First, two experiments are carried out to test the experimentâĂŹs testbed capability and reliability. The first one is the evaluative experiment for the 6 DOF master manipulator; its workspace and force/torque feedback capabilities are explored. The master manipulator is also tested in both haptics and teleoperation applications. Then the kinematics of the redundant slave manipulator are studied; a wrist singularity avoidance algorithm is applied.

After testing the system testbed, we conducted the kinesthetic exploration experiments. The next three experiments have a similar protocol, but investigated different kinesthesia factors: weight, center of gravity and inertia distribution. These properties are closely related to kinesthetic feedback and force reflection. During experiments for each kinesthesia factor, a direct contact haptic perception experiment is carried out as a comparison group. This experiment provides the ideal case result for the haptic exploration task in a teleoperator scenario. This is because the ideal feedback in a teleoperation system should be able to mimic the exact motion and force interaction in the slave workspace, as if the operator is interacting with the remote space directly. Then the new controller is used through teleoperation to perform the same tasks. Lastly, a PD control architecture is provided as another control group.

The system testbed discussed in the previous chapter is the overall experimental platform.

6.1 Evaluation of the Innovative Master Manipulator with Six Degree of Freedom Force/Torque Feedback

In this experiment, the master controller system, consisting of four haptic devices, is tested. Results show the reliability of the novel system. First, the system is manipulated by an operator mimicking a normal haptics exploration scenario to test its kinematics algorithms. Then a static virtual wall is used to test the force feedback capability. Since the master manipulator would be in direct contact with operators, its stability is crucial for the safety of the operators.

6.1.1 Kinematics Evaluation

The kinematics algorithm proposed is evaluated in this experiment. The position and orientation of the master controller is generated based on the position information of the four Omnis. The computational capability of our computer is high enough to maintain a 1 kHz update rate when communicating with all four Omnis in every iteration. During this experiment, the operator attempted to test the workspace boundaries, first in linear motion along the three axes, then in rotational motion around the three axes.

Discussion

The data showed that the new system we built achieved the proposed workspace. All four Phantoms are in their own workspace during the process. Although one particular Phantom may be in its wrist singularity position at its workspace limit,

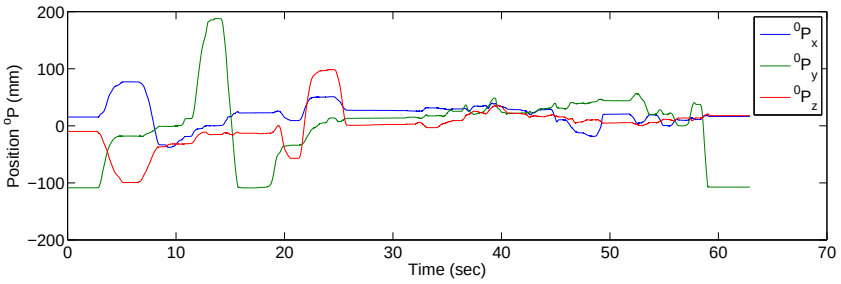

Figure 6.1: Position of the Master Controller

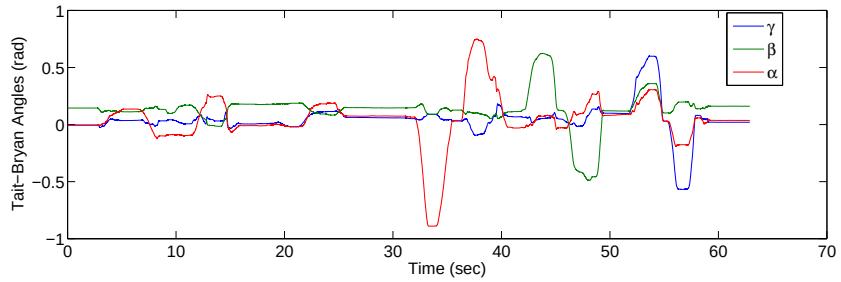

Figure 6.2: Orientation of the Master Controller

the system configuration is still stable due to the fact that we used only the Phantoms' position information to determine the master system configuration. The master system orientation is determined by the relative positions of the Phantoms. When computing the system position, all four PhantomsâĂŹ positions are used; this makes the data more accurate in that the process of taking the average helps reduce the random noise from the encoders.

In the first half of the experiment, the manipulator translated in its workspace, first along the x axis, then the y axis, then the z axis, while the four Phantoms moved accordingly, as is shown in Fig. 6.1 and 6.2. The second and third Phantoms, as shown in Fig. 6.4 and 6.5, have their coordinate systems paralleled to that of the manipulator system; therefore, their position curves are very similar to 6.1 during the first half of the experiment. In the second half of the experiment, the manipulator rotated around the x, y and z axes, respectively. The angles α, β and γ were defined

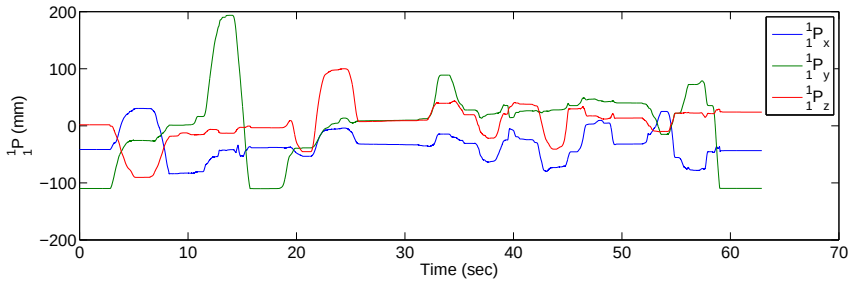

Figure 6.3: Position of Phantom Omni No. 1

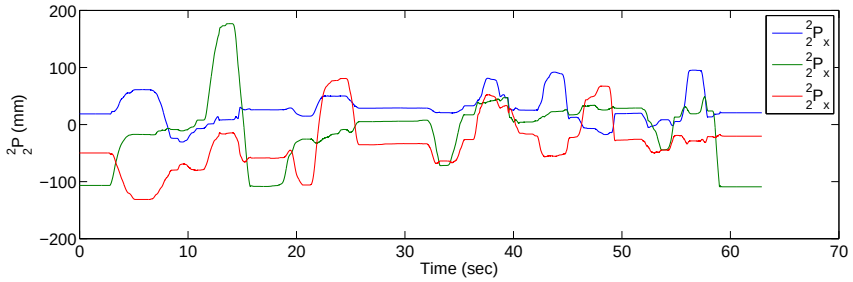

Figure 6.4: Position of Phantom Omni No. 2

according to Appendix E. The rotational angles were able to achieve the proposed specifications.

6.1.2 Haptics Experiment

A virtual wall with a stiffness of 300N/m and a rotational stiffness of 50Nm/rad was established. The system is able to interact with this flexible wall in a virtual environment (VE).

The virtual wall passes through the origin and is perpendicular to the z axis. Its force and torque feedback functions are defined in Eqs. 6.1 and 6.2. The desired joint position is computed using the kinematics of the new system, and the figure shows that the singularity problem is avoided because of the method we used. The force collaboration between the Omnis is shown in Fig. 6.7 and Fig. 6.8. All of them are

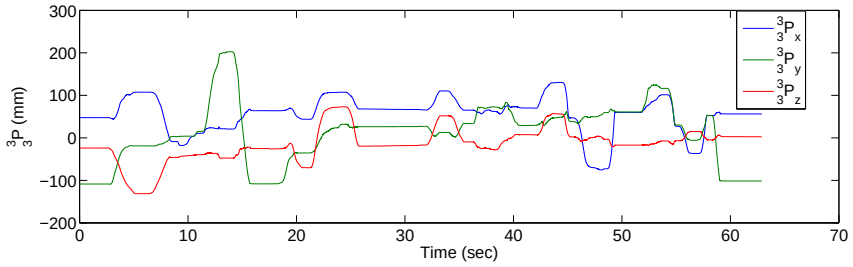

Figure 6.5: Position of Phantom Omni No. 3

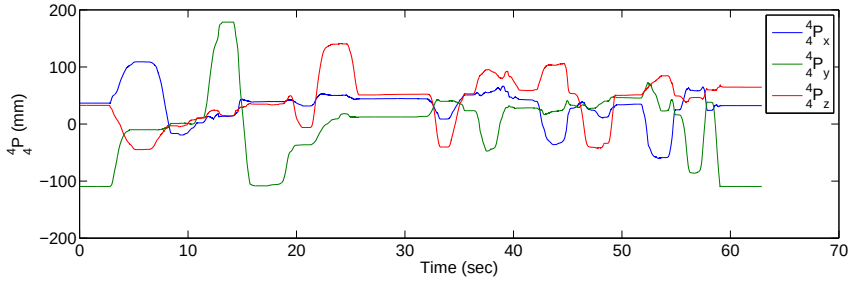

Figure 6.6: Position of Phantom Omni No. 4

shown in the end-effector frame of the Omnis.

$$F = \begin{cases} k_p({}^{O}_{h}P - P_o) & z > 0 \\ 0 & z < 0 \end{cases} \tag{6.1}$$

$$\tau = \begin{cases} k_t({}^{O}_{h}\theta - \theta_o) & z > 0 \\ 0 & z < 0 \end{cases} \tag{6.2}$$

Where P_o is the point where the haptic device enters the virtual wall in VE, θ_o is the orientation of the device when it enters the virtual wall. k_t and k_p are the wall's translational and rotational stiffness, respectively. The dynamics of the virtual wall is simulated using a passive integrator proposed in [32].

When the master manipulator enters the wall, a resistant force is created that pushes the manipulator back to its point of entry. Also, the rotational resistant force pushes the manipulator toward its original orientation when it enters the virtual wall.

This type of modeling is widely accepted in haptics research because it can emulate typical interactions between objects. A large stiffness coefficient is suitable for a more rigid material while a small stiffness coefficient corresponds to a more flexible object. During the process, an operator may push the limit of the force capability, first in translational motion and then in rotational motion.

Disucussion

The force and torque applied by the manipulator during the interaction with the virtual wall is shown in Fig. 6.7 and 6.8. In the first half of the experiment, the manipulator translated inside the virtual wall to test its force feedback capability. Then it was rotated around its point of entry to generate a torque feedback; as shown in Fig. 6.8. From Fig. 6.9 to Fig. 6.12, we can see the four Phantoms worked collectively to generate the desired force and torque. For example, between 30 and 35 seconds, torque along the y axis is applied. For all the Phantoms, force along their negative x and negative z axis is applied accordingly. The force is multiplied with leverage, in this case the distance between the pressure point and the center of the handle, to derive the equivalent torque. The operator was able to feel a resistant force/torque against the relative motion between the master manipulator and the virtual wall simulated.

We also developed a graphic rendering of the virtual wall. As shown in Fig. 6.14, the red sphere represents the position of the master device in the virtual environment as it interacts with the deformable virtual wall.

6.1.3 Teleoperation Experiment

Experiment Setup

In this experiment, the omni-based system we developed is used as the master robot in a teleoperation system. The WAM was used as the slave robot as shown in Fig. 5.1. Two computers are used as the master and slave controllers. The master controller

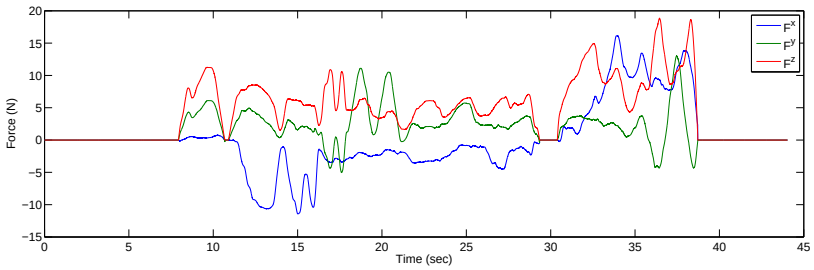

Figure 6.7: Force Applied by the Device

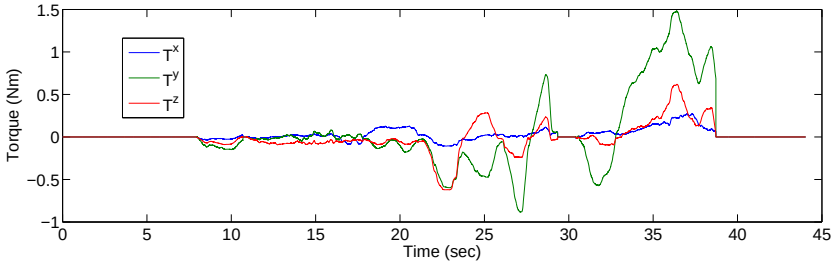

Figure 6.8: Torque Applied by the Device

is connected to the master robot through Firewire cable, and the slave controller is connected to the slave robot through Control Area Network (CAN) bus. The position, orientation and force information is transmitted between the computers through the Ethernet. 2-Channel controllers are used to enforce position and force tracking [41, 27, 56].

Experimental Results

The new master controller system shows great potential in the experiment. As in Fig. 6.13, the joint angles of the slave robot track the master robot well. The singularities of the Phantoms are successfully avoided due to our kinematics computation. The desired angles generated by the master manipulator are stable and smooth, making it possible for the slave manipulator to track them smoothly. The slave manipulator was able to track the master robot well because of its mechanism and controller design. The data from this experiment confirmed that the system was ready for the kinesthetic exploration experiments.

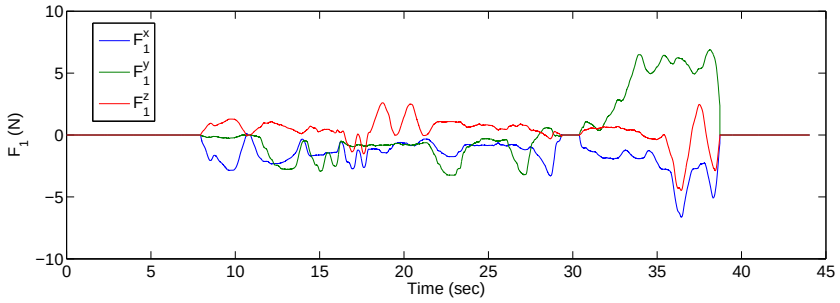

Figure 6.9: Force Applied by Phantom Omni No. 1

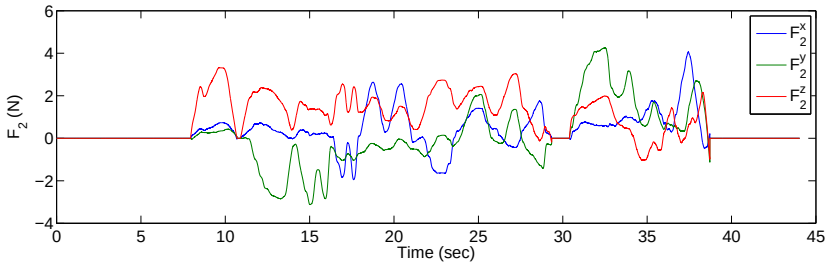

Figure 6.10: Force Applied by Phantom Omni No. 2

6.2 Kinematics of the Redundant Slave Robot

The purpose of this experiment is to test the efficacy of the wrist singularity avoidance algorithm. We focused on avoiding wrist singularity because the workspace of the following experiments is in the most dexterous space of the robot and, therefore, significantly eliminates the possibility of other singularities. The wrist singularity occurs when the determinant of its Jacobian Matrix equals zero.

$$\dot{x} = J(\theta)\dot{\theta} \tag{6.3}$$

$$J(\theta) = \begin{pmatrix} Z_0 \times (o_n - o_0) & \cdots & Z_{n-1} \times (o_n - o_{i-1}) \\ Z_0 & \cdots & Z_{n-1} \end{pmatrix} \tag{6.4}$$

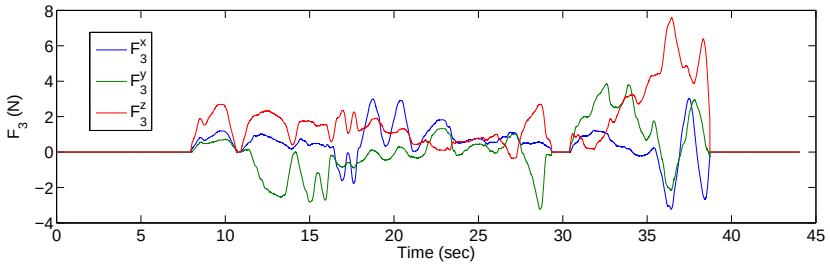

Figure 6.11: Force Applied by Phantom Omni No. 3

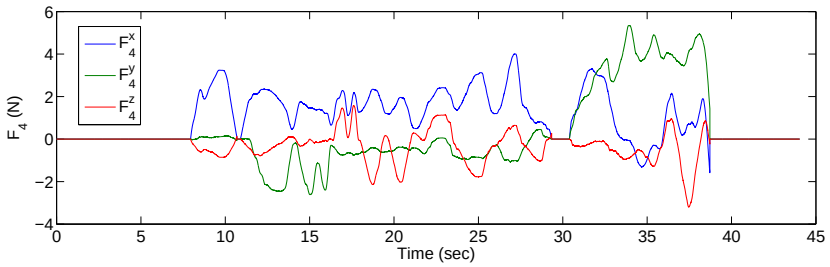

Figure 6.12: Force Applied by Phantom Omni No. 4

Applying the property of spherical wrist, the Jacobian matrix can be simplified into:

$$= \begin{pmatrix} J_{11} & 0 \\ J_{12} & J_{22} \end{pmatrix} \tag{6.5}$$

Taking its determinant, we have:

$$|J| = |J_{11}||J_{22}| \tag{6.6}$$

$$|J_{22}| = \sin(\theta_6) \tag{6.7}$$

Therefore, the wrist singularity happens when:

$$\theta_6 = 0 \tag{6.8}$$

What we designed is an intuitive algorithm, when θ_6 approaches 0, for example smaller than a constant threshold α, joint three is activated and provides a pivot motion that

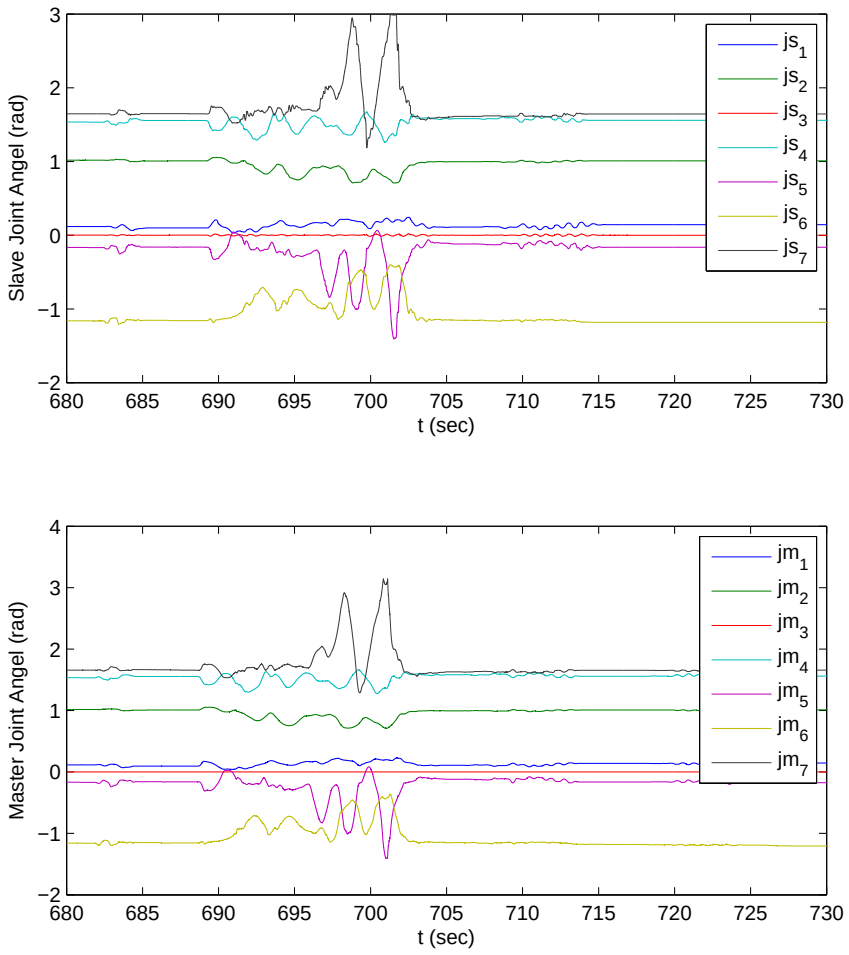

Figure 6.13: Position Tracking of the Teleoperation System

holds the wrist position, but places its orientation in a way where θ_6 is no longer zero, and the arm is ϕ degrees with respect to the original configuration. Also, the robot needs a smooth transition between the cases when the singularity avoidance is and is not activated, so we define:

$$\phi = \begin{cases} \phi = k_\phi(\theta_6 - \alpha), & \text{if} \quad \theta_6 \leq \alpha \\ 0, & \text{otherwise} \end{cases}$$

Therefore, when θ_6 enters the singularity zone, joint three will be activated smoothly; details can be found in Appendix. C.

6.2.1 Results and Discussion

We used RoboWorks to simulate the WAM manipulator as the slave manipulator. The reason why we did not use the real manipulator was that when close to the singularity configuration, the joint velocities can become large. The robot can have a brief but very violent motion, and then shutdown. This is because in order to generate a small velocity at the end effector space, a set of very large velocities in the joint space is required. This set of large velocities usually exceeds the maximum velocity allowed by the robot, and the control system shuts down operation as a safety measure.

The results of the singularity avoidance algorithm are shown in Fig. 6.15 and Fig. 6.16. In Fig. 6.15, the angle of joints five and seven change drastically when joint six approaches zero, and joint three stays constant at zero (it is shown as the red line), which mimics a singularity an anthropomorphic arm can encounter. In Fig. 6.16, joint three is activated when the robot approaches the wrist singularity, as shown by the red line; therefore, all of the joints travel smoothly. This singularity avoidance algorithm was essential to our application because most of the singularities we encountered were wrist singularities.

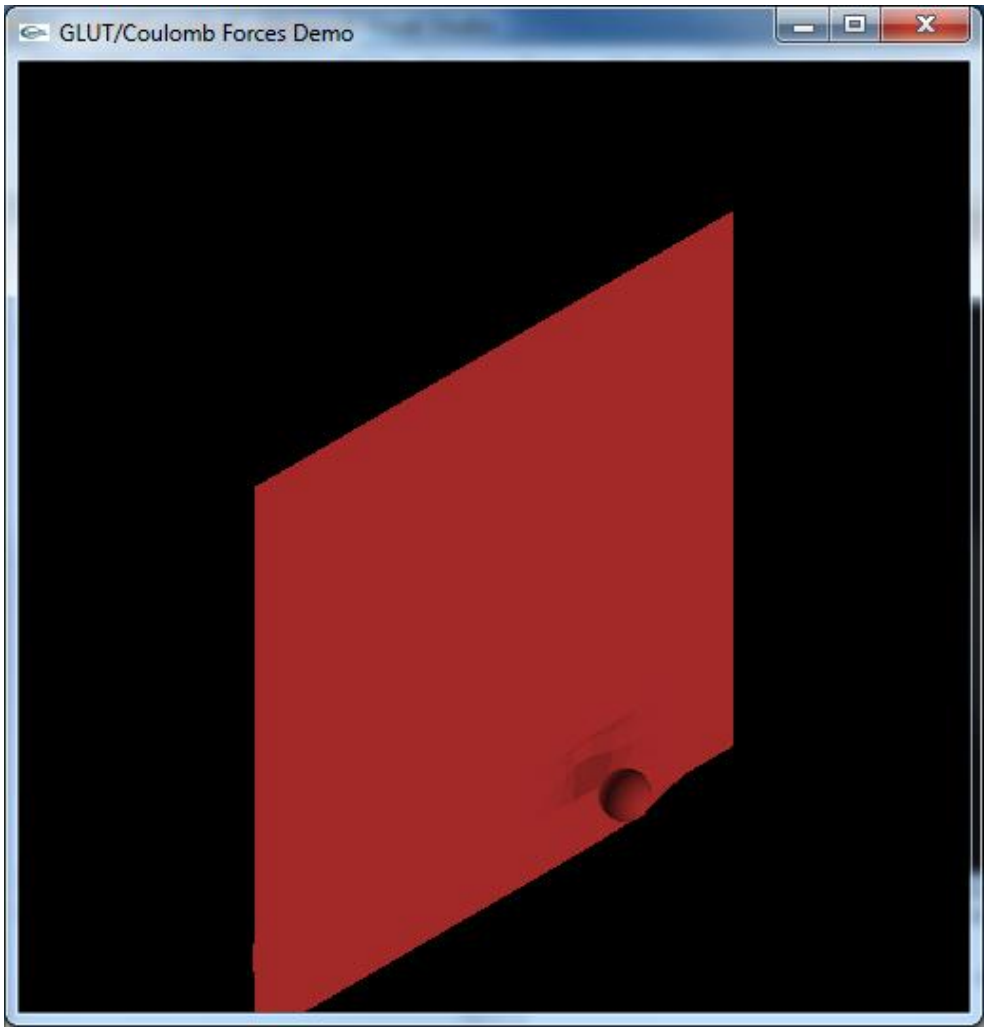

Figure 6.14: Haptics Application
The red sphere shows the position of the master controller in the virtual environment. The red rectangle shows the position of the deformable virtual wall. The cave on the wall is caused by the force exerted by the red sphere.

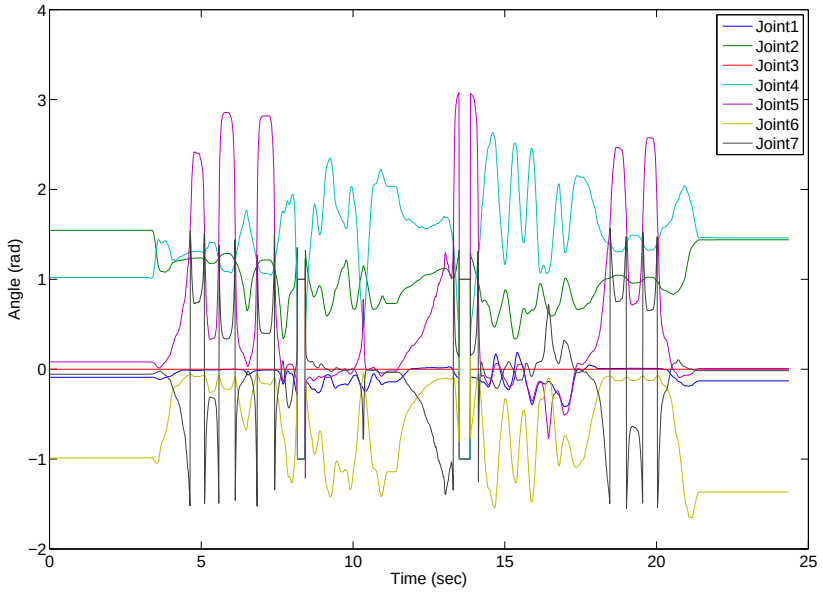

Figure 6.15: Joint Angles of WAM without Singularity Avoidance

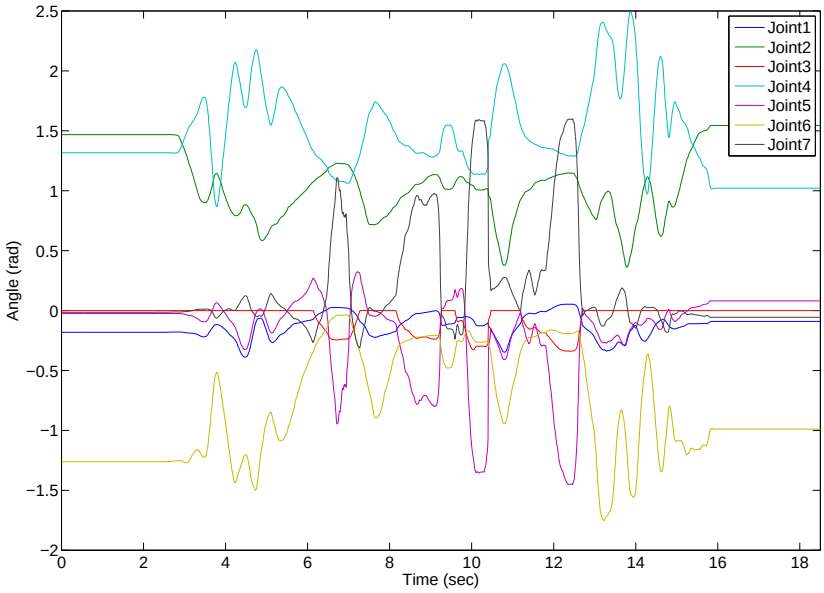

Figure 6.16: Joint Angles of WAM with Singularity Avoidance

6.3 Weight Perception

As mentioned in Chapter. 3, two sets of equations govern the motion of an object:

$$f_d = ma + mg \tag{6.9}$$

$$\tau_d = I\alpha + \omega^T I \times \omega + \tau_g(\theta) \tag{6.10}$$

In this experiment, the participants were asked to judge the weight of the object, which is the term m and I in Eq. 6.9 and Eq. 6.10. The other terms were kept constant.

6.3.1 Methods

The experiment presented here is the first one of a series of experiments. In this experiment, haptics exploration tasks were studied in both teleoperation and direct interactions. Weight perception was used as the kinesthetic exploration task. The operators interacted with test objects that look identical. They would answer questions about the weight of test objects. It took approximately half an hour for each subject to complete the experiments.

Design of the Test Objects

A test object used in the experiment is shown in Fig. 6.17. It is made up of three parts: the handle, the extra weight and the cardboard box around them. The handle is where the subject would grasp. On top of the handle, there is a piece of sheet aluminum. The purpose of the aluminum is to make it easier for the robot to grasp the test object. Every time the robot grasped the test object, the top piece was first placed onto the palm part of the hand, and then the robotic fingers are closed to provide gripping force. These combined mechanisms ensured a firm grasp. A threaded rod passed through a hole at the bottom of the handle and was bolted down

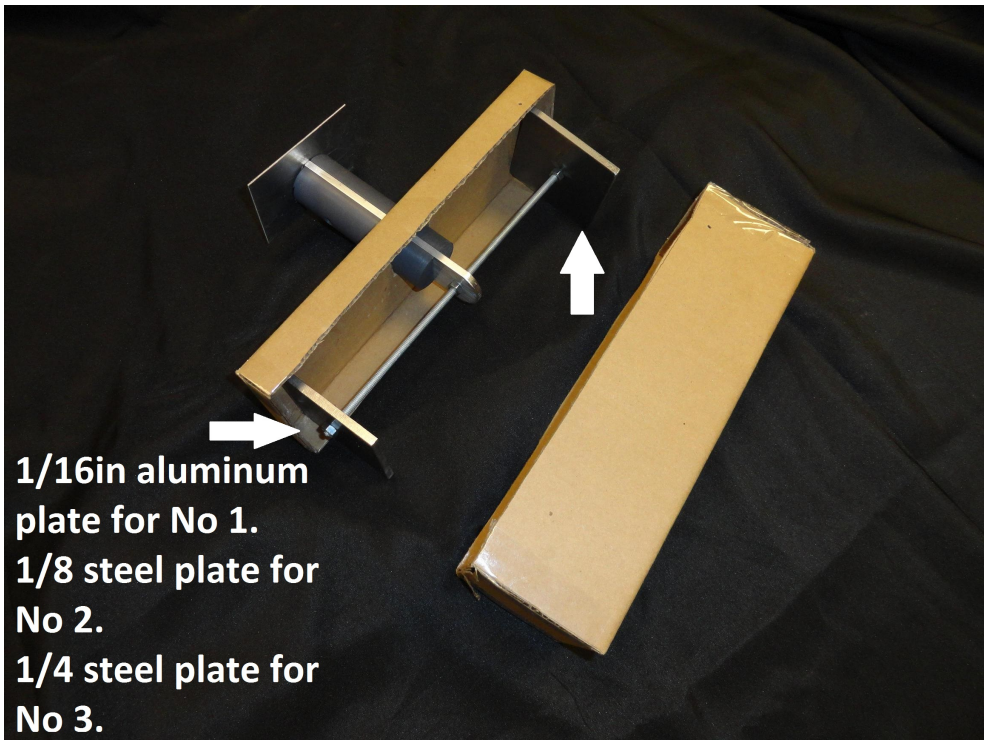

Figure 6.17: A Test object With the Cardboard Box Open

Table 6.1: Weight of the Test Objects

No.	Weight (W_a Unit:kg)	Normalized Weight (W_n)
1	0.6030	6.865
2	0.8774	9.987
3	1.2909	14.70
Comparison	0.8784 (W_c)	10.00

at its midpoint. The extra weights were fastened on the two ends of the threaded rod. Every test object had a cardboard box around it, and all the boxes had identical appearances. This is to ensure that the subjects could not receive any additional visual information about the weight of the object. Also, since the material of the handles was identical, there was no appreciable tactile sensing difference between the objects. The normalized weight is defined according to Eq. 6.11.

$$W_n = \frac{W_a}{W_c} \times 10 \tag{6.11}$$

Where W_a is the actual weight shown in the second column of Table 6.1. W_c is 0.8784 kg, the actual weight of the comparison objects, as shown in the last row, second column in Table 6.1. The purpose of this normalization is to eliminate bias from the subjectsâĂŹ previous experiences. It is easier and more meaningful to test the relative weight perception than the quantitative weight perception capability.

There were three testing methods used: direct contact haptics exploration, teleoperation haptics exploration with a two channel controller, and teleoperation haptics exploration with a three channel controller. In the direct contact exploration, the subjects manipulated the test objects directly using their dominant hand, so the force the participants experienced was exactly the amount of force needed to manipulate the objects. In the teleoperation experiments, the participants manipulated the objects through a teleoperation system shown in Fig. 5.1. In every section, three test objects were used, so for each participant there were nine trials in total.

The perception time was recorded as a performance index. In direct contact exploration tests, perception time was the interval from when the subject picked up the object until they laid down the object. In teleoperation exploration tests, the perception time was the time interval where the force feedback was enabled. The subjects were unaware that the time they spent was a type of data we were collecting, but before the experiment started, they were all informed that the process would be videotaped.

Procedure and Instructions

In the experiment, the participant was asked to come in and sit comfortably on the chair next to the table where the direct haptic exploration was going to take place. An introduction about the experiments was given to the participant by the examiner. Then the direct contact exploration experiment started. The subject was first given the comparison object to manipulate. They were told that the weight of this object was ten units and that they needed to remember this weight. The object was then

taken away from the participant and a test object was presented to them. They then picked up the test object and manipulated it before telling the examiner the weight of the test object. This process was repeated two more times for the other two test objects. Then the direct contact exploration experiment ended. The test objects were presented to the participants following a random sequence generated by a computer program.

Before the teleoperation kinesthetic tasks started, the subjects were given two minutes of recess while the examiner set up and initialized the robot. At the beginning of the three channel controller teleoperation exploration section, the subjects were given a brief introduction about the system. Then the experiment started. The experiments shared the same procedure as the direct contact experiments. They were given the comparison object every time before the test object to review.

After finishing the three channel control section, the robot went back to its home position. The participants were given a two minutes recess while the examiner made changes to the controller. Then the same procedure was carried out one more time using the two channel controller.

System Testbed

A 7 DOF WAM was used as the slave robot. An innovative 6 DOF master controller was used as the master robot. Its details are explained in Chapter 5.

One camera on the slave side was directly connected to a monitor on the master side to provide visual feedback for the subjects. A large piece of black cloth hanging between the slave robot and the master side prevented the subjects from seeing the slave side directly. This was to ensure that the subjects received visual feedback from the slave side only through the monitors to mimic an actual teleoperation scenario.

When we implemented the three channel controller, a new issue emerged. The force/torque sensor reading from the slave robot contained a high frequency noise. When it was reflected to the master controller, there was an audible, high pitch noise from the actuators of the master controller, so we implemented a first-order low pass

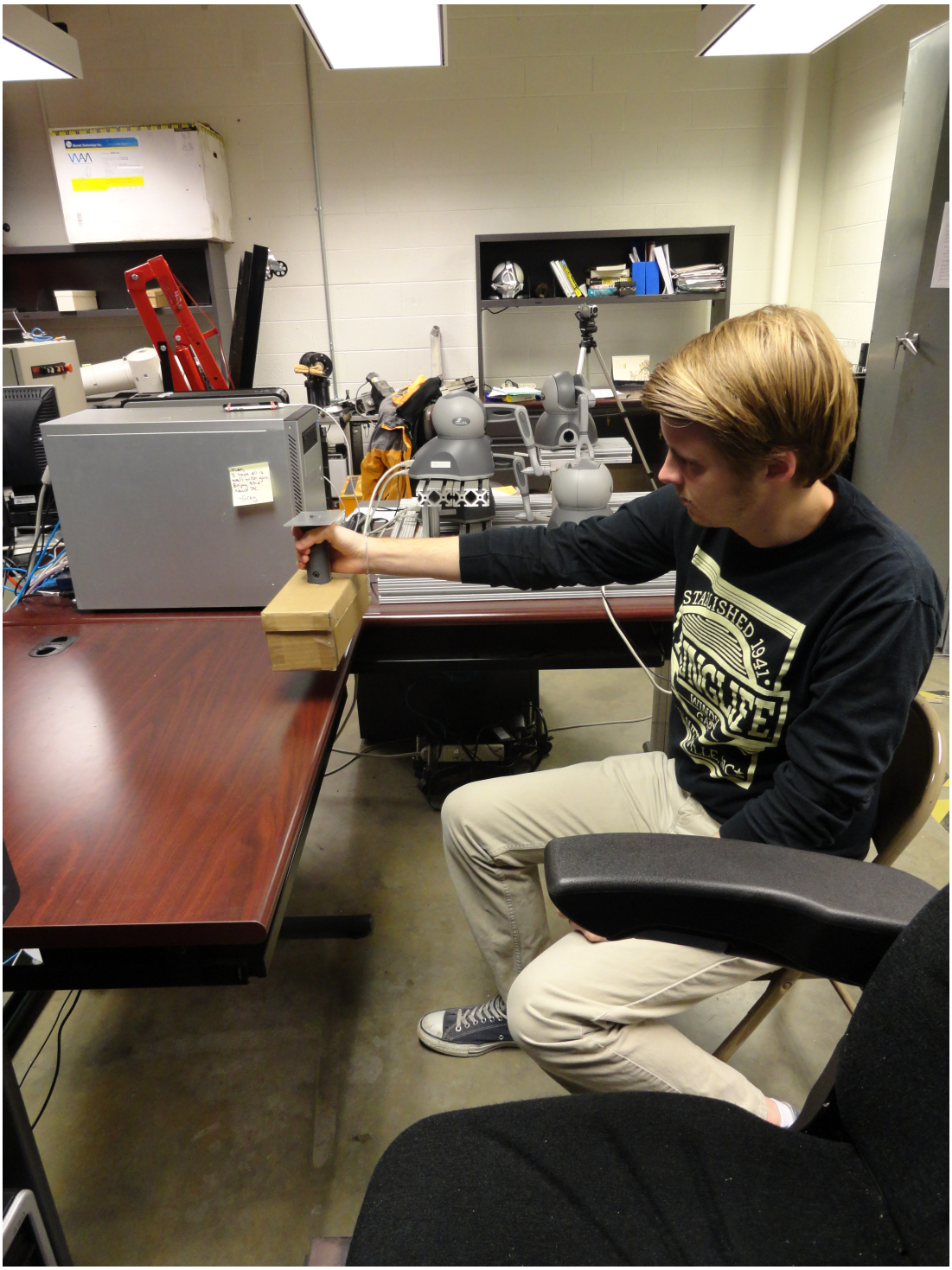

Figure 6.18: Direct Contact Exploration

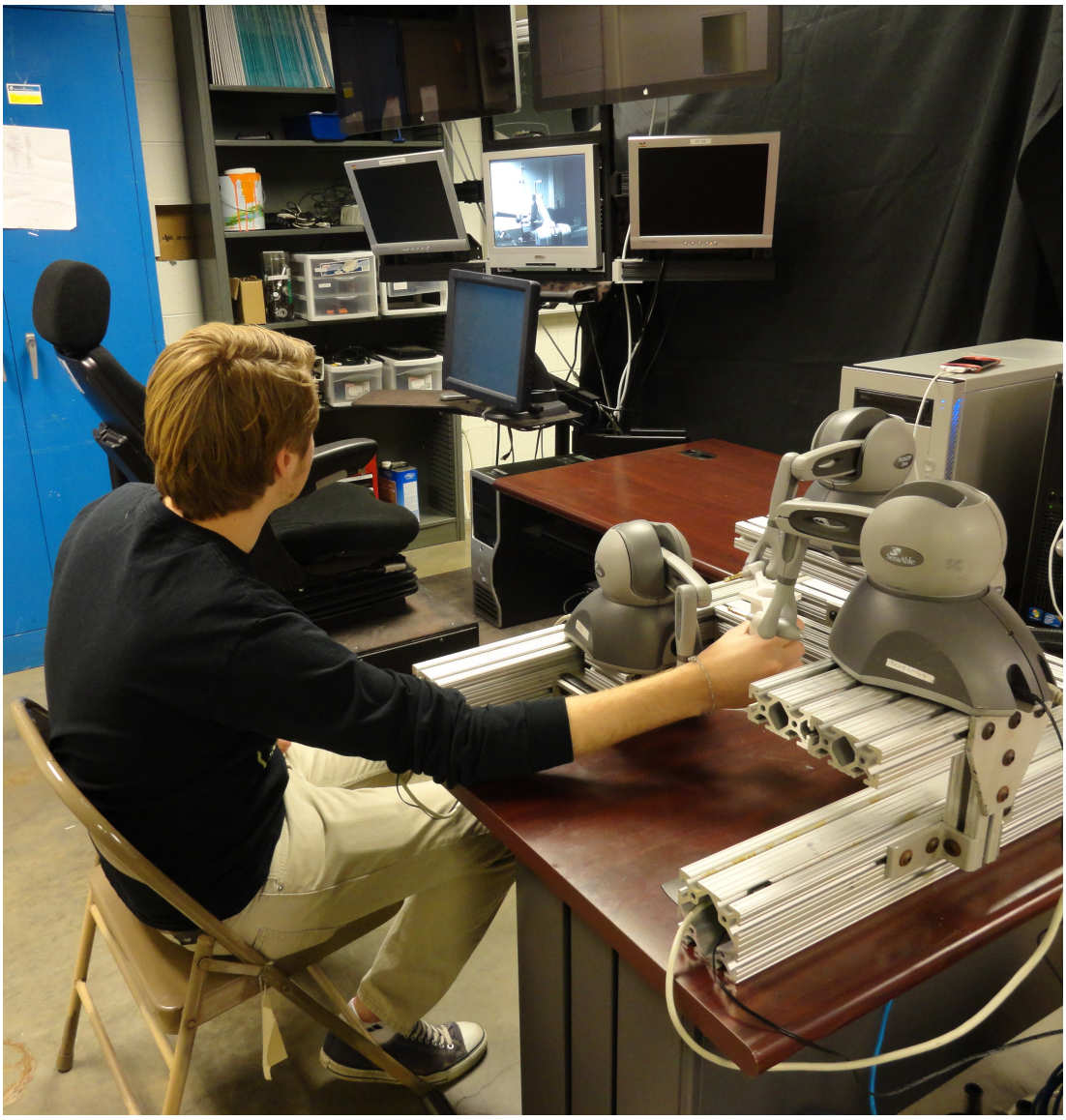

Figure 6.19: Teleoperation Exploration

filter for sensor measurements value, as shown in Eq. 6.12. Its cutoff frequency was set to 5 Hz, because when converted to the frequency domain, most of human motion is under 5 Hz. [20]

$$\tilde{f}_{ffd}(k) = \alpha f_{ffd}(k) + (1-\alpha)\tilde{f}_{ffd}(k-1) \tag{6.12}$$

Where α is the low pass filter constant, denote T as the update period of the master controller and τ as the filter constant, then when $T << \tau$, we have the following equation:

$$\alpha = \frac{T}{\tau} \tag{6.13}$$

Another issue was that the f_{ffd} was given with respect to the robotic hand coordinate frame, which must be transformed into the world coordinate frame. This was achieved by multiplying the coordinate transformation matrix which can be derived through the robotâĂŹs forward kinematics. Also the force feedback was scaled down to ensure that the desired force did not exceed the capacity of the haptic devices.

$$\tilde{f}_{ffd} = k_f {}^0_7R \tilde{f}_{ffd} \tag{6.14}$$

$$k_f = 0.5 \tag{6.15}$$

$${}^0_7R = {}^0_7R(\theta_1, \theta_2, \theta_3, \theta_4, \theta_5, \theta_5, \theta_6, \theta_7). \tag{6.16}$$

Where k_f is the force scaling factor, and ${}^0_7R$ is the coordinate transformation between the gripper frame and the world frame and is a function of the robot configuration as shown in Eq. 6.16, its analytical expression can be found in Appendix B. Therefore, combining Eqs. 6.12 to 6.16, results in the C_4 block in Fig. 5.5.

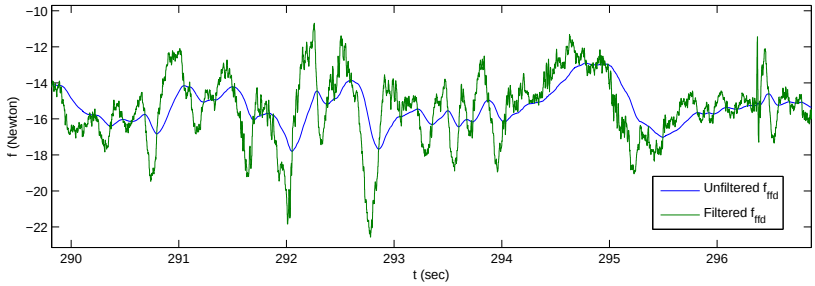

Figure 6.20: Filtered Force/Torque Sensor Data and Unfiltered Force/Torque Sensor Reading

Participants

Five individuals, aged from 24-30, volunteered to be the participants in these experiments. All of them were right-handed and two of them were females. None of them had participated in any experiments on this setup before.

6.3.2 Results and Analysis

The perceived weights were recorded and their average and variance were computed according to Eq. 6.17.

$$\tilde{x} = \frac{1}{N}\sum_{k=1}^{N} x_j$$
$$\sigma^2 = \frac{1}{N-1}\sum_{k=1}^{N}(x_j - \tilde{x})^2 \tag{6.17}$$

The ideal perceived weight should be exactly proportional to the actual weight of the test object, so the ideal curve would be a 45 degree straight line that passes through the origin. As shown in Fig. 6.21, the blue line, which represents where the subjects were tested in direct contact exploration tasks, shows the curve of a roughly proportional relationship. According to the dashed black line in Fig. 6.21, the subjects cannot tell the difference between the test objects. This is due to the fact that the position tracking error between the master and the slave robots was so low;

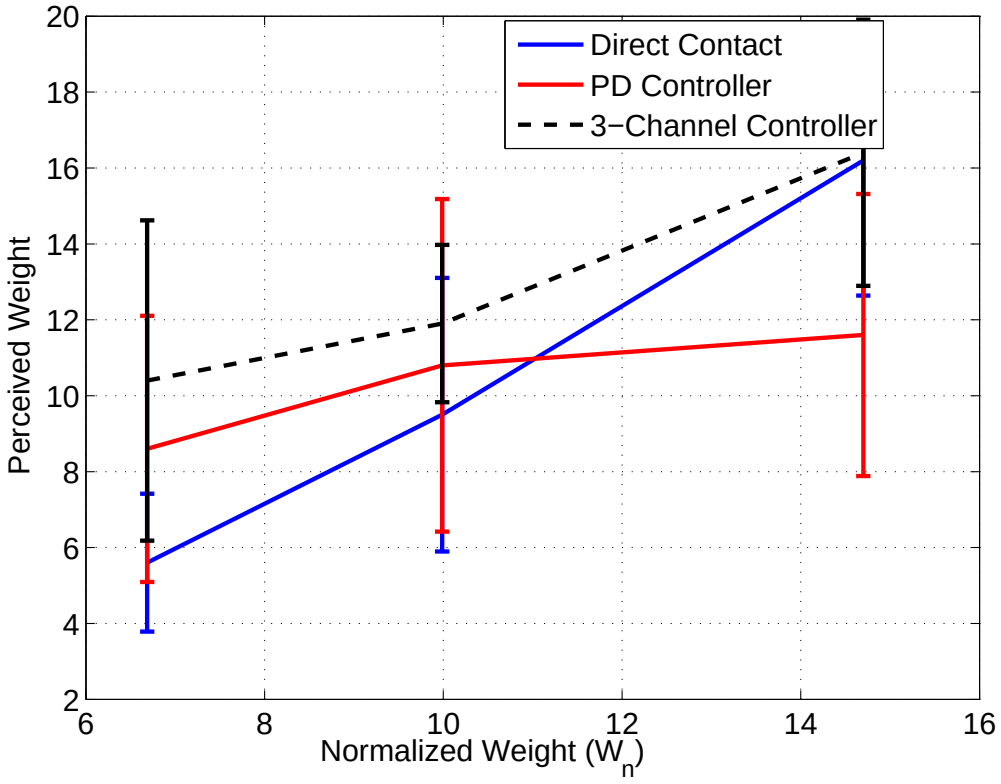

Figure 6.21: Perceived weight vs. Actual Weight in Direct Contact (top), Two-Channel Control (Middle) and Three-Channel Controller (bottom)

the force feedback was very close to zero, as shown in Fig. 6.13. In the blue line of Fig. 6.21, where the force feedback channel was enabled, the performance improved greatly, especially for the heavy object. These results show significant improvement from the results in [43].

The perception time also confirms our expectations. In Fig. 6.22, trials 1-3 show the perception time for the three trials in direct contact exploration, trials 4-6 show the time spent on the two channel controller time, and trials 7-9 show the time spent on the three channel teleoperation experiments. Note for each section of the experiment,

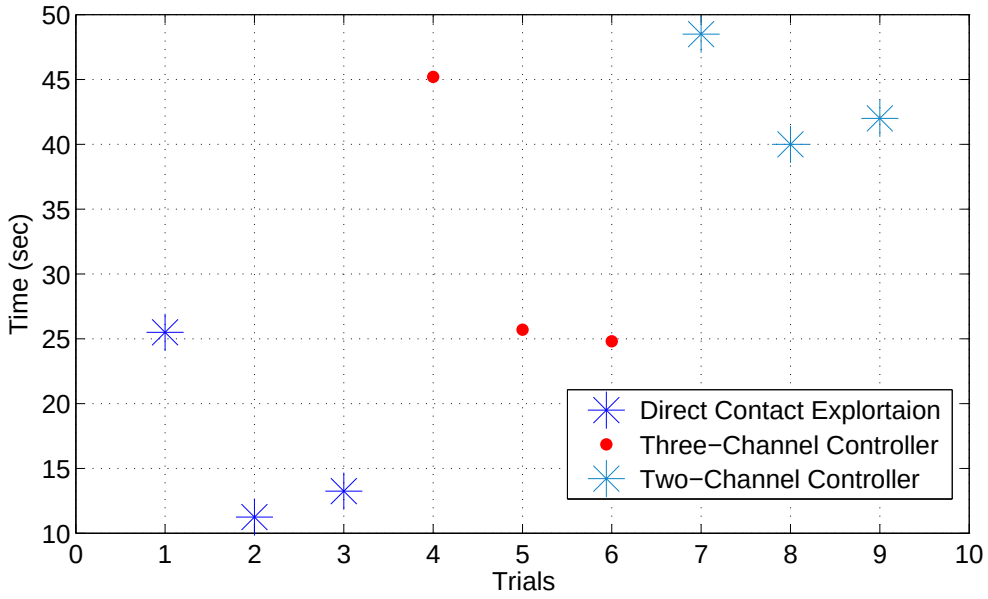

Figure 6.22: Perception Time Vs. Trials

the first trials (trial 1, 4 and 7) always take longer than the rest. This is because the subjects needed time to get used to the experimental setup. The second and third trial used in the three channel controller cases (trial 8 and 9) are significantly shorter than those of the two channel controller case (trial 5 and 6). This shows that the three channel controller provides better weight perception than the two channel controller, but is still worse than the direct haptics exploration.

6.4 Center of Gravity Perception

When holding an object, not only does a person have to provide the grasping force to cancel the gravity, but he/she also has to provide torque to compensate for the unbalanced object if he/she is not holding it at the center of gravity; otherwise the heavier side would drop. This can also be seen from Eq. 6.9, where the third term $\tau_g(\theta)$ is a gravitational torque term. In this experiment, we try to determine the

perception accuracy. The term m was kept the same for the three test objects used in this experiment.

In the teleoperation exploration experiments, this unbalancing effect can be reflected back to the subject through the teleoperator. The force/torque sensor can measure the torque generated by the unbalanced load. These experiments are used to test the operators' ability to the unbalanced objects during the direct contact and teleoperation experiments.

6.4.1 Methods

Apparatus

In this experiment, three boxes with identical appearances and weights were used. The weights on them were distributed differently to provide different locations for the center of gravity. The configurations of the objects are shown in Tab. 6.3 and Fig. 6.23. The unbalanced object added a torque along the axis that is perpendicular to the handle and the threaded rod.

Table 6.2: Apparatus Configuration for Center of Gravity Experiment (Units: m)

No.	Left*	Right*	L_c
0	0	1.3×10^{-2}	8.6×10^{-2}
1	3.2×10^{-3}	9.5×10^{-3}	4.3×10^{-2}
2	6.4×10^{-3}	6.4×10^{-3}	0

* shows the thickness of the metal plate. The plates have identical area, so the thickness is proportional to its weight.

Procedure

Before the experiments, each participant was given brief instructions about the experiment. He/she was given enough time to get comfortable with the teleoperation system. Participants were also instructed to adjust their seats as comfortable as possible.

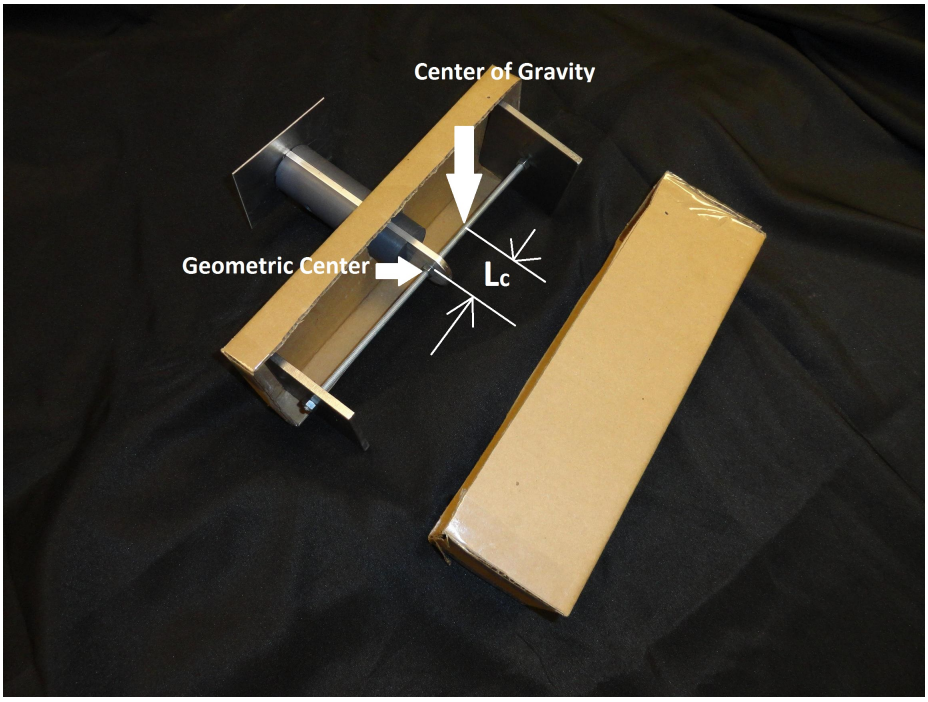

Figure 6.23: A Test Object in the Center of Gravity Perception

There are three sections for each participant, each experiment testing method corresponding to one type of method mentioned in the last part. The first testing method is, again, the direct contact exploration. Two kinds of system control architectures were tested: a simple PD controller and the advanced transparency enhanced controller. The procedures of the three testing methods were identical. Each section had five trials in total. The three objects were presented to the participant in a random order.

In the direct contact section, the lab examiner put an object in front of the participant and asked him/her to pick it up using his/her dominant hand. They were asked to hold it only at its handle. After the participant was asked to state which end of the box was heavier. There are only two possible results for each trial 0 (wrong) and 1 (right).

During each trial in the teleoperation sections, the laboratory personnel put the test object between the fingers of the gripper and closed the gripper of the robot.

Then, the participants were asked to pick up the handle of the master robot and try to determine the objectâĂŹs center of gravity based on the force feedback. When he/she felt comfortable enough, he/she was advised to release the master manipulator. The same question was asked and answered. The participants were only able to see the slave side in a television view connected to a CCD camera on the slave side. This is to simulate the actual remote handling process. The time spent on each trial was also recorded, but the participants were unaware of that.

Participants

People with various backgrounds volunteered for the experiments. A recruiting flier was used to recruit volunteers. They were given free T-shirts for the time they spent.

6.4.2 Results and Analysis

The average accuracy and execution time are taken as the haptics index of the corresponding trials according to Eq. 6.17. The results are given in Fig. 6.24 and Fig. 6.25. The trend of the bar chart clearly supports what was hypothesized. In the direct interaction case, the participants spent the least amount of time and had the highest accuracy. In the three channel controller, the participants had lower accuracy and spent more time in reaching their decision. In the PD controller case, the participants spent very long times with very low accuracy.

6.5 Inertia Perception

This experiment tries to test inertia perception resolution. The difference between the first two experiments and this one is that acceleration is required to generate the force difference that helps distinguish objects, as shown in Eq. 6.9 and Eq. 6.10. The m term was the same for all the objects. Also there is no noticeable $\tau_g(\theta)$ term because the gravity center was at the geometric center of the objects.

Table 6.3: Results of Center of Gravity Perception

Participants Number	DC			3C			2C		
1	✓	✓	✓	✓	✓	✓	×	×	×
	2"	3"	2"	14"	5"	3"	10"	12"	14"
Accuracy		100%			100%			0%	
Time		2.3"			7.3"			12"	
2	×	✓	✓	✓	✓	✓	×	✓	×
	2"	2"	2"	18"	6"	11"	25"	13"	10"
Accuracy		66.7%			100%			33.3%	
Time		2"			11.6"			16"	
3	✓	✓	✓	✓	×	✓	×	×	×
	13"	10"	3"	12"	12"	8"	19"	14"	10"
Accuracy		100%			66.7%			0%	
Time		8.7"			10.7"			14.3"	
4	✓	✓	✓	✓	×	×	×	×	×
	13"	3"	8"	15"	12"	22"	12"	22"	14"
Accuracy		100%			33.3%			0%	
Time		8"			16.3"			16"	
5	✓	✓	✓	✓	×	✓	×	×	×
	2"	2"	2"	7"	3"	4"	8"	10"	6"
Accuracy		100%			66.7%			0%	
Time		2"			4.7"			8"	
Average Time		4.6"			10.2"			13.3"	
Standard Deviation		3.4"			4.4"			3.4"	
Average Accuracy		93.3%			73%			6.7%	
Standard Deviation		0.15			0.28			0.15	

6.5.1 Methods

Procedure

The experiments still have three sections: direct contact exploration, teleoperation exploration with PD controller and teleoperation exploration with advanced controller. In each section, there were three trials, and in each trial, the participants were given two objects one after the other. They were asked to compare the second one with the first one in terms of mass. So, there were three possible answers: more massive,

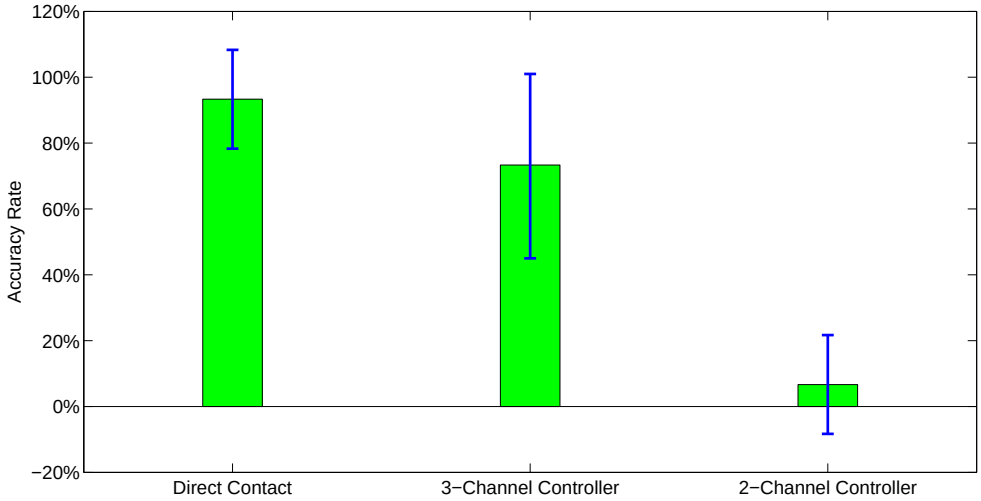

Figure 6.24: Average Accuracy in Center of Gravity perception

less massive and the same. If they answered with "the same", the answer would be treated as incorrect because none of the objects had the same inertia. During the experiments, the participants were instructed to only compare the test objects in the same trial and discard all previous experiences.

Apparatus

The same 0.3m-long, 1.30kg-weight test objects were used in this experiment. The weights used were the quarter-inch thick steel plate with both a width and height three and a half inches. There were three objects used, as shown Tab. 6.4 and Fig. 6.26. Each object had two weights. They were placed symmetrically to each other on objects. The first one has them at 1.9×10^{-2}m from the center of the threaded rod; this is the closest they can get because of the size of the handle. The second one has them placed at 7.4×10^{-2}m. And the third one has them at the furthest possible location: 1.5×10^{-1}m from the center. The location of the weights on the second object is chosen so that the radius of gyration and the square root of total effective inertia of the three of them forms an arithmetic progression.

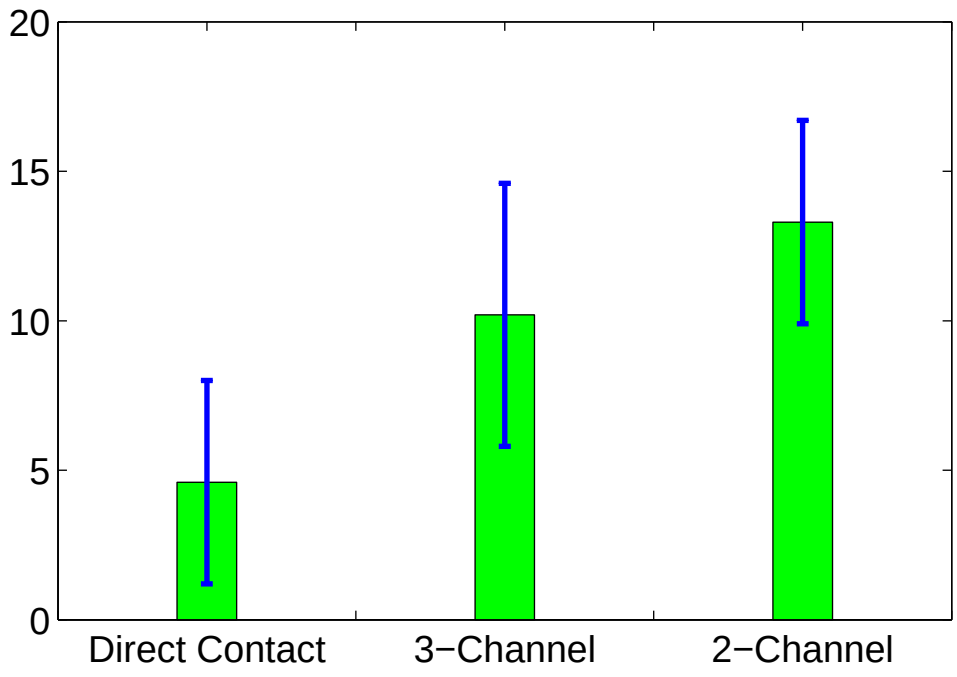

Figure 6.25: Average Time Spent by the Participants in Each Section in Center of Gravity Perception

Participants

Five people, aged from 19 to 30, volunteered for the experiments. They were given free T-shirts for their time. The same flyer used in the previous experiment was used here.

6.5.2 Results and Analysis

The raw data of this part of the experiment is in Tab. 6.5. The accuracy and time spent on each trial was recorded. The time accounted for was from the time the participant picked up the object to the time he/she came up with an answer to our question. Fig. 6.27 and 6.28 shows the bar chart of the experiment results. As we can see, the accuracy rate of the PD controller is lower and the exploration time is longer. This supports our hypothesis that the advanced controller provides better

Figure 6.26: A Test Object in Inertia Perception

transparency in the kinesthetic exploration tasks. However, we have to point out that this part of the experiment proved to be the most difficult of the three. This is because inertia manifests itself through motion acceleration, which may be ambiguous to some people. So, the accuracy rate is very low even in the direct contact exploration part. Given the limited workspace and the force capacity of the manipulators, the result has merit.

6.6 Discussion

The first two experiments tested the functionality of the experimental testbed. The last three experiments used the testbed to carry out the proposed kineshtetic exploration tasks. The same kinesthetic experimental framework is used in the three different kinesthetic perception experiments. Based on the performance in the kinesthetic exploration tasks, it is obvious that the teleoperational exploration can be further improved, since the performance in direct contact experiments is much better

Table 6.4: Apparatus Configuration for Inertia Experiment (Units: m)

NO.	L_x	Radius of Gyration
0	1.9×10^{-2}	1.7×10^{-2}
1	7.4×10^{-2}	5.7×10^{-2}
2	1.5×10^{-1}	1.14×10^{-1}

* shows the thickness of the metal plate. The plates have identical area, so the thickness is proportional to its weight.

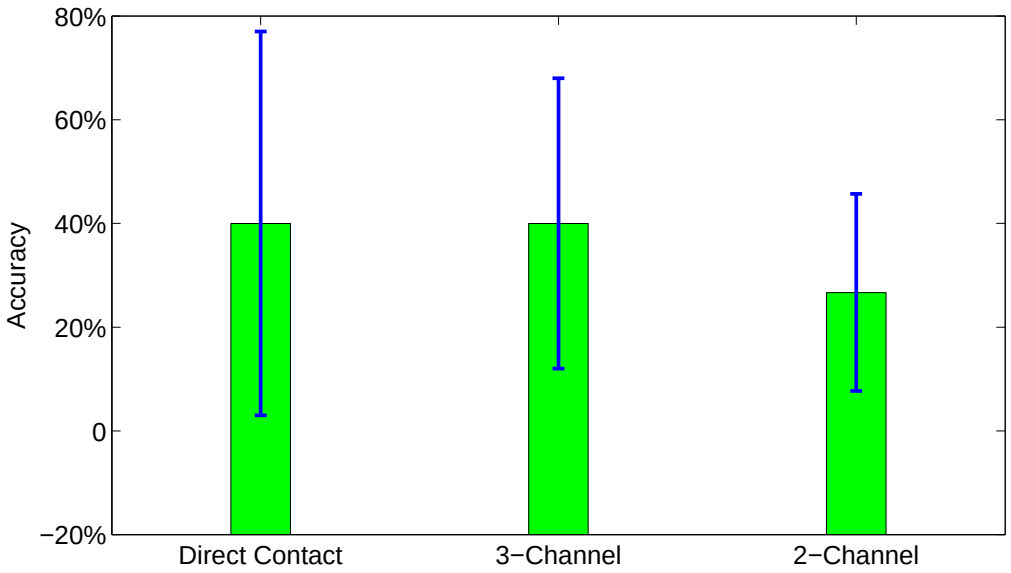

Figure 6.27: Average Accuracy vs. Experimental Methods

than in the teleoperation case. Possible methods include the hardware, the controller design and so on. This has been the drive of teleoperations research for over four decades.

In this experiment, the controller design significantly influenced the results. The better the force feedback provided to the operator, the better the experiment result is. These experiments show that the more advanced control algorithms can improve kinesthetic perception. This is consistent with earlier research results showing that a better control system can improve the system transparency [26, 29].

Table 6.5: Results of Inertia Perception

Participants Number	DC			TA			TPD		
1	✓	✓	✓	×	✓	×	×	✓	×
	15"	13"	8"	25"	30"	24"	23"	24"	15"
Accuracy		100%			33.3%			33.3%	
Time		12"			26.3"			20.6"	
2	✓	✓	✓	✓	×	✓	×	✓	✓
	17"	20"	20"	28"	24"	20"	40"	26"	23"
Accuracy		100%			66.7%			66.7%	
Time		19"			24"			29.7"	
3	✓	×	×	✓	×	×	×	×	✓
	30"	26"	28"	71"	74"	67"	69"	54"	100"
Accuracy		33.3%			100.0%			66.7%	
Time		28"			70.7"			74.3"	
4	×	✓	×	✓	✓	✓	✓	×	✓
	61"	97"	23"	52"	31"	60"	97"	84"	50"
Accuracy		33.3%			100%			66.7%	
Time		60.3"			47.7"			77"	
5	×	×	✓	×	✓	✓	×	×	✓
	20"	28"	14"	29"	26"	21"	19"	27"	22"
Accuracy		33.3%			66.7%			33.3%	
Time		20.7"			25.3"			22.7"	
Average Time		28.0"			38.8"			44.8"	
Standard Deviation		18.7"			20.3"			28.3"	
Accuracy Rate		60%			60%			46.7%	
Standard Deviation		0.37			0.28			0.19	

Human factors are very important in any experiment involving human subjects. The more subjects there are, the less potential for bias in the results. For example, females tended to over-rate the weight of the objects and males were more likely to underestimate the weight of the objects. The expertise of the subjects in related areas can also play a very important role. Someone who is familiar with the experimental setup can produce much better results than a person naive about teleoperation systems. Therefore, in our experiments, the subjects were given brief introductions to the experiments and the system testbed to make them familiar with the environment.

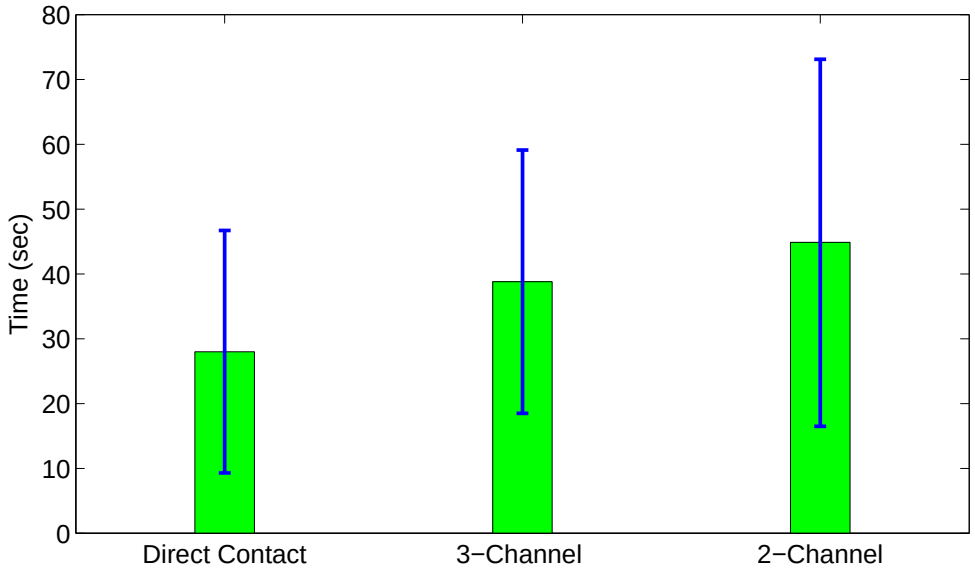

Figure 6.28: Average Perception Time vs. Experimental Methods

Another important factor about human subjects is the issue of fatigue. People get tired which leads to overrating weights as the experiment proceeds, so a proper resting period during the experiment is crucial.

The goal for a kinesthetic teleoperation system is to provide a sense of immersion so that the operator perceives as if it can mimic a direct hand interaction. The results of these experiments show that the performance of current teleoperation systems is still not high enough to provide that level of feedback. Both the hardware and control design of the system may be posing limitations to the performance. In this experiment, teleoperational and direct kinesthetic exploration were investigated. Different controllers for the teleoperation system were used in the experiments. Weight estimation, center of gravity perception and inertia perception experiments were considered. The result suggested that the controller with a better transparency provided better performance. Several factors were discussed and analyzed. There are a lot of open questions that may be promising research topics, for example, comparing the hardware systems using the same controller and experiment protocol.

Chapter 7

Conclusions

7.1 Overview

In this dissertation, kinesthetic perception in teleoperation systems was investigated. During the course of this research, two major issues have been addressed: system testbed configuration and experimental protocol development. The system testbed configuration issue includes the kinematic redundancy of the slave robot, the actuation redundancy of the master robot and the kinematics of the master robot. The experimental protocol issue includes the design of test objects, the setup of the experimental environment and the development of the experimental procedure. Experiments were conducted which demonstrated the influence of the controllers on the performance of the teleoperation systems.

7.2 Slave Robot Redundancy Resolution

In the slave kinematic redundancy problem, we adopted a geometric approach. The redundancy of the robot was utilized to avoid the wrist singularity. A simulated slave manipulator was used to test the algorithm. The advantage of this approach is obvious: every step of computation is based on a geometric method that has clear physical meaning. It is easier to compute and interpret. Commonly used

pseudo inverse based algorithms require taking the inverse of the Jacobian matrix, which consumes much computational power. Previously, geometric approach inverse kinematics methods are only applied on non-redundant robots. Also, this algorithm is easy to apply to robots with different kinematics.

The disadvantage of this algorithm is that it only solved the singularity in one particular configuration. It is still an open question for the other singularity configurations and for the joint limit avoidance.

7.3 Master Controller Design

Through research, people are always trying to push the limits of human knowledge; therefore, proper equipment may not always be off-the-shelf. For this reason, custom-designed experimental equipment has been widely used. We designed a master manipulator that can offer the necessary force feedback. The novel master manipulator is the integration of four off-the-shelf haptic devices and some other custom-designed parts. When solving the master actuation redundancy problem, four haptic devices were integrated into one system; the convex optimization method was used to resolve the redundancy. Using the collaboration between small scale robots to provide a large force capability is beneficial in that it makes the system more expandable and flexible. Also, it helps reduce the cost of the equipment.

Recently developed advanced prototyping methods have made the design and production of new conceptual products much easier. 3D printing is the most important development. It was used to manufacture the prototype. This brings a whole new dimension to parts design. Previously, engineers had to consider the availability of the material in their designs; now the 3D printer can print objects of any shape as long as they can be contained in the 3D printer work space. Also, the material used in 3D printing is far lighter than most other materials used in the prototyping process. This makes the new robot more transparent. However current

3D printing technology is not perfect; its material still suffers from weakness and lack of heat-resisting capability.

7.4 Kinesthesia Experiments

The experimental protocol developed was based on previous human factor analysis research and experimental psychology methods. Using a standardized protocol made the results of the experiments more valuable. Every experiment had at least five participants; most of them were naive about the experiment.

The results of the experiments support the hypothesis: a controller that provides better force tracking can improve kinesthetic exploration performance. In the weight and center of gravity perceptions, the average perception time decreased when the three channel controller was used, and the average accuracy rate increased. For the inertia perception, the trend of the curves still supports what we expected. But the differences resulting from the use of using different controllers is not very significant. We think it is due to the fact that the acceleration generated by the teleoperation system is not noticeable to human perception. Also, we think that the low pass filter may have had a side effect in the kinesthetic perception tasks. It created a significant lag in the force feedback and some force/torque associated with the dynamics of the object was lost because of this low pass filtering mechanism.

7.5 General Discussion

Experiments were presented and the kinesthetic exploration tasks in both direct contact and teleoperation cases were investigated. Experimental protocols, control algorithms and hardware were constructed centered on the concept of testing and enhancing kinesthetics feedback. There were three fundamental contributions: 1) an experimental framework was proposed to test the kinesthetic exploration tasks in both teleoperation and direct contact cases; 2) different controllers were used

in the experiments to analyze their role in kinesthetic exploration tasks; and 3) a singularity avoidance algorithm was used to improve the performance of the kinesthetic exploration tasks. The results show that as the force feedback was enhanced, the participants' performance improved. The direct contact exploration and PD controller were used as the comparison. If the force feedback is further improved, there should be better results. The experiments were very fundamental and can be applied to other teleoperation applications.

Chapter 8

Future Work

This dissertation demonstrates the concept of testing the kinesthetic perception in teleoperation systems. A system testbed was configured and an experimental framework was proposed. We can further explore this concept along many possible avenues. The following sections explain areas in which future research work can be conducted.

8.1 Kinematic Redundancy

A geometric approach based inverse kinematic algorithm was used to avoid wrist singularity. It can also be generalized to avoid other singularities such as elbow or shoulder singularity. The algorithm we proposed considered the wrist Jacobian matrix; if we can use the same method to analyze other portions of the Jacobian matrix, we would be able to solve the singularity problem of the whole arm. In other words, the robot will be able to travel inside its workspace without encountering any singularities. Also, it would be useful to use the redundancy in avoiding the joint limits and in avoiding collision with other objects in the workspace. It would also be interesting to optimize the impedance of the robotic arm by utilizing its redundancy. The impedance of the robot in Cartesian space is different given different configurations, although the individual joint controllers used are the same.

8.2 Master Controller

We built an innovative master controller by integrating off-the-shelf haptic devices. Kinematics and force feedback algorithms were proposed.

One potential way to upgrade the current master controller would be to install switches to increase its functionality. Most teleoperation systems require many inputs from the operators, such as the control command of the open/close motion of the gripper or the activation/deactivation of many other types of end-effectors. Also, we can install those tactile sensors or force torque sensors on the handle to take force/torque measurements from the master side and then send these measurements to the slave side. This way, a four-channel control architecture would be formed, and then it could be used in the kinesthetic perception experiments.

3D printing technology has been developing faster than ever before. If the 3D metal printer becomes more affordable, many more robots parts will become easy to custom-designed. We can have those switches mechanically built in the handle so that it would not require any assembly. This would make the handle much easier to manufacture and have a very consistent appearance.

Another new type of master controller that might be interesting has the exoskeleton style structure. That type of structure mimics the kinematics of a human arm, has a very large workspace and usually does not have a singularity problem.

8.3 Control Algorithms

A lot of controller algorithms have been proposed to enhance the performance of teleoperation systems. In this dissertation, only two of them were explored. The most transparent four-channel controller was not tested. The additional channel we did not use was the force measurement from the master controller. This is due to the fact that the master controller is relatively small and it is challenging to integrate an extra component into the system. More measurements taken and more signals

transferred usually can improve the sense of immersion, but more signals transmitted also require better communication channels. So it would be very interesting to see whether increased system complexity increases kinesthetic feedback. Even for the same type of controller, there are a lot of parameters that we can tweak, for example, the gains of the controllers and the scaling factors.

Also, there are significant numbers of passivity enforced controllers that perform well in maintaining the stability of teleoperation system. It would be useful to test their transparency in kinesthetic exploration tasks. The tradeoff between performance and stability is the central issue of controller design. A system that has very high sensitivity may tend to go unstable, but a very stable system usually has slow response.

8.4 Integrating Kinesthetic and Tactile Sensation

Kinesthetic and tactile sensing are the two subareas of haptics. They are closely related. For example, when a person lifts an object and tries to determine its weight, he/she relies on both kinesthetic and tactile information. The gravity the wrist and the arm perceive is a projection of the load onto the muscles, and the fingers perceive the deformation and discomfort caused by the load. There has been little effort to use this combined information comprehensively. Different types of haptics sensing have different advantages. When one perceives the weight of a relatively small object, tactile sensing is the major perception method. When trying to handle a large object, kinesthetic sensing is the major factor. If we can fuse the two types of data together, we may be able to generate complete information about the environment. The equipment in our lab currently has this capability. The Barretthand has a touch pad that provides tactile sensing information on the finger tips and the palm. This information may be important when determining the shape or the weight of the object. Also, when the object is light, the sensors on the joints and wrist may not be

accurate because their ranges are large, but the tactile sensors can be very useful in this case.

Tactile sensing can also provide extra information, for instance, temperature or texture of the objects. If an artificial intelligence algorithm can be used, such information can be used together to determine the attributes of the object. Another challenge to this issue is miniaturizing the various types of sensors.

8.5 Experimental Protocol Improvements

Human factors are also very important to the performance of teleoperation systems. A well-trained operator is usually more effective than a naive operator. But there is also a maximum performance level that is limited by the natural perception capabilities of human beings. So by analyzing the minimum amount of effort spent on the operators' training, we can make the training more cost effective and affordable. Also, gender, age, race and many other factors could be influential. These results would be useful when trying to pick operator candidates from the general population.

Also, in our experiments, the examiners interacting with the subjects knew the actual attributes of the testing objects. This may have brought extra information to the subjects inadvertently. It would be best to use the double-blind experimental protocol where two examiners are used. One of them does the object configuration tasks and therefore knows the answers to the questions but does not interact with the subjects, while the other examiner interacts with the subjects but knows nothing about the actual test objects being used.

Bibliography

[1] Eric L Amazeen and MT Turvey. Weight perception and the haptic size–weight illusion are functions of the inertia tensor. *Journal of Experimental Psychology: Human Perception and Performance*, 22(1):213, 1996. xiv, 10, 11

[2] Robert J Anderson and Mark W Spong. Bilateral control of teleoperators with time delay. *Automatic Control, IEEE Transactions on*, 34(5):494–501, 1989. 7

[3] Robert J Anderson and Mark W Spong. Asymptotic stability for force reflecting teleoperators with time delay. *The International Journal of Robotics Research*, 11(2):135–149, 1992. 25

[4] Technology Inc. Barrett. Wam user manual. 2003. 112

[5] Stephen Poythress Boyd and Lieven Vandenberghe. *Convex optimization*. Cambridge university press, 2004. 45

[6] Joel Wakeman Burdick. *Kinematic analysis and design of redundant robot manipulators*. PhD thesis, Stanford University, 1988. 9

[7] M.C. Cavusoglu, D. Feygin, and F. Tendick. A critical study of the mechanical and electrical properties of the phantom haptic interface and improvements for highperformance control. *Presence: Teleoperators & Virtual Environments*, 11(6):555–568, 2002. 34

[8] M.C. Çavusoglu, A. Sherman, and F. Tendick. Design of bilateral teleoperation controllers for haptic exploration and telemanipulation of soft environments. *Robotics and Automation, IEEE Transactions on*, 18(4):641–647, 2002. 8

[9] Tan Fung Chan and Rajiv V Dubey. Design and experimental studies of a generalized bilateral controller for a teleoperator system with a six dof master and a seven dof slave. In *Intelligent Robots and Systems' 94.'Advanced Robotic Systems and the Real World', IROS'94. Proceedings of the IEEE/RSJ/GI International Conference on*, volume 1, pages 415–422. IEEE, 1994. 6

[10] Tan Fung Chan and Rajiv V Dubey. A weighted least-norm solution based scheme for avoiding joint limits for redundant joint manipulators. *Robotics and Automation, IEEE Transactions on*, 11(2):286–292, 1995. 6

[11] Peter Corke. Matlab toolbox, November 2013. 50

[12] Philippe Desbats, Franck Geffard, Gérard Piolain, and Alain Coudray. Force-feedback teleoperation of an industrial robot in a nuclear spent fuel reprocessing plant. *Industrial Robot: An International Journal*, 33(3):178–186, 2006. 8, 9

[13] Force Dimension. Force dimension products, 2014. 11

[14] John V Draper. Teleoperators for advanced manufacturing: Applications and human factors challenges. *International Journal of Human Factors in Manufacturing*, 5(1):53–85, 1995. 10

[15] Rajiv Dubey and John Luh. Redundant robot control using task based performance measures. *Journal of robotic systems*, 5(5):409–432, 1988. 9

[16] Rajiv V Dubey, Tan Fung Chan, and Steve E Everett. Variable damping impedance control of a bilateral telerobotic system. *Control Systems, IEEE*, 17(1):37–45, 1997. 6

[17] RV Dubey, JA Euler, and SM Babcock. An efficient gradient projection optimization scheme for a seven-degree-of-freedom redundant robot with spherical wrist. In *Robotics and Automation, 1988. Proceedings., 1988 IEEE International Conference on*, pages 28–36. IEEE, 1988. 9

[18] Iman Ebrahimi, Juan A Carretero, and Roger Boudreau. 3-prrr redundant planar parallel manipulator: Inverse displacement, workspace and singularity analyses. *Mechanism and Machine Theory*, 42(8):1007–1016, 2007. 9

[19] M. Fotoohi, S. Sirouspour, and D. Capson. Stability and performance analysis of centralized and distributed multi-rate control architectures for multi-user haptic interaction. *The International Journal of Robotics Research*, 26(9):977–994, 2007. 9

[20] Hironobu Fujiyoshi, Alan J Lipton, and Takeo Kanade. Real-time human motion analysis by image skeletonization. *IEICE TRANSACTIONS on Information and Systems*, 87(1):113–120, 2004. 72

[21] Geomagic. Phantom premium, 2014. 11

[22] J.H. Ginsberg. *Advanced engineering dynamics*. Cambridge University Press, 1998. 109

[23] R.C. Goertz. Fundamentals of general-purpose remote manipulators. *Nucleonics (US) Ceased publication*, 10, 1952. 5, 6

[24] William R Hamel and Pamela Murray. Observations concerning internet-based teleoperations for hazardous environments. In *Robotics and Automation, 2001. Proceedings 2001 ICRA. IEEE International Conference on*, volume 1, pages 638–643. IEEE, 2001. 8

[25] B. Hannaford and J.H. Ryu. Time-domain passivity control of haptic interfaces. *Robotics and Automation, IEEE Transactions on*, 18(1):1–10, 2002. 7

[26] Blake Hannaford. A design framework for teleoperators with kinesthetic feedback. *Robotics and Automation, IEEE Transactions on*, 5(4):426–434, 1989. 8, 83

[27] Jonghyun Kim, Pyung Hun Chang, and Hyung-Soon Park. Transparent teleoperation using two-channel control architectures. In *Intelligent Robots and Systems, 2005.(IROS 2005). 2005 IEEE/RSJ International Conference on*, pages 1953–1960. IEEE, 2005. 59

[28] R.L. Klatzky, S.J. Lederman, and D.E. Matula. Haptic exploration in the presence of vision. *Journal of Experimental Psychology: Human Perception and Performance*, 19(4):726, 1993. 8

[29] Dale A Lawrence. Stability and transparency in bilateral teleoperation. *Robotics and Automation, IEEE Transactions on*, 9(5):624–637, 1993. xiv, 7, 27, 28, 83

[30] S.J. Lederman and R.L. Klatzky. Extracting object properties through haptic exploration. *Acta Psychologica*, 84(1):29–40, 1993. 8, 10

[31] Susan J Lederman and Roberta L Klatzky. Hand movements: A window into haptic object recognition. *Cognitive psychology*, 19(3):342–368, 1987. 10

[32] DJ Lee and Ke Huang. On passive non-iterative varying-step numerical integration of mechanical systems for haptic rendering. In *ASME Dynamic Systems & Control Conf*, 2008. 57

[33] Dongjun Lee and Perry Y Li. Passive bilateral feedforward control of linear dynamically similar teleoperated manipulators. *Robotics and Automation, IEEE Transactions on*, 19(3):443–456, 2003. 7

[34] Zhijun Li, Liang Ding, Haibo Gao, Guangren Duan, and Chun-Yi Su. Trilateral teleoperation of adaptive fuzzy force/motion control for nonlinear teleoperators with communication random delays. *IEEE Trans. Fuzzy Syst*, 21(4):610–624, 2013. 6

[35] Yun Lin and Yu Sun. 5-d force control system for fingernail imaging calibration. In *Robotics and Automation (ICRA), 2011 IEEE International Conference on*, pages 1374–1379. IEEE, 2011. 12

[36] Pawel Malysz and Shahin Sirouspour. A kinematic control framework for single-slave asymmetric teleoperation systems. *Robotics, IEEE Transactions on*, 27(5):901–917, 2011. 6

[37] Pawel Malysz and Shahin Sirouspour. Trilateral teleoperation control of kinematically redundant robotic manipulators. *The International Journal of Robotics Research*, 30(13):1643–1664, 2011. 6

[38] Karan A. Manocha, Norali Pernalete, and Rajiv V. Dubey. Variable position mapping based assistance in teleoperation for nuclear cleanup. In *Robotics and Automation, 2001. Proceedings 2001 ICRA. IEEE International Conference on*, volume 1, pages 374–379. IEEE, 2001. 8, 9

[39] HL Martin and WR Hamel. Joining teleoperation with robotics for remote manipulation in hostile environments. In *Conference Proceedings Robots 8, Robotics International of Society of Manufacturing Engineers*, volume 1, 1980. 6

[40] Max Q-H Meng, Polley R Liu, William LC Shek, and Peter X Liu. Psychophysics, soft-haptics and information acquisition for internet-based robotic teleoperation. *International Journal of Information Acquisition*, 1(02):191–200, 2004. 10

[41] Edvard Naerum and Blake Hannaford. Global transparency analysis of the lawrence teleoperator architecture. In *Robotics and Automation, 2009. ICRA'09. IEEE International Conference on*, pages 4344–4349. IEEE, 2009. 7, 59

[42] Newtonium. Robowork, May 2008. 51

[43] Mark W Noakes, Thomas W Burgess, and John C Rowe. Remote systems experience at the oak ridge national laboratory–a summary of lessons learned. 2011. 5, 8, 74

[44] A.M. Okamura and M.R. Cutkosky. Feature detection for haptic exploration with robotic fingers. *The International Journal of Robotics Research*, 20(12):925–938, 2001. 8

[45] J. Park and O. Khatib. A haptic teleoperation approach based on contact force control. *The International Journal of Robotics Research*, 25(5-6):575, 2006. 34

[46] J. Park and O. Khatib. http://www.sensable.com/products-haptic-devices.htm. *The International Journal of Robotics Research*, 25(5-6):575, 2006. 34

[47] Quanser. Haptics wand, 2014. 11

[48] SE Salcudean. Control for teleoperation and haptic interfaces. *Lecture notes in control and information sciences*, pages 51–66, 1998. 7

[49] Sensable. Phantom omin user guide. Technical report, SensAble Technologies, Inc., 2008. 36, 37

[50] Aman V Shah, Scott Teuscher, Eric W McClain, and Jake J Abbott. How to build an inexpensive 5-dof haptic device using two novint falcons. In *Haptics: Generating and Perceiving Tangible Sensations*, pages 136–143. Springer, 2010. 12

[51] X. Shen, J. Zhou, A. El Saddik, and N.D. Georganas. Architecture and evaluation of tele-haptic environments. In *Distributed Simulation and Real-Time Applications, 2004. DS-RT 2004. Eighth IEEE International Symposium on*, pages 53–60. IEEE, 2004. 9

[52] T.B. Sheridan. Space teleoperation through time delay: Review and prognosis. *Robotics and Automation, IEEE Transactions on*, 9(5):592–606, 1993. 7

[53] Bruno Siciliano. Kinematic control of redundant robot manipulators: A tutorial. *Journal of Intelligent and Robotic Systems*, 3(3):201–212, 1990. 9

[54] Hyoung Il Son, Tapomayukh Bhattacharjee, Hoeryong Jung, and Doo Yong Lee. Psychophysical evaluation of control scheme designed for optimal kinesthetic perception in scaled teleoperation. In *Robotics and Automation (ICRA), 2010 IEEE International Conference on*, pages 5346–5351. IEEE, 2010. 7, 10

[55] Tsu T Soong. *Fundamentals of probability and statistics for engineers*. Wiley. com, 2004. 39

[56] John E Speich, K Fite, and M Goldfarb. Transparency and stability robustness in two-channel bilateral telemanipulation. *Transactions of the ASME*, 123:400–4007, 2001. 59

[57] Aaron Steinfeld, Terrence Fong, David Kaber, Michael Lewis, Jean Scholtz, Alan Schultz, and Michael Goodrich. Common metrics for human-robot interaction. In *Proceedings of the 1st ACM SIGCHI/SIGART conference on Human-robot interaction*, pages 33–40. ACM, 2006. 10

[58] P. Ström, L. Hedman, L. Särnå, A. Kjellin, T. Wredmark, and L. Felländer-Tsai. Early exposure to haptic feedback enhances performance in surgical simulator training: a prospective randomized crossover study in surgical residents. *Surgical endoscopy*, 20(9):1383–1388, 2006. 9

[59] Anthony Talvas, Maud Marchal, Clément Nicolas, Gabriel Cirio, Mathieu Emily, and Anatole Lécuyer. Novel interactive techniques for bimanual manipulation of 3d objects with two 3dof haptic interfaces. In *Haptics: Perception, Devices, Mobility, and Communication*, pages 552–563. Springer, 2012. 12

[60] Yuichi Tsumaki, H Naruse, Dragomir N Nenchev, and Masaru Uchiyama. Design of a compact 6-dof haptic interface. In *Robotics and Automation, 1998. Proceedings. 1998 IEEE International Conference on*, volume 3, pages 2580–2585. IEEE, 1998. 12

[61] Michael T Turvey. Dynamic touch. *American Psychologist*, 51(11):1134, 1996. 10

[62] RQ Van der Linde, P. Lammertse, E. Frederiksen, and B. Ruiter. The hapticmaster, a new high-performance haptic interface. In *Proc. Eurohaptics*, pages 1–5, 2002. 9

[63] Minh Hung Vu and Uhn Joo Na. A new 6-dof haptic device for teleoperation of 6-dof serial robots. *Instrumentation and Measurement, IEEE Transactions on*, 60(11):3510–3523, 2011. 12

[64] D. Wang, K. Tuer, M. Rossi, L. Ni, and J. Shu. The effect of time delays on tele-haptics. In *Haptic, Audio and Visual Environments and Their Applications, 2003. HAVE 2003. Proceedings. The 2nd IEEE Internatioal Workshop on*, pages 7–12. IEEE, 2003. 9

[65] Ki Young Woo, Byoung Dae Jin, and Dong-Soo Kwon. A 6-dof force-reflecting hand controller using the fivebar parallel mechanism. In *Robotics and Automation, 1998. Proceedings. 1998 IEEE International Conference on*, volume 2, pages 1597–1602. IEEE, 1998. 12

[66] Gordon Wood. *Fundamentals of psychological research.* Little, Brown Boston, 1974. 10

[67] Renbin Zhou, William R Hamel, AS Hariharan, and Mark W Noakes. Using the wam as a master controller. In *Proceedings of the ANS 2006 International Joint Topical Meeting*, 2006.

Appendix

Appendix A

Testing Object Design

The dimensions of the testing objects are shown in Fig. A.1. Every testing object is made up of a center rod, a handle and several pieces of sheet metal. The handle is fastened to on the center rod. The metal sheets are attached to both ends of the center rod. n_1 and n_2 represent the numbers of metal plates attached to each side of the center rod. The dimension of each sheet of metal is $d \times a \times a$ in^3. The variable l_{x1} and l_{x2} shows the location of the handle on the center rod. The center rod has a length of l and cross-sectional area of A. The handle is made up of a a quarter inch aluminum plate with two pieces of PVC on each side. So the weight of the testing object is:

$$m = m_1 + m_2(n_1 + n_2) + m_3 + m_4 \tag{A.1}$$

$$m_1 = \rho_1 l A \tag{A.2}$$

$$m_2 = a_w^2 d_w \rho_2 \tag{A.3}$$

$$m_3 = \rho_3 \pi R_h^2 L_h \tag{A.4}$$

$$m_4 = \rho_4 L_h R_h d_h \tag{A.5}$$

Where ρ_1 and ρ_2 are the mass densities of the materials as shown in Tab. A.1. So

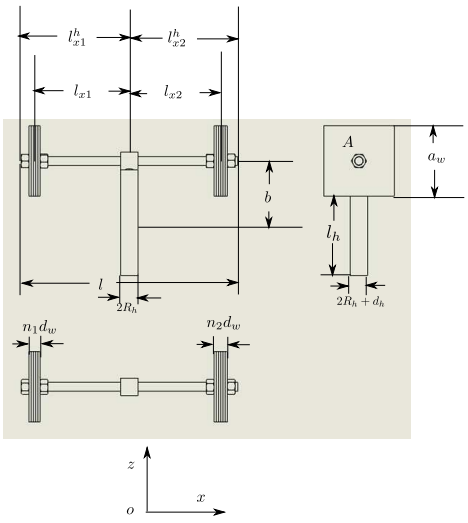

Figure A.1: Dimension of Testing Objects

Table A.1: Mass Density of the Material Used in the Objects

	ρ_1	ρ_2	ρ_3
Material	Aluminum	PVC	Steel
Unit: kg/m^3	2.7×10^3	1.35×10^3	7.8×10^3

the inertia matrix of the center rod with respect to its geometricy center is:

$$I_1 = \begin{pmatrix} 0 & 0 & 0 \\ 0 & \frac{1}{12}m_1 l^2 & 0 \\ 0 & 0 & \frac{1}{12}m_1 l^2 \end{pmatrix} \tag{A.6}$$

Where

$$m_1 = 0.0536kg \tag{A.7}$$

$$l = 0.3048m \tag{A.8}$$

Plugging in the numbers, we can get

$$I_1 = \begin{pmatrix} 0 & 0 & 0 \\ 0 & 4.15 \times 10^{-4} & 0 \\ 0 & 0 & 4.15 \times 10^{-4} \end{pmatrix} \tag{A.9}$$

The inertia matrix of a metal sheet with respect to its geometricy center is:

$$I_2 = \begin{pmatrix} \frac{1}{6} m_2 a_w^2 & 0 & 0 \\ 0 & \frac{1}{12} m_2 (a_w^2 + d_w^2) & 0 \\ 0 & 0 & \frac{1}{12} m_2 (a_w^2 + d_w^2) \end{pmatrix} \tag{A.10}$$

where

$$a_w = 0.0889m \tag{A.11}$$

$$d_w = 0.00635m \tag{A.12}$$

$$m_2 = 0.388kg \tag{A.13}$$

for steel plates and

$$a_w = 0.0889m \tag{A.14}$$

$$d_w = 1.58 \times 10^{-3}m \tag{A.15}$$

$$m_2 = 0.0338g \tag{A.16}$$

for aluminum. So

$$I_2 = \begin{pmatrix} 5.13 \times 10^{-4} & 0 & 0 \\ 0 & 2.56 \times 10^{-4} & 0 \\ 0 & 0 & 2.56 \times 10^{-4} \end{pmatrix} \tag{A.17}$$

for the steel. The inertia matrix of the outer pieces of the handle with respect to their its geometricy center is:

$$I_3 = \begin{pmatrix} \frac{1}{12}m_3(3R_h^2 + l_h^2) & 0 & 0 \\ 0 & \frac{9\pi^2-32}{18\pi^2}m_3R_h^2 & 0 \\ 0 & 0 & \frac{9\pi^2-64}{36\pi^2}m_3R_h^2 + \frac{1}{12}m_3(l_h^2) \end{pmatrix} \tag{A.18}$$

where

$$R_h = 1.91 \times 10^{-2}m \tag{A.19}$$

$$l_h = 1.02 \times 10^{-1}m \tag{A.20}$$

$$m_3 = 0.101kg \tag{A.21}$$

Plug in the values, we have

$$I_3 = \begin{pmatrix} 9.7 \times 10^{-5} & 0 & 0 \\ 0 & 4.7 \times 10^{-5} & 0 \\ 0 & 0 & 9.9 \times 10^{-4} \end{pmatrix} \tag{A.22}$$

The inertia matrix of the center piece of the handle is separated into two pieces, with the upper half a rectangular shaped object and the lower half a semicylindrical er shaped object. The inertia of the upper half with respect to its geometricy center is:

$$I_4 = \begin{pmatrix} \frac{1}{12}m_4(l_{ha}^2 + l_{ha2}^2) & 0 & 0 \\ 0 & \frac{1}{12}m_4(l_{ha2}^2 + d_h^2) & 0 \\ 0 & 0 & \frac{1}{12}m_4(l_{ha}^2 + d_h^2) \end{pmatrix} \tag{A.23}$$

where

$$m_4 = 9.8 \times 10^{-2} kg \tag{A.24}$$

$$d_h = 6.35 \times 10^{3} m \tag{A.25}$$

$$l_{ha} = 0.15 m \tag{A.26}$$

$$l_{ha2} = 2R_h = 3.81 \times 10^{-2} m \tag{A.27}$$

Plug in the values

$$I_4 = \begin{pmatrix} 1.96 \times 10^{-4} & 0 & 0 \\ 0 & 1.22 \times 10^{-5} & 0 \\ 0 & 0 & 1.84^{-4} \end{pmatrix} \tag{A.28}$$

The inertia of the lower half with respect to its geometricy center is:

$$I_5 = \begin{pmatrix} \frac{9\pi^2-32}{18\pi^2} m_5 R_h^2 & 0 & 0 \\ 0 & \frac{9\pi^2-64}{36\pi^2} m_5 R_h^2 + \frac{1}{12} m_5 d_h^2 & 0 \\ 0 & 0 & \frac{1}{12} m_5 (l_{ha}^2 + d_h^2) \end{pmatrix} \tag{A.29}$$

where

$$m_5 = 7.1 \times 10^{-3} kg \tag{A.30}$$

$$d_h = 6.35 \times 10^{-3} m \tag{A.31}$$

$$R_h = 1.9 \times 10^{-2} m \tag{A.32}$$

$$\tag{A.33}$$

Table A.2: Location of the Origins and of and the Mass of the Components

	m (Unit:kg)	x (Unit:m)	y (Unit:m)	z (Unit:m)
1	0.0536	0	8.89×10^{-2}	0
2	0.388	0.15	8.89×10^{-2}	0
3	0.101	1.13×10^{-2}	0	0
4	9.8×10^{-2}	0	1.27×10^{-2}	0
5	7.1×10^{-3}	0	9.7×10^{-2}	0

Plug in the values

$$I_5 = \begin{pmatrix} 8.2 \times 10^{-7} & 0 & 0 \\ 0 & 2.56 \times 10^{-6} & 0 \\ 0 & 0 & 8.83 \times 10^{-7} \end{pmatrix} \tag{A.34}$$

We chose the center of the handle as the inertia coordinate for the object;, therefore, the inertia matrix of the parts with respect to their its own geometricy center needed to be shifted to coincide with the new frame. The shift between the two frames is shown in Tab. A.2 Using the parallel axis theorems for moments of inertia [22]

$$I_{x'x'} = I_{xx} + m(y_{o'}^2 + z_{o'}^2) \tag{A.35}$$

$$I_{y'y'} = I_{yy} + m(x_{o'}^2 + z_{o'}^2) \tag{A.36}$$

$$I_{z'z'} = I_{zz} + m(x_{o'}^2 + y_{o'}^2) \tag{A.37}$$

$$I_{x'y'} = I_{xy} + mx_{o'}y_{o'} \tag{A.38}$$

$$I_{y'z'} = I_{yz} + my_{o'}z_{o'} \tag{A.39}$$

$$I_{x'z'} = I_{xz} + mx_{o'}z_{o'} \tag{A.40}$$

and summing up the inertia matrices of all components, we can derive the inertia matrix of the testing objects as follows:

$$I = \begin{pmatrix} I_{11} & I_{12} & I_{13} \\ I_{21} & I_{22} & I_{23} \\ I_{31} & I_{32} & I_{33} \end{pmatrix} \tag{A.41}$$

$$I_{11} = m_1 b^2 + \frac{n_1 + n_2}{6} m_2 a^2 + (n_1 + n_2) m_2 b^2 + \frac{1}{12} m_3 (R_h^2 + l_h^2) \tag{A.42}$$

$$+ \frac{1}{12} m_4 (l_h^2 + d_h^2) \tag{A.43}$$

$$I_{12} = 0 \tag{A.44}$$

$$I_{13} = m_1 b (\frac{l}{2} - l_{x1}^h) \tag{A.45}$$

$$I_{21} = 0 \tag{A.46}$$

$$I_{22} = \frac{1}{12} m_1 l^2 + m_1 (\frac{l}{2} - l_{x1})^2 + \frac{n_1 + n_2}{12} m_2 (a^2 + d^2)$$

$$+ n_1 m_2 (l_{x1}^2 + b^2) + n_2 m_2 (l_{x2}^2 + b^2) + \frac{1}{48} m_3 (4R_h^2 + 4l_h^2 + d_h^2) \tag{A.47}$$

$$+ \frac{1}{12} m_4 (d_h^2 + l_h^2) \qquad I_{23} = 0 \tag{A.48}$$

$$I_{31} = m_1 b (\frac{l}{2} - l_{x1}^h) \tag{A.49}$$

$$I_{32} = 0 \tag{A.50}$$

$$I_{33} = \frac{1}{12} m_1 l^2 + m_1 b^2 + \frac{1}{12} m (a^2 + d^2)$$

$$+ n_1 m_2 b l_{x1} + n_2 m_2 b l_{x2} + \frac{1}{2} m_3 R^2 + \frac{1}{12} m_4 (d_h^2 + d_h^2) \tag{A.51}$$

And the final result is shown in Tab. A.3

Table A.3: Inertia of the Object with Two One-Quarter Inch Steel Plate on Each Side

	Qt.	I'_{xx} $(kgcm^2)$	I'_{yy} $(kgcm^2)$	I'_{zz} $(kgcm^2)$	I'_{xy} $(kgcm^2)$	I'_{yz} $kgcm^2$	I'_{xz} $kgcm^2$
1	1	4.2×10^3	4.2×10^3	8.4×10^3	0	0	0
2	2	7.2×10^4	1.9×10^5	2.5×10^5	1.1×10^5	0	0
3	2	1.9×10^3	1.2×10^3	2.0×10^4	0	0	0
4	1	2.1×10^3	1.2×10^2	2.0×10^3	0	0	0
5	1	676.2	25.6	676.9	0	0	0
Sum		8.0×10^4	1.9×10^5	2.8×10^5	1.1×10^5	0	0
Model		8.4×10^4	1.9×10^5	2.6×10^5	9.5×10^4	0	0

Appendix B

Kinematics of WAM

The forward kinematics is used to determine the position and orientation of the end effector based on the joint angles. The general form of a transformation is given in Eq. 5.3

$$T = \begin{pmatrix} c\theta_i & -s\theta_i & 0 & a_{i-1} \\ s\theta_i c\alpha_{i-1} & c\theta_i c\alpha_{i-1} & -s\alpha_{i-1} & -sa_{i-1}d \\ s\theta_i s\alpha_{i-1} & c\theta_i s\alpha_{i-1} & c\alpha_{i-1} & -ca_{i-1}d \\ 0 & 0 & 0 & 1 \end{pmatrix} \tag{B.1}$$

The following equations shows the transformation of the joints [4].

$${}^0T_1 = \begin{pmatrix} c_1 & -s_1 & 0 & 0 \\ s_1 & c_1 & 0 & 0 \\ 0 & 0 & 1 & 0 \\ 0 & 0 & 0 & 1 \end{pmatrix} \tag{B.2}$$

$$
{}^{1}T_{2} = \begin{pmatrix} c_2 & -s_2 & 0 & 0 \\ 0 & 0 & 1 & 0 \\ -s_2 & -c_2 & 0 & 0 \\ 0 & 0 & 0 & 1 \end{pmatrix} \tag{B.3}
$$

$$
{}^{2}T_{3} = \begin{pmatrix} c_3 & -s_3 & 0 & 0 \\ 0 & 0 & -1 & -L_3 \\ -s_3 & -c_3 & 0 & 0 \\ 0 & 0 & 0 & 1 \end{pmatrix} \tag{B.4}
$$

$$
{}^{3}T_{4} = \begin{pmatrix} c_4 & -s_4 & 0 & d_3 \\ 0 & 0 & 1 & 0 \\ -s_4 & -c_4 & 0 & 0 \\ 0 & 0 & 0 & 1 \end{pmatrix} \tag{B.5}
$$

$$
{}^{4}T_{5} = \begin{pmatrix} c_5 & -s_5 & 0 & -d_3 \\ 0 & 0 & -1 & -L_4 \\ s_5 & c_5 & 0 & 0 \\ 0 & 0 & 0 & 1 \end{pmatrix} \tag{B.6}
$$

$$
{}^{5}T_{6} = \begin{pmatrix} c_6 & -s_6 & 0 & 0 \\ 0 & 0 & 1 & 0 \\ -s_6 & -c_6 & 0 & 0 \\ 0 & 0 & 0 & 1 \end{pmatrix} \tag{B.7}
$$

$$
{}^6T_7 = \begin{pmatrix} c_7 & -s_7 & 0 & 0 \\ 0 & 0 & -1 & -L_7 \\ s_7 & c_7 & 0 & 0 \\ 0 & 0 & 0 & 1 \end{pmatrix} \tag{B.8}
$$

Then

$$
{}^0T_2 = {}^0T_1 {}^1T_2 \tag{B.9}
$$

$$
= \begin{pmatrix} c_1c_2 & -c_1s_2 & -s_1 & 0 \\ c_2s_1 & -s_1s_2 & c_1 & 0 \\ -s_2 & -c_2 & 0 & 0 \\ 0 & 0 & 0 & 1 \end{pmatrix} \tag{B.10}
$$

$$
{}^0T_3 = {}^0T_1 {}^1T_2 {}^2T_3 \tag{B.11}
$$

$$
= \begin{pmatrix} s_1s_3 + c_1c_2c_3 & c_3s_1 - c_1c_2s_3 & c_1s_2 & L_3c_1s_2 \\ c_2s_3s_1 - c_1s_3 & -c_1c_3 - c_2s_1s_3 & s_1s_2 & L_3s_1s_2 \\ -c_3s_2 & -s_2s_3 & c_2 & L_3c_2 \\ 0 & 0 & 0 & 1 \end{pmatrix} \tag{B.12}
$$

$$
{}^0T_4 = {}^0T_1 {}^1T_2 {}^2T_3 {}^3T_4 \tag{B.13}
$$

$$
= \begin{pmatrix} c_4(s_1s_3 + c_1c_2c_3) - c_1s_2s_4 & -s_4(s_1s_3 + c_1c_2c_3) - c_1c_4s_2 & c_3s_1 - c_1c_2s_3 & o_3^x \\ -c_4(c_1s_3 - c_2c_3s_1) - s_1s_2s_4 & s_4(c_1s_3 - c_2c_3s_1) - c_4s_1s_2 & -c_1c_3 - c_2s_1s_3 & o_3^y \\ -c_2s_4 - c_3c_4s_2 & c_3s_2s_4 - c_2c_4 & s_2s_3 & o_3^z \\ 0 & 0 & 0 & 1 \end{pmatrix} \tag{B.14}
$$

Where

$$o_3^x = L_3 c_1 s_2 + d_3 s_1 s_3 + d_3 c_1 c_2 c_3 \tag{B.15}$$

$$o_3^y = L_3 s_1 s_2 - d_3 c_1 s_3 + d_3 c_2 c_3 s_1 \tag{B.16}$$

$$o_3^z = L_3 c_2 - d_3 c_3 s_2 \tag{B.17}$$

$$^0T_5 = {}^0T_1\,{}^1T_2\,{}^2T_3\,{}^3T_4\,{}^4T_5 \tag{B.18}$$

$$= \begin{pmatrix} r_{11} & r_{12} & r_{13} & o_4^x \\ r_{21} & r_{22} & r_{23} & o_4^y \\ r_{31} & r_{32} & r_{33} & o_4^z \\ 0 & 0 & 0 & 1 \end{pmatrix} \tag{B.19}$$

Where

$$r_{11} = c_5(c_4(s_1 s_3 + c_1 c_2 c_3) - c_1 s_2 s_4) + s_5(c_3 s_1 - c_1 c_2 s_3) \tag{B.20}$$

$$r_{12} = c_5(c_3 s_1 - c_1 c_2 s_3) - s_5(c_4(s_1 s_3 + c_1 c_2 c_3) - c_1 s_2 s_4) \tag{B.21}$$

$$r_{13} = s_4(s_1 s_3 + c_1 c_2 c_3) + c_1 c_4 s_2 \tag{B.22}$$

$$r_{21} = -c_5(c_4(c_1 s_3 - c_2 c_3 s_1) + s_1 s_2 s_4) - s_5(c_1 c_3 + c_2 s_1 s_3) \tag{B.23}$$

$$r_{22} = s_5(c_4(c_1 s_3 - c_2 c_3 s_1) + s_1 s_2 s_4) - c_5(c_1 c_3 + c_2 s_1 s_3) \tag{B.24}$$

$$r_{23} = c_4 s_1 s_2 - s_4(c_1 s_3 - c_2 c_3 s_1) \tag{B.25}$$

$$r_{31} = s_2 s_3 s_5 - c_5(c_2 s_4 + c_3 c_4 s_2) \tag{B.26}$$

$$r_{32} = s_5(c_2 s_4 + c_3 c_4 s_2) + c_5 s_2 s_3 \tag{B.27}$$

$$r_{33} = c_2 c_4 - c_3 s_2 s_4 \tag{B.28}$$

$$o_4^x = L_3 c_1 s_2 + d_3 s_1 s_3 - d_3 c_4 (s_1 s_3 + c_1 c_2 c_3) + L_4 s_4 (s_1 s_3 + c_1 c_2 c_3) \tag{B.29}$$

$$+ d_3 c_1 c_2 c_3 + L_4 c_1 c_4 s_2 + d_3 c_1 s_2 s_4 \tag{B.30}$$

$$o_4^y = L_3 s_1 s_2 - d_3 c_1 s_3 + d_3 c_4 (c_1 s_3 - c_2 c_3 s_1) - L_4 s_4 (c_1 s_3 - c_2 c_3 s_1) \tag{B.31}$$

$$+ d_3 c_2 c_3 s_1 + L_4 c_4 s_1 s_2 + d_3 s_1 s_2 s_4 \tag{B.32}$$

$$o_4^z = L_3 c_2 + L_4 c_2 c_4 - d_3 c_3 s_2 + d_3 c_2 s_4 + d_3 c_3 c_4 s_2 - L_4 c_3 s_2 s_4 \tag{B.33}$$

$$^0T_6 = {}^0T_1 {}^1T_2 {}^2T_3 {}^3T_4 {}^4T_5 {}^5T_6 \tag{B.34}$$

$$= \begin{pmatrix} r_{11} & r_{12} & r_{13} & o_5^x \\ r_{21} & r_{22} & r_{23} & o_5^y \\ r_{31} & r_{32} & r_{33} & o_5^z \\ 0 & 0 & 0 & 1 \end{pmatrix} \tag{B.35}$$

Where

$$r_{11} = c_6(c_5(c_4(s_1 s_3 + c_1 c_2 c_3) - c_1 s_2 s_4) + s_5(c_3 s_1 - c_1 c_2 s_3))$$

$$- s_6(s_4(s_1 s_3 + c_1 c_2 c_3) + c_1 c_4 s_2) \tag{B.36}$$

$$r_{12} = -c_6(s_4(s_1 s_3 + c_1 c_2 c_3) + c_1 c_4 s_2) - s_6(c_5(c_4(s_1 s_3 + c_1 c_2 c_3) - c_1 s_2 s_4)$$

$$+ s_5(c_3 s_1 - c_1 c_2 s_3))$$

$$r_{13} = c_5(c_3 s_1 - c_1 c_2 s_3) - s_5(c_4(s_1 s_3 + c_1 c_2 c_3) - c_1 s_2 s_4) \tag{B.37}$$

$$r_{21} = s_6(s_4(c_1 s_3 - c_2 c_3 s_1) - c_4 s_1 s_2) - c_6(c_5(c_4(c_1 s_3 - c_2 c_3 s_1)$$

$$+ s_1 s_2 s_4) + s_5(c_1 c_3 + c_2 s_1 s_3)) \tag{B.38}$$

$$r_{22} = c_6(s_4(c_1 s_3 - c_2 c_3 s_1) - c_4 s_1 s_2) + s_6(c_5(c_4(c_1 s_3 - c_2 c_3 s_1) + s_1 s_2 s_4) \tag{B.39}$$

$$+ s_5(c_1 c_3 + c_2 s_1 s_3)) \tag{B.40}$$

$$r_{23} = s_5(c_4(c_1 s_3 - c_2 c_3 s_1) + s_1 s_2 s_4) - c_5(c_1 c_3 + c_2 s_1 s_3) \tag{B.41}$$

$$r_{31} = -c_6(c_5(c_2s_4 + c_3c_4s_2) - s_2s_3s_5) - s_6(c_2c_4 - c_3s_2s_4) \tag{B.42}$$

$$r_{32} = s_6(c_5(c_2s_4 + c_3c_4s_2) - s_2s_3s_5) - c_6(c_2c_4 - c_3s_2s_4) \tag{B.43}$$

$$r_{33} = s_5(c_2s_4 + c_3c_4s_2) + c_5s_2s_3 \tag{B.44}$$

$$o_5^x = L_3c_1s_2 + d_3s_1s_3 - d_3c_4(s_1s_3 + c_1c_2c_3) + L_4s_4(s_1s_3 + c_1c_2c_3) \tag{B.45}$$

$$+ d_3c_1c_2c_3 + L_4c_1c_4s_2 + d_3c1s2s4 \tag{B.46}$$

$$o_5^y = L_3s_1s_2 - d_3c_1s_3 + d_3c_4(c_1s_3 - c_2c_3s_1) - L_4s_4(c_1s_3 - c_2c_3s_1) \tag{B.47}$$

$$+ d_3c_2c_3s_1 + L_4c_4s_1s_2 + d_3s_1s_2s_4 \tag{B.48}$$

$$o_5^z = L_3c_2 + 291c_2c_4 - d_3c_3s_2) + d_3c_2s_4 + d_3c_3c_4s_2 - L_4c_3s_2s_4 \tag{B.49}$$

$$^0T_7 = {}^0T_1{}^1T_2{}^2T_3{}^3T_4{}^4T_5{}^5T_6{}^6T_7 \tag{B.50}$$

$$= \begin{pmatrix} r_{11} & r_{12} & r_{13} & o_5^x \\ r_{21} & r_{22} & r_{23} & o_5^y \\ r_{31} & r_{32} & r_{33} & o_5^z \\ 0 & 0 & 0 & 1 \end{pmatrix} \tag{B.51}$$

where

$$r_{11} = -c_7(s_6(s_4(s_1s_3 + c_1c_2c_3) + c_1c_4s_2) - c_6(c_5(c_4(s_1s_3 + c_1c_2c_3) \tag{B.52}$$

$$- c_1s_2s_4) + s_5(c_3s_1 - c_1c_2s_3))) - s_7(s_5(c_4(s_1s_3 + c_1c_2c_3) - c_1s_2s_4) \tag{B.53}$$

$$- c_5(c_3s_1 - c_1c_2s_3)) \tag{B.54}$$

$$r_{12} = s_7(s_6(s_4(s_1s_3 + c_1c_2c_3) + c_1c_4s_2) \tag{B.55}$$

$$- c_6(c_5(c_4(s_1s_3 + c_1c_2c_3) - c_1s_2s_4) + s_5(c_3s_1 - c_1c_2s_3))) \tag{B.56}$$

$$- c_7(s_5(c_4(s_1s_3 + c_1c_2c_3) - c_1s_2s_4) - c_5(c_3s_1 - c_1c_2s_3)) \tag{B.57}$$

$$r_{13} = c_6(s_4(s_1s_3 + c_1c_2c_3) + c_1c_4s_2) \tag{B.58}$$

$$+ s_6(c_5(c_4(s_1s_3 + c_1c_2c_3) - c_1s_2s_4) + s_5(c_3s_1 - c_1c_2s_3)) \tag{B.59}$$

$$r_{21} = c_7(s_6(s_4(c_1s_3 - c_2c_3s_1) - c_4s_1s_2) \tag{B.60}$$

$$- c_6(c_5(c_4(c_1s_3 - c_2c_3s_1) + s_1s_2s_4) + s_5(c_1c_3 + c_2s_1s_3))) \tag{B.61}$$

$$+ s_7(s_5(c_4(c_1s_3 - c_2c_3s_1) + s_1s_2s_4) - c_5(c_1c_3 + c_2s_1s_3)) \tag{B.62}$$

$$r_{22} = c_7(s_5(c_4(c_1s_3 - c_2c_3s_1) + s_1s_2s_4) - c_5(c_1c_3 + c_2s_1s_3)) \tag{B.63}$$

$$- s_7(s_6(s_4(c_1s_3 - c_2c_3s_1) - c_4s_1s_2) - c_6(c_5(c_4(c_1s_3 - c_2c_3s_1) + s_1s_2s_4) \tag{B.64}$$

$$+ s_5(c_1c_3 + c_2s_1s_3))) \tag{B.65}$$

$$r_{23} = -c_6(s_4(c_1s_3 - c_2c_3s_1) - c_4s_1s_2) \tag{B.66}$$

$$- s_6(c_5(c_4(c_1s_3 - c_2c_3s_1) + s_1s_2s_4) \tag{B.67}$$

$$+ s_5(c_1c_3 + c_2s_1s_3)) \tag{B.68}$$

$$r_{31} = s_7(s_5(c_2s_4 + c_3c_4s_2) + c_5s_2s_3) \tag{B.69}$$

$$- c_7(c_6(c_5(c_2s_4 + c_3c_4s_2) - s_2s_3s_5) \tag{B.70}$$

$$+ s_6(c_2c_4 - c_3s_2s_4)) \tag{B.71}$$

$$r_{32} = c_7(s_5(c_2s_4 + c_3c_4s_2) + c_5s_2s_3) \tag{B.72}$$

$$+ s_7(c_6(c_5(c_2s_4 + c_3c_4s_2) - s_2s_3s_5) \tag{B.73}$$

$$+ s_6(c_2c_4 - c_3s_2s_4)) \tag{B.74}$$

$$r_{33} = c_6(c_2c_4 - c_3s_2s_4) \tag{B.75}$$

$$- s_6(c_5(c_2s_4 + c_3c_4s_2) - s_2s_3s_5) \tag{B.76}$$

$$o_6^x = L_3c_1s_2 + d_3s_1s_3 - d_3c_4(s_1s_3 + c_1c_2c_3) \tag{B.77}$$

$$+ L_4s_4(s_1s_3 + c_1c_2c_3) \tag{B.78}$$

$$+ d_3c_1c_2c_3 + L_4c_1 *_4 s_2 + d_3c_1s_2s_4 \tag{B.79}$$

$$o_6^y = L_3 s_1 s_2 - d_3 c_1 s_3 + d_3 c_4 (c_1 s_3 - c_2 c_3 s_1) \tag{B.80}$$

$$- L_4 s_4 (c_1 s_3 - c_2 c_3 s_1) + d_3 c_2 c_3 s_1 + L_4 c_4 s_1 s_2 \tag{B.81}$$

$$+ d_3 s_1 s_2 s_4 \tag{B.82}$$

$$o_6^z = L_3 c2 + L_4 c_2 c_4 - d_3 c_3 s_2 + d_3 c_2 s_4 \tag{B.83}$$

$$+ d_3 c_3 c_4 s_2 - L_4 c_3 s_2 s_4 \tag{B.84}$$

$$J^T = \begin{pmatrix} z_0 \times (o_7 - o_0) & z_1 \\ z_1 \times (o_7 - o_1) & z_2 \\ z_2 \times (o_7 - o_2) & z_3 \\ z_3 \times (o_7 - o_3) & z_4 \\ z_4 \times (o_7 - o_4) & z_5 \\ z_5 \times (o_7 - o_5) & z_6 \\ z_6 \times (o_7 - o_6) & z_7 \end{pmatrix} \tag{B.85}$$

Since WAM has a spherical joint, then

$$o_7 - o_6 = 0 \tag{B.86}$$

$$o_7 - o_5 = 0 \tag{B.87}$$

$$o_7 - o_4 = 0 \tag{B.88}$$

Then the Jacobian matrix of WAM can be simplified into

$$J^T = \begin{pmatrix} z_0 \times (o_7 - o_0) & z_1 \\ z_1 \times (o_7 - o_1) & z_2 \\ z_2 \times (o_7 - o_2) & z_3 \\ z_3 \times (o_7 - o_3) & z_4 \\ 0 & z_5 \\ 0 & z_6 \\ 0 & z_7 \end{pmatrix} \tag{B.89}$$

Appendix C

Inverse Kinematics of WAM

A general inverse kinematics for a redundancy is complicated, but the axes of the last three joints of WAM intersect at one point; this reduces the complexity of the computation. Because this is equivalent to having a spherical joint at the wrist, it decouples the inverse kinematics problem into two sub-problems: inverse position kinematics and inverse orientation kinematics. The inverse position kinematics generates the desired angle for the first four joints from the base. The orientation kinematics considers the remaining three. where And the joint limitations are:

Table C.1: Denavit-Hartenberg Parameters for WAM

Joint	a_{i-1}	α_{i-1}	d_i	θ_i
1	0	0	0	θ_1
2	0	$-\frac{\pi}{2}$	0	θ_2
3	0	$\frac{\pi}{2}$	L_3	θ_3
4	d_3	$-\frac{\pi}{2}$	0	θ_4
5	$-d_3$	$\frac{\pi}{2}$	L_4	θ_5
6	0	$-\frac{\pi}{2}$	0	θ_6
7	0	$\frac{\pi}{2}$	L_7	θ_7

Table C.2: Link Parameter Values

Parameter	Value
L_3	55.8cm
L_4	29.1cm
L_7	6.5cm
d_3	4.76cm

Table C.3: Joint Limits

Joint	Maximum Joint Angle (radians)	Minimum Joint Angle (radians)
1	2.46	-2.46
2	1.9	-1.9
3	2.74	2.74
4	3.14	-0.9
5	3.14	-3.14
6	4.7	-1.57
7	2.35	-2.35

C.1 WAM Inverse Kinematics with Joint Three Set to Zero

The first step to solving the inverse kinematics of WAM is to turn WAM into a non-redundant robot by setting joint two equal to zero.

C.1.1 Inverse Position Kinematics: - A Geometric Approach

The geometric variables are defined in Fig. C.1. The third joint is held at zero to eliminate the redundancy at the first joint. Define x_d, y_d and z_d as the desired manipulator position and $\theta_1, \theta_2, \theta_3$ and θ_4 are desired angles. We first set

$$\theta_3 = 0.0 \tag{C.1}$$

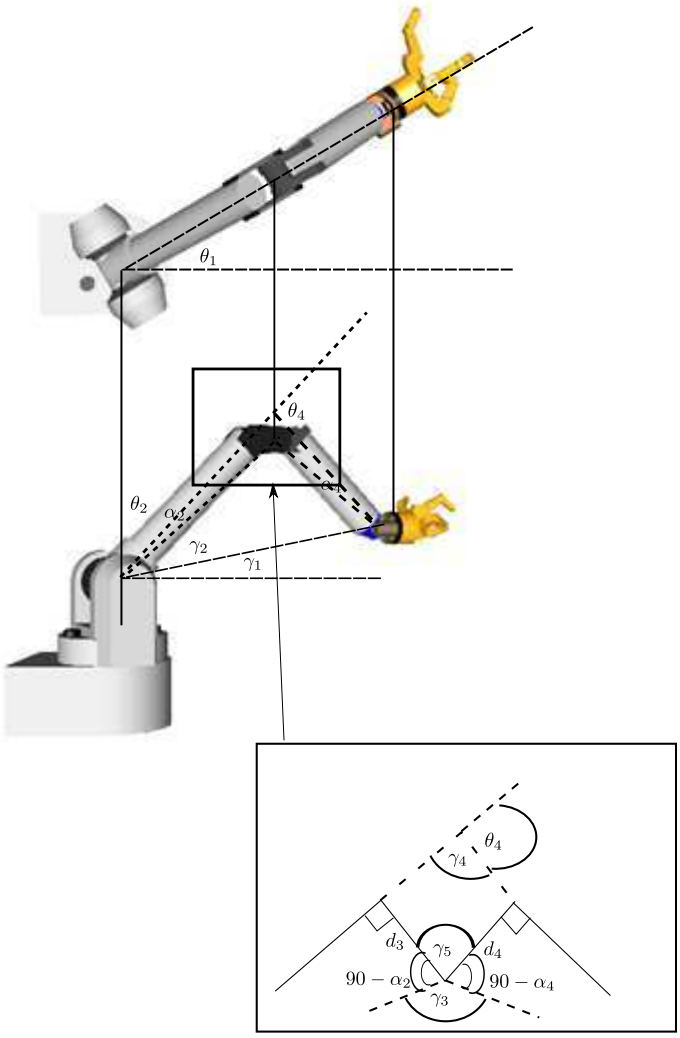

Figure C.1: Elbow Kinematics of WAM

Then the first joint is easy to find according to the following equation:

$$\theta_1 = \arctan(x_d/y_d) \tag{C.2}$$

Since the rotation axis of Joint 4 does not intercept with axis three and five, in order to simplify the computation we compute four offset values for the robot.

$$l'_3 = \sqrt{l_3^2 + d_3^2} \tag{C.3}$$

$$\alpha_2 = \arctan \frac{d_3}{l_3} \tag{C.4}$$

$$l'_4 = \sqrt{l_4^2 + d_4^2} \tag{C.5}$$

$$\alpha_4 = \arctan \frac{d_3}{l_4} \tag{C.6}$$

Then we can solve for the values of joints 1, 2 and 4. The first joint angle can be given by Eq. C.2.

$$l_{d2} = \sqrt{x_d^2 + y_d^2 + z_d^2} \tag{C.7}$$

$$\gamma_1 = \arcsin(\frac{z_d}{l_{d2}}) \tag{C.8}$$

$$\gamma_2 = \arccos(\frac{l_{d1}^2 + l'^2_3 - l'^2_4}{2 l_{d1} l'_3}) \tag{C.9}$$

$$\gamma_3 = \arccos(\frac{l'^2_3 + l'^2_4 - l_{d1}^2}{2 l'_3 l'_4}) \tag{C.10}$$

$$\theta_2 = \gamma_1 + \gamma_2 + \alpha_2 \tag{C.11}$$

$$\theta_4 = 180 - \gamma_4 \tag{C.12}$$

$$= 180 - (360 - \gamma_5 - 90 - 90) \tag{C.13}$$

$$= \gamma_5 \tag{C.14}$$

$$= 360 - (90 - \alpha_2) - (90 - \alpha_4) - \gamma_3 \tag{C.15}$$

$$= 180 + \alpha_2 + \alpha_4 - \gamma_3 \tag{C.16}$$

Then add the constant offset angles given by Eq. C.3-Eq. C.6.

C.1.2 Inverse Orientation Kinematics

$$T = \begin{pmatrix} c_5c_6c_7 - s_5s_7 & -c_7s_5 - c_5c_6s_7 & c_5s_6 \\ c_7s_6 & -s_6s_7 & -c_6 \\ c_5s_7 + c_6c_7s_5 & c_5c_7 - c_6s_5s_7 & s_5s_6 \end{pmatrix} = \begin{pmatrix} r_{11} & r_{12} & r_{13} \\ r_{21} & r_{22} & r_{23} \\ r_{31} & r_{32} & r_{33} \end{pmatrix} \tag{C.17}$$

Using an inverse trigonometric, we can find eight possible solutions.

$$\theta_6 = -\arccos(-r_{23}) \tag{C.18}$$

$$\theta_5 = \arctan(r_{33}/r_{13}) \tag{C.19}$$

$$\theta_7 = \arctan(-\frac{r_{22}}{r_{21}}) \tag{C.20}$$

C.2 General Inverse Kinematics of WAM

In this section, the method of computing the inverse kinematics of the WAM, without locking joint 3, will be presented. First, denote the plane shown in the zoomed-in picture in Fig. C.1 as the reference plane. When the constraint on joint 3 is released, the robot elbow joint will be able to go around in a circle without changing the position and orientation of the end-effector. Define the new plane that link three and link four formed as the arm plane. Denote the angle between the planes as ζ. The

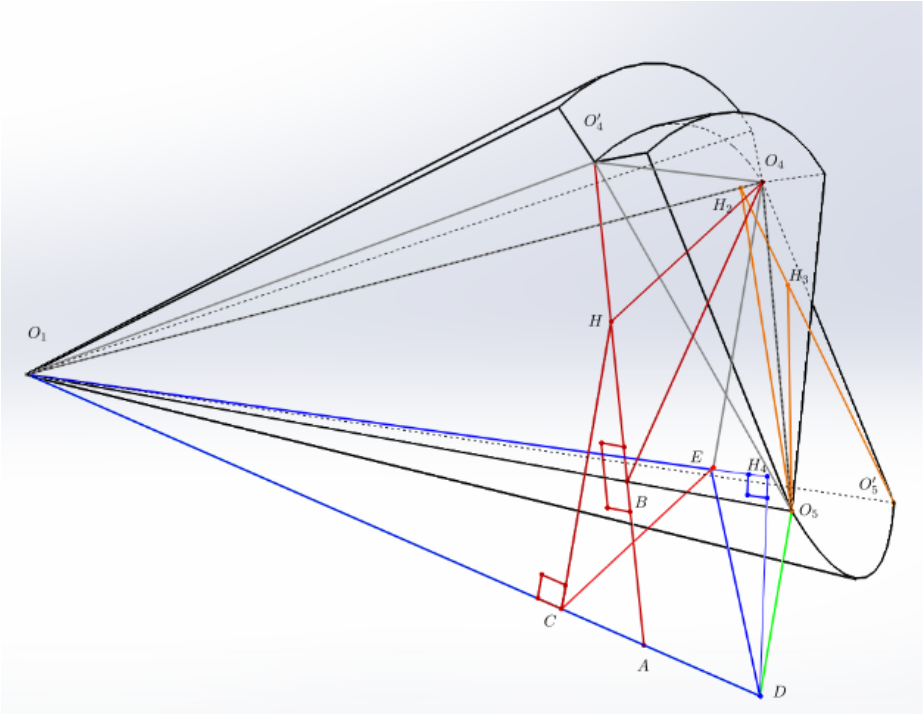

Figure C.2: Inverse Kinematics of Lower Arm of WAM

variables, γ_1, γ_2, l_{d2}, γ_3, α_3 and α_4 are all defined the same way as in the last section and they can be found with the same equations. First draw a line on the arm plane from O_4' and perpendicular to O_1O_5 , then

$$O_1B = \cos\gamma_2 L_3' \tag{C.21}$$

$$BA = \tan\gamma_1 O_1B \tag{C.22}$$

Draw a line from o_4 that is perpendicular to O_1O_5. This line is going to intersect with O_1O_5 at B, then

$$HB = \cos\phi BO_4 \tag{C.23}$$

$$HC = (HB + BA)\cos\gamma_1 \tag{C.24}$$

$$= (\cos\phi BO_4' + \tan\gamma_1 O_1B)\cos\gamma_1 \tag{C.25}$$

$$= (\cos\phi BO_4' + \tan\gamma_1\cos\gamma_2 L_3')\cos\gamma_1 \tag{C.26}$$

$$= \cos\gamma_1\cos\phi\sin\gamma_2 L_3' + \sin\gamma_1\cos\gamma_2 L_3' \tag{C.27}$$

Then we can find θ_3

$$\theta_2 = \arcsin(\frac{HC}{L_3'}) \tag{C.28}$$

$$= \arcsin(\frac{\cos\gamma_1\cos\phi\sin\gamma_2 L_3' + \sin\gamma_1\cos\gamma_2 L_3'}{L_3'}) \tag{C.29}$$

$$= \arcsin(\cos\gamma_1\cos\phi\sin\gamma_2 + \sin\gamma_1\cos\gamma_2) \tag{C.30}$$

$$\theta_1' = \arcsin(\frac{EC}{O_1E}) \tag{C.31}$$

$$= \arcsin(\frac{O_4H}{\cos(\theta_2)L_3'}) \tag{C.32}$$

$$= \arcsin(\frac{\sin\phi O_4B}{\cos(90-\theta_2)L_3'}) \tag{C.33}$$

$$= \arcsin(\frac{\sin\phi\sin\gamma_2 L_3'}{\cos(90-\theta_2)L_3'}) \tag{C.34}$$

$$= \arcsin(\frac{\sin\phi\sin\gamma_2}{\sin\theta_2}) \tag{C.35}$$

Therefore the $\tilde{\theta}_1$ is:

$$\tilde{\theta}_1 = \theta_1' + \theta_1 \tag{C.36}$$

Where θ_1 is given by Eq. C.2. By inspection, θ_4 will be constant when the end-effector position and orientation are constant. The last thing unknown on the lower

arm is the θ_3. Draw a line from O_5 that is perpendicular to O_1O_4 at H_2, connect H_2 and O_5'. H_2O_5' perpendicular to O_1O_4 at H_2. Therefore, the surface $H_2O_5O_5'$ is perpendicular to the surface $O_1O_5O_5'$. Draw a line from O_5' to H_2O_5' at H_3. This line is perpendicular to the $O_1O_4O_5'$ surface. Draw a line from D perpendicular to O_1E at H_4.

$$O_5H_3 = DH_4 \tag{C.37}$$

DH_4 can be found by the following equation:

$$DH_4 = \sin\theta_1' O_1D \tag{C.38}$$

$$= \sin\theta_1' \sqrt{x_d^2 + y_d^2} \tag{C.39}$$

And O_5H_2 can be given by

$$O_5H_2 = \sin\gamma_2 O_1O_5 \tag{C.40}$$

$$= \sin\gamma_2 \sqrt{x_d^2 + y_d^2 + z_d^2} \tag{C.41}$$

Therefore, θ_3 is given by

$$\theta_3 = \arcsin(\frac{O_5H_3}{O_5H_2}) \tag{C.42}$$

$$= \arcsin(\frac{DH_4}{O_5H_2}) \tag{C.43}$$

$$= \arcsin(\frac{\sin\theta_1' \sqrt{x_d^2 + y_d^2}}{\sin\gamma_2 \sqrt{x_d^2 + y_d^2 + z_d^2}}) \tag{C.44}$$

Plug in Eq. C.35:

$$= \arcsin\left(\frac{\sin\phi \sin\gamma_2 \sqrt{x_d^2 + y_d^2}}{\sin\theta_2 \sin\gamma_2 \sqrt{x_d^2 + y_d^2 + z_d^2}}\right) \tag{C.45}$$

$$= \arcsin\left(\frac{\sin\phi \sqrt{x_d^2 + y_d^2}}{\sin\theta_2 \sqrt{x_d^2 + y_d^2 + z_d^2}}\right) \tag{C.46}$$

Then we can derive the rotational transformation matrix:

$${}^0_4R^4_7R = {}^0_7R \tag{C.47}$$

$${}^4_7R = {}^4_0R^0_7R \tag{C.48}$$

Plug the result into Eq. C.17. The method of solving for the last three wrist joints is the same as shown in Eq. C.18-Eq. C.20.

Appendix D

WAM-Phantom Teleoperation System Startup and Operational Procedure

D.1 Startup

D.1.1 Phantom Omni

The Omnis are connected to a windows PC through a firewire cable. The Omnis can be connected in a series, where the lower female connector should be connected to the one closer to the Omni, and the upper one should be connected to the Omni further away from the computer. Check the connectivity before turning them on.

Turn on the power plug in the panel; now the blue LED lights inside the inkwell of the Omnis should be blinking. Then turn on the computer and type in the password and username to log in the computer. There are two programs on the screen, one called "Phantom Setup" and another one called "Phantom Control". Launch "Phantom Control" and check to see whether all the serial numbers of the Omnis show up on the drop-down list. If any one does not show up, recycle the power of the Omnis.

Go to network settings and make sure that the netmask is set to "255.255.255.0" and the IP address is set as "192.168.7.24". Launch "Visual Studio 2005" and start the solution called "ColumnbForce"; click "start without debugging." Now all the

Omnis are actuated, and the computer is sending position commands to the WAM computer.

D.1.2 WAM

Turn on the power supply of WAM, an AC to 48VDC converter. Turn on WAM external PC; it takes the computer more than one minute to start-up. The login passcode is "WAM." Type "sudo ifconfig eth0 192.168.7.27 netmask 255.255.255.0" to set up the ethernet. Then the computer will ask for a password again; type "WAM." Type "robot" as the username and "WAM" as the passcode. Go to "cd tianqiu/modified_examples." Now the control program of WAM is launched. Follow the direction to shift+idle and shift+activate WAM. Type enter three times and then you can see the first command position received from the Phantom computer. See if they are close to "0,45,0,90,0,-45,0," because that is the origin of the slave workspace. If it is close enough, hit enter and the robot will go to the desired position. During this process, do not move the master controller; otherwise, there will be big jerk when starting the teleoperation mode. When the slave robot reaches the desired position, hit enter again, and now the robot is in teleoperation mode.

D.2 Shutdown

The shutdown procedure is basically the reverse of the initialization. First hit the "Enter" key on the WAM computer. Then close the gripper by hitting the "Enter" key three more times. Then type "q" to quit the teleoperation mode. The robot will move back to its home position; hit shift+idle the robot and quit the program. For the Omnis' PC, simply right click the Opengl window and click "quit."

Appendix E

Euler Angle and Robot Angle Tracking Error

In this section, we will discuss using the robot end-effector orientation matrices to determine the orientation angle tracking error, therefore determining the torque to be provided by the PID controller. The orientation difference matrix is defined as:

$$R^{diff} = R_s(R_m)^{-1} \tag{E.1}$$

Then in order to determine the difference angle, we need to apply the Euler angle transformation.

$$R^{diff} = Z(\alpha)Y(\beta)X(\gamma) \tag{E.2}$$

$$= \begin{bmatrix} \cos\alpha & -\sin\alpha & 0 \\ \sin\alpha & \cos\alpha & 0 \\ 0 & 0 & 1 \end{bmatrix} \begin{bmatrix} \cos\beta & 0 & \sin\beta \\ 0 & 1 & 0 \\ -\sin\beta & 0 & \cos\beta \end{bmatrix} \begin{bmatrix} 1 & 0 & 0 \\ 0 & \cos\gamma & -\sin\gamma \\ 0 & \sin\gamma & \cos\gamma \end{bmatrix} \tag{E.3}$$

$$= \begin{bmatrix} \cos\alpha\cos\beta & \cos\alpha\sin\beta\sin\gamma - \cos\gamma\sin\alpha & \sin\alpha\sin\gamma + \cos\alpha\cos\gamma\sin\beta \\ \cos\beta\sin\alpha & \cos\alpha\cos\gamma + \sin\alpha\sin\beta\sin\gamma & \cos\gamma\sin\alpha\sin\beta - \cos\alpha\sin\gamma \\ -\sin\beta & \cos\beta\sin\gamma & \cos\beta\cos\gamma \end{bmatrix} \tag{E.4}$$

Therefore the Euler angles can be found using Eq.

$$\beta = -\arcsin R_{31}^{diff} \tag{E.5}$$

$$\gamma = -\arccos \frac{R_{33}^{diff}}{\cos\beta} \tag{E.6}$$

$$\alpha = \arccos \frac{R_{11}^{diff}}{\cos\beta} \tag{E.7}$$

Vita

Mr. Tian Qiu was born in the city of Beijing, China in 1987 to Chang Liu and Ning Qiu. His family lived in Beijing for all his childhood and teenage life. He graduated from the experimental high school attached to Beijing Normal University in spring 2005 with honors. He entered Tsinghua University the following fall and majored in automation, where he took courses in computer, electrical and mechanical engineering. After graduating from Tsinghua, he moved to Knoxville, Tennessee to join the University of Tennessee. He was accepted by the interactive network robotics lab in the mechanical, aerospace and biomedical engineering department, where he worked on passive controllers in haptics interaction and haptics perception with the presence of noise. In the summer of 2011, the principle investigator of the lab, Dr. Lee, went back to Korea. Mr. Qiu began working in the robotics system lab under Dr. Hamel, when he started to work on teleoperation systems. His dissertation focuses on kinesthetic perception with teleoperation systems.